

**A case study for Skukuza: Estimating biophysical  
properties of fires using EOS-MODIS satellite data**

**Dissertation  
zur Erlangung des Doktorgrades  
der Mathematisch-Naturwissenschaftlichen Fakultäten  
der Georg-August-Universität zu Göttingen**

vorgelegt von

**Dipl. Geogr. Tobias Landmann**

aus Elim (Südafrika)

Göttingen 2003

D 7

Referentin/Referent: Prof. Dr. G. Gerold

Korreferentin/Korreferent: Prof. Dr. M. Kappas

Tag der mündlichen Prüfung: 11.02.2003

## *Vorwort*

Savannenbrände in Afrika, speziell in Südafrika, tragen zu einem großen Anteil an der jährlichen feuerbedingten Aerosol- und Gasemissionen in die Atmosphäre bei. Sowohl von der Häufigkeit als auch von der verbrannten Biomasse her (35 % der globalen jährlichen Biomasseverluste durch Feuer) besitzt Südafrika eine Schlüsselrolle in Untersuchungen zum feuerbeeinflussten Savannenökosystem, für das Feuermonitoring und Feuermanagement im Zusammenhang mit den Savannen-Nationalparks und für die Analyse und Modellierung der Emissionen in die Atmosphäre. Eine wesentliche Grundlage dafür stellt die weitflächige satellitengestützte Analyse der brennbaren Biomasse, Zahl und Lokalität der Feuer sowie Erfassung der Feuerintensität dar.

Unter Beteiligung am SAFARI-2000-Programm (Southern Africa Regional Science Initiative) konnten mit dieser Dissertation am Beispiel des Krüger-Nationalparks in Südafrika sowohl im Feld leicht einsetzbare Methoden zur Analyse der brennbaren Biomasse wie auch neue Algorithmen zur pixelgenauen Erfassung von Feuerintensität und Brandflächen über MODIS- und Landsat-ETM-Daten entwickelt werden. Ihre Anwendbarkeit für bessere regionale Emissionsmodelle - wie für ein effektives Feuermanagement im Nationalpark - wird in dieser Arbeit aufgezeigt und ist auf andere Savannenbrände übertragbar.

Dank der guten Unterstützung über die Gottlieb Daimler und Karl-Benz-Stiftung, der südafrikanischen Forschungseinrichtungen und Kollegen (CSIR Environmentek) und der Universität Göttingen konnte diese Dissertation erfolgreich abgeschlossen werden.

Göttingen, den 1. November 2003

## *Prologue*

Biomass burning in Africa, explicitly in Southern Africa, contributes excessively to the annual aerosol loading and pyrogenic gas emissions within the African atmospheric system. The frequency of burning and the extensive size of burned areas in Southern Africa (wildfires in Southern Africa account for 35% of global annual fire biomass fuel consumptions) make South Africa suitable for fire related research. Research regarding the fire effects on ecosystem function, the development of spatial fire monitoring mechanisms and fire management practises in protected areas is necessary to develop, improve and analyse models that predict regional pyrogenic emissions. Spatial fire information from remote sensing can be used as tool to rigorously and effectively detect and analyse biomass fuel available for burning, fire count locations as well as fire severity.

This dissertation was accomplished within the context of the 2000 Southern Africa Regional Science (SAFARI-2000) Initiative, using the Kruger National Park in South Africa as a 'casestudy' savanna ecosystem. Methods to analyse pre-burn biomass fuel loads, spatially explicit algorithms to detect fire severity, and fire scar mapping and detection methods using Landsat ETM+ and MODIS satellite imagery were developed. The applicability of these methods and algorithms to effectively improve regional emissions models and fire management practices in protected areas are shown. The new methods developed within the context of this dissertation may be applicable to similar savanna ecosystems. This dissertation could be completed successfully and thankfully with the support of the Gottlieb Daimler and Karl-Benz Foundation, South African Research Institutions (especially CSIR Environmentek) and the University of Goettingen in Germany.

Göttingen, 1<sup>st</sup> of November 2003

## **Abstract**

**Context Abstract.** The Southern African Regional Science Initiative (SAFARI-2000) program provides the working context of this study. SAFARI-2000 aims to explore study and address linkages between land-atmosphere processes and the relationship between biogenic, anthropogenic emissions and the consequences of their deposition to the functioning of the biogeophysical and biogeochemical systems (SWAP *et al.*, 2001). The interdisciplinary nature of SAFARI allows an integrative data analyses approach. Through collaborative SAFARI research, fire study sites in South Africa were identified for *in situ* validation and refinement of fire information from the MODerate resolution Imaging Spectroradiometer (MODIS) using high-resolution satellite data and field data observations at representative validation sites. Biomass burning contributes significantly to global budgets of many atmospheric gases, the rising levels of which are implied with potential climate forcing factors and global change. Global satellite estimates of biomass burning with high accuracies are thus required to provide exact figures for gas fluxes derived from this source. Only satellite data combined with well-defined numeric models can provide these data.

**Summary Abstract.** Biomass burning in Southern African savannas has the potential to emit large amounts of trace gases and aerosols to the atmosphere. There are large uncertainties in methods that quantitatively measure sub-pixel fire effect, spatial explicit fuel biomass parameters, biomass consumption rates and combustion efficiencies rigorously and effectively over large physiological diverse savanna landscapes. Savannas in Southern Africa are characterized by a highly differential nature of fire behavior mainly due to fragmented land cover. This thesis will utilize the improved remote sensing capabilities provided by Earth Observing System (EOS) MODerate resolution Imaging Spectroradiometer (MODIS) and Landsat ETM+ to measure fire effects at the Skukuza-area in the Kruger National Park (KNP), South Africa. *In situ* aboveground fuel biomass data and fire spectral properties were collected at the KNP site and investigated to feed combustion completeness, sub-pixel area fractions burnt and fire severity models from contemporary 30-meter Landsat ETM+ data, using appropriate wavelengths. Implications are made for automated and effective fire scar monitoring techniques in multi-temporal MODIS data sets. Further, the study illustrates how spatial explicit Landsat ETM+ fuel biomass satellite calculations that account for the fuel type complexity in each pixel, combustion completeness and area burnt from contemporary MODIS overpasses as well as *in situ* emission factors can be used to accurately estimate gas

and particulate emissions for the KNP-area. This method is shown to reduce some uncertainties in local emission estimates. Finally the results show that MODIS and Landsat ETM+ spectral and spatial properties of fires can effectively be used to corroborate fire management policies in the KNP.

# TABLE OF CONTENTS

<b>PROLOGUE.....</b>	<b>I-II</b>
<b>ABSTRACT.....</b>	<b>III</b>
<b>TABLE OF CONTENTS.....</b>	<b>V</b>
<b>LIST OF FIGURES .....</b>	<b>IX</b>
<b>LIST OF TABLES .....</b>	<b>XV</b>
<b>LIST OF MAPS.....</b>	<b>XVI</b>

## SECTION 1: INTRODUCTION..... 1

1.1 DETERMINANTS OF FIRES IN SOUTHERN AFRICA.....	2
1.1.1 Regional fire patterns.....	2
1.1.2 Landscape and landform fire patterns.....	4
1.2 SCIENCE RATIONAL FOR REMOTE SENSING FIRE INFORMATION .....	5
1.2.1. Fire regimes as sources or sink.....	6
1.2.2. Atmospheric chemistry effects.....	6
1.2.3. Ecosystem effects .....	7
1.3 THE HERITAGE OF FIRE REMOTE SENSING .....	8
1.3.1 Past, current and future fire detection sensors.....	8
1.3.2 Current MODIS status .....	11
1.4 STUDY SITES .....	12
1.5 SATELLITE DATA CORRECTIONS .....	16
1.5.1 Landsat ETM+ calibration to reflectance.....	16
1.5.2 Landsat ETM+ atmospheric correction .....	17
1.6 OBJECTIVES AND STUDY OUTLINE.....	18
1.7 OVERVIEW OF MATERIALS USED AND METHODS .....	21
1.7.1 Field sampling .....	22
1.7.2 Statistical methods and satellite data.....	24
1.7.3 Satellite data.....	25

**SECTION 2: MAIN RESULTS..... 27**

**2.1 FUEL SAMPLING PROTOCOL FOR SOUTHERN AFRICA ..... 27**

2.1.1 BACKGROUND..... 27

2.1.2 SAMPLING STRATEGY ..... 28

    2.1.2.1 Site set up..... 28

    2.1.2.2 Description of site ..... 28

    2.1.2.3 Fuel sampling and tree cover density ..... 29

2.1.3 CALCULATIONS..... 31

    2.1.3.1 Tree cover density ..... 31

    2.1.3.2 Fuels..... 31

    2.1.3.3 Combustion completeness ..... 32

2.1.4 DISCUSSION ..... 32

    2.1.4.1 Error thresholds ..... 32

    2.1.4.2 General relevance ..... 33

2.1.5 APPLICATION OF THIS PROTOCOL TO THE SAFARI SITES ..... 34

2.1.6 PRACTICAL CONSIDERATIONS ..... 37

2.1.6 SUMMARY ..... 37

**2.2 CHARACTERIZING THE SURFACE HETEROGENEITY OF FIRE EFFECTS  
USING MULTI-TEMPORAL REFLECTIVE WAVELENGTH DATA ..... 39**

2.2.1 INTRODUCTION ..... 39

2.2.2 MODELING..... 41

2.2.3 STUDY AREA ..... 42

2.2.4 SATELLITE DATA ..... 44

2.2.5 FIELD MEASUREMENTS ..... 46

    2.2.5.1 Pre-fire field measurements ..... 46

    2.2.5.2 Post-fire measurements..... 47

2.2.6 REFLECTANCE SPECTRA RESULTS..... 48

2.2.7 ILLUSTRATIVE MODELING RESULTS ..... 49

2.2.8 COMPARISON OF LANDSAT ETM+ REFLECTANCE AND GROUND MEASUREMENTS ..... 56

2.2.9 CONCLUSIONS..... 61

2.2.10 SUMMARY..... 63

**2.3 ESTIMATING FIRE INTENSITY AND FIRE SEVERITY FROM REMOTE SENSING INFORMATION FOR EXPERIMENTAL FIRES IN THE KRUGER NATIONAL PARK (KNP) ..... 65**

2.3.1 INTRODUCTION..... 65

2.3.2 METHODOLOGY ..... 67

    2.3.2.1 Site description..... 67

    2.3.2.2 Field data collection..... 68

    2.3.2.3 Satellite data..... 70

    2.3.2.4 Theoretical Approach ..... 70

2.3.3 RESULTS ..... 74

    2.3.3.1 Fire intensity..... 74

    2.3.3.2 Fire severity mapping ..... 77

2.3.4 DISCUSSION AND CONCLUSION..... 80

2.3.5 SUMMARY..... 82

**2.4 IMPROVED FIRE EMISSIONS ESTIMATES FROM THE KRUGER NATIONAL PARK (KNP) USING SATELLITE DERIVED BIOMASS AND BURNED AREA DATA AND *IN SITU* AIRBORNE EMISSION FACTORS (EF) ..... 85**

2.4.1 INTRODUCTION..... 85

2.4.2 METHODS ..... 89

    2.4.2.1 Study area..... 89

    2.4.2.2 Fuel sampling ..... 91

    2.4.2.3 Satellite data..... 93

    2.4.2.4 Emissions modeling approach..... 94

2.4.3 RESULTS AND DISCUSSION ..... 98

    2.4.3.1 Predicting fuel mass and greenness ..... 98

    2.4.3.2 Satellite fire information..... 102

    2.4.3.3 Emissions estimates..... 104

2.4.4 CONCLUSION..... 109

2.4.5 SUMMARY..... 110

<b><u>2.5 THE RELEVANCE OF REMOTE SENSING BURNED AREA INFORMATION FOR FUTURE FIRE MANAGEMENT POLICIES IN THE KRUGER NATIONAL PARK (KNP)</u></b> .....	<b>113</b>
2.5.1 INTRODUCTION .....	113
2.5.2 BACKGROUND.....	115
2.5.2.1 Imaging characteristics and data description .....	115
2.5.2.2 Description of the KNP Integrated Fire Policy.....	118
2.5.3 TECHNICAL APPROACH .....	120
2.5.3.1 Spectral analyses of burnt areas .....	120
2.5.3.2 Spatial corrections .....	121
2.5.4 MAPPING THE FIRE-AFFECTED AREA.....	121
2.5.4.1 Spectral considerations in Landsat .....	121
2.5.4.2 Temporal considerations.....	124
2.5.4.3 Validating MODIS fire information.....	125
2.5.5 RELEVANCE OF RESULTS FOR FIRE KNP FIRE MANAGEMENT.....	126
2.5.5.1 Fire mapping .....	126
2.5.5.2 Fire regime monitoring .....	127
2.5.6 CONCLUSIONS AND RECOMMENDATIONS .....	129
2.5.7 SUMMARY.....	131
<b><u>SECTION 3: OVERALL DISCUSSION AND CONCLUSION</u></b> .....	<b>133</b>
3.1 CHARACTERIZING THE FIRE-AFFECTED AREA.....	133
3.2 VALIDATION IMPLICATION.....	134
3.3 LOCAL EMISSION ESTIMATES .....	135
3.4 THE UTILITY OF RESULTS FOR FIRE MANAGEMENT IN THE KNP.....	136
<b>4 REFERENCES .....</b>	<b>139</b>
<b>APPENDIX .....</b>	<b>157</b>
<b>ACKNOWLEDGEMENTS.....</b>	<b>159</b>

# LIST OF FIGURES

## SECTION 1: INTRODUCTION

**Figure 1** Physiological relationship between environmental factors, floristic, structural vegetation characteristics and fire frequency distributions & herbivory in Southern Africa ... 3

**Figure 2** A Catena profile for a slope typically found on granite and undulating areas in semi-arid savanna landforms. Dominant tree species are shown on corresponding soils. Broad-leaved sites on the scarp or crest slope (left in the diagram) produce more biomass fuels than fine-leaved savanna sites on the mid-slope (from SCHOLES, 1997). ..... 5

**Figure 3** Comparison of a fire-affected area in Landsat ETM+ imagery as a red, green blue (visible) band composite over the KNP uncorrected for atmospheric effect in (a) and the same area corrected for atmospheric effect in (b). No image enhancements were applied.... 18

**Figure 4** Summary methodology diagram showing field and laboratory study components and working steps as flow arrows or lines. Key issues addressed in each manuscript paper are shown as numbers: manuscript paper one [fuel sampling technique], manuscript paper two [CC= Combustion completeness], manuscript three [FS= Fire severity], manuscript four [KNP emission estimates], and manuscript paper five [relevance of fire information for KNP fire management policies]. The ASD (Analytical Spectral Devise) refers to spectral reflectance measurements recorded on fire-affected areas using a hand-held ASD radiometer..... 21

## SECTION 2: MAIN RESULTS

### 2.1 Fuel sampling protocol for Southern Africa

**Figure 5** Effective sampling design position showing the 15 sampling quadrats, the woody fuel transect and possible sequence to record disc meter heights..... 30

**Figure 6** The non-linear relationship (black line) using 95% confidence intervals (grey line) wood and grass phytomass (t/ha) and Landsat ETM+ tasseled cap brightness index data. The below 2 meter wood portion was calculated using allometry equations according to Netshiluvhi and Scholes (2001) and grass was accounted for by disc pasture meter heights. .... 34

**Figure 7:** The non-linear relationship using 95% confidence limits between field combustion completeness (CC) from phytomass measurements and Landsat ETM+ reflectance CC from ETM+ band 4 (0.78-0.9  $\mu\text{m}$ )..... 35

**Figure 8** The upper image from MODIS shows a wildfire that burned over a 12-day period in September 2000. The fire destroyed approximately 3065 km<sup>2</sup> in an area (rectangle) to the east of the Etosha National Park pan, Namibia. Based on methods presented in the protocol, the lower rectangle relating combustion completeness to tree cover and fuel loads has been produced (from Alleaume *et al*, 2002, *submitted*)..... 36

## 2.2 Characterizing the surface heterogeneity of fire effects using multi-temporal reflective wavelength data

**Figure 9** Reflectance spectra of black and white ash and non-photosynthetically active 'brown' vegetation fuel samples made using an ASD radiometer. The samples collected from the Kruger National Park (KNP) and the Madikwe Game Reserve (MGR), South Africa. .... 48

**Figure 10** Modeled reflectances for a hypothetical observation sensed over a fire-affected area with different combustion completeness and fraction of the observation area that burned. Reflectances modeled using the average of the KNP and MGR 'brown' fuel vegetation and black ash 1240nm ASD reflectance measurements ( $r_u = 0.325$  and  $r_b = 0.046$ ). .... 50

**Figure 11** Modeled reflectances for a hypothetical observation sensed over a fire-affected area with combustion completeness = 0.5 (top) and combustion completeness = 0.9 (bottom) plotted as a function of the fraction of the observation area that burned. Reflectances modeled at 1240nm (solid line) and 2130nm (dashed line) using the average of the KNP and MGR 'brown' fuel vegetation and black ash ASD reflectance measurements at these wavelengths (1240nm:  $r_u = 0.325$  and  $r_b = 0.046$ ; 2130nm:  $r_u = 0.242$  and  $r_b = 0.074$ ). .... 51

**Figure 12** Modeled spectral index values for a hypothetical observation sensed over a fire-affected area with combustion completeness = 0.5 (top) and combustion completeness = 0.9 (bottom) plotted as a function of the fraction of the observation area that burned. Spectral index values computed as  $(r_{1240nm} - r_{2130nm}) / (r_{1240nm} + r_{2130nm})$  using the reflectance data illustrated in Figure 3. .... 52

**Figure 13** Modeled absolute (left) and relative (right) change in reflectance for a hypothetical observation sensed over of fire-effected areas with different combustion completeness ( $cc$ ) and fractions of the observation area that burned ( $f$ ), illustrating a small and/or incomplete fire ( $f*cc = 0.25$ ) and a larger and/or more complete fire ( $f*cc = 0.5$ ). Reflectances modeled using the average of the KNP and MGR 'brown' fuel vegetation and black ash 1240nm ASD reflectance measurements ( $r_u = 0.325$  and  $r_b = 0.046$ ). The dashed

line shows modeled  $1\sigma$  errors computed assuming normally distributed 1240nm reflectance errors with a mean value of zero and  $1\sigma = 0.013$ . ..... 53

**Figure 14** Modeled absolute change (after - before fire) reflectance for a hypothetical observation sensed over a fire-affected area with different combustion completeness and fractions of the observation area that burned. Model results shown separately for the MGR 'brown' fuel vegetation and black ash 1240nm ASD reflectance measurements ( $r_u = 0.269$  and  $r_b = 0.047$ ) and the KNP 'brown' fuel vegetation and black ash 1240nm ASD reflectance measurements ( $r_u = 0.378$  and  $r_b = 0.046$ ). ..... 55

**Figure 15** Landsat ETM+ surface reflectance data acquired before prescribed fires (open circles) and after prescribed fires (closed circles) at 13 sites in the Kruger National Park (KNP) (top) and at 7 sites in the Madikwe Game Reserve (MGR) (bottom). The mean reflectance of the cloud-free 30m pixels falling within each 120m x 120m site are shown for Landsat bands 1 (450-515nm), 2 (525-605nm), 3 (630-690nm), 4 (750-900nm), 5 (1550-1750nm) and 7 (2090-2350nm). ..... 56

**Figure 16** Change in Landsat ETM+ band 4 surface reflectance data acquired before and after prescribed fires at 13 sites in the Kruger National Park (KNP) (top) and at 7 sites in the Madikwe Game Reserve (MGR) (bottom) plotted as a function of site-level estimates of combustion completeness. The change in reflectance for cloud-free 30m pixels falling within each 120m x 120m site (dots) with simple linear regression fits of these data (solid lines) and regression fits of the mean of the pixel values at each site (dashed lines,  $R^2$  in parentheses) are shown. .... 58

**Figure 17** Change in Landsat ETM+ band 4 surface reflectance data acquired before and after prescribed fires at 13 sites in the Kruger National Park (KNP) (top) and at 7 sites in the Madikwe Game Reserve (MGR) (bottom) plotted as a function of site-level estimates of the fraction of the site area that burned. .... 59

**Figure 18** Change in Landsat ETM+ band 4 surface reflectance data acquired before and after prescribed fires at 13 sites in the Kruger National Park (KNP) (top) and at 7 sites in the Madikwe Game Reserve (MGR) (bottom) plotted as a function of the product of estimates of the fraction of the site area that burned and the site-level combustion completeness. .... 60

### 2.3 Estimating fire intensity and fire severity from remote sensing information for experimental fires in the Kruger National Park (KNP)

**Figure 19** Shown are spectral ash reflective curves to simulate different percent white ash contents in 'greyish' ash and non-photosynthetic vegetation. The most bottom ash curve has nine percent white ash in it and is the reflection of the black ash as collected in the

field. The positions of narrow band Landsat ETM+ near-IR, short mid-IR (SMIR) and long mid-IR (LMIR) bands (and corresponding MODIS centre wavelengths) are marked with the grey vertical lines. .... 71

**Figure 20** Scatter diagram showing the abundance of grey ash (1-x) and concurrent black ash (1-x) on Experimental Burn Plots (EBP) in the southern KNP. The values represent relative abundances from 0 to 1 (1-x) of black and grey ash endmembers. .... 75

**Figure 21** Abundances of grey ash (1-x) in Landsat ETM+ data and Landsat ETM+ modelled pre fire fuel loads [g/m<sup>2</sup>] for the Kambeni Experimental Burn Plots (EBP). The pre fire image was acquired on the 12 June 2000 and used to derive the pre burn phytomass. .... 76

**Figure 22** Relationship between abundances of grey ash (1-x) from the linear unmixing and Landsat ETM+ combustion completeness (CC) per pixel ..... 77

**Figure 23** Relationship between residual non-photosynthetic (brown) phytomass abundances (1-x) from the linear unmixing and Landsat ETM+ combustion completeness (CC) per fire-affected pixel. .... 77

**Figure 24** The amplitude of fire severity and absolute reflection change (before fire – after) in Landsat ETM+ using the SMIR band. The hypothetical model shows ( $R^2=1$ ) a lesser sensitivity to the burn severity amplitude. The actual data ( $R^2=0.53$ ) is a non-linear function that is most determined by fire intensity than by the change in reflection in between two images. The same reflection change can exhibit different fire severity levels ..... 78

**Figure 25** The left images show the abundance output band of ‘grey’ ash from the linear unmixing result for Kambeni 5 and Kambeni respectively. The right column shows the fire severity as a product of the abundance of grey ash and combustion completeness. Evidently, Kambeni 5 exhibits brighter that is higher fire severity pixel values than Kambeni 7 (bottom). No image enhancements or stretching was applied..... 79

## 2.4 Improved fire emissions estimates from Kruger National Park (KNP) using satellite derived biomass and fire estimates and Airborne Emission Factor (EF) data

**Figure 26** The map shows Southern African states and the location of the two biomass sampling sites. The Kruger National Park (KNP) is located near the border to Mozambique and Madikwe Game Reserve (MGR) is situated on the western border of South Africa, 900 kilometres west from the KNP. .... 89

**Figure 27** Sampling design (120 by 120 meter) implied on prescribed burn plots. The settling height of grass was recorded every 6 m with a disc pasture meter (DPM) and also clipped in 50 cm quadrats every 30 m. Dry matter leaf litter and twig fall (=1.5 cm) was also collected in the quadrats, dried and weighted. Wood mass was sampled before and after the fire in three randomly selected 10-meter plots in the centre of the sampling frame using non-destructive measurement methods..... 92

**Figure 28** Aboveground grass and woody mass (=2 meter in height) including twig litter (gDM/m<sup>2</sup>) sampled on prescribed burn plots during 2000 and 2001 as a function of Landsat ETM+ Tasseled Cap (?) brightness. The regression was derived from field data sampled in several savanna types in the Kruger National Park and Madikwe Game Reserve. The regressions are shown with 95 % prediction intervals (widely defined as the bold, dashed line), the prediction intervals at 95% (narrow defined, dashed) for cloud-free 30m pixel averages pertaining to each 120m x 120m site (dots) and with non-linear and linear regression fits of these data (solid lines)..... 99

**Figure 29** Recommended two-way approach that can be used to predict litter [gDM/m<sup>2</sup>] (grass and leaf litter). The site measured tree cover density [%] is significantly linearly related to Landsat ETM+; the tree cover density [%] can be used to predict the litter amount [gDM/m<sup>2</sup>] using the above non-linear regression. The regressions are shown with 95 % prediction intervals (widely, dashed line), the prediction intervals at 95% (narrow defined, dashed). ..... 100

**Figure 30** Percent [%] greenness from field observations on fractional land cover components and corresponding NDVI from Landsat ETM+. The regressions are shown with 95 % prediction intervals, the confidence intervals at 95% and with a non-linear regression fit of data points (solid lines)..... 101

**Figure 31** Regression equation showing 250-meter resolution MODIS CC using the near-IR channel (841-876 nm) fire information as a function of the same information from co-located 30-meter resolution data from fires in the KNP. The regression shows that CC can be continuously and accurately (R<sup>2</sup>=0.87) estimated with daily MODIS fire information using the near-IR band. .... 103

**Figure 32** Cumulative CO emissions (kg) for the 30-day satellite observation period in September 2001 ..... 108

**Figure 33** Cumulative NO<sub>x</sub> emissions (kg) for the 30-day satellite observation period in September 2001 ..... 108

**Figure 34** Cumulative CH<sub>3</sub>COOH emissions (kg) for the 30-day satellite observation period in September 2001 ..... 109

**Figure 35** Cumulative CH<sub>4</sub> emissions (kg) for the 30-day satellite observation period in September 2001 .....109

2.5 The relevance of remote sensing burned area information for future fire management policies in the Kruger National Park (KNP)

**Figure 36** Simulated reflectance spectra of ASD derived ash reflectance, fire scar spectra and biomass reflectance spectra (solid lines). The non-photosynthetic biomass and ash spectra were derived from laboratory measurements using an ASD radiometer (grey and black line). The one week old fire scar reflectance spectra was derived using hand held field ASD radiometer measurement (averages) on one week old burn scars in the KNP (dark grey solid line with points). The photosynthetic biomass reflectance spectra was derived from the USGS spectral library (grey line with points). The simulated reflectance (y-axis) is shown as a function of the resampled Landsat ETM+ wavebands from 0.47 μm to 2.2 μm. The fire scar sensitive central wavebands are marked with vertical dotted lines..

.....122

**Figure 37** Temporal compositing of fire affected pixels using Landsat ETM+ bands 3 (0.66μm) to 7 (2.2μm). The exact burn day was gathered from field fire protocols made during the SAFARI 2000 intensive field campaign. The Landsat acquisition dates were: 15 August 2000, 31 August 2000 and the 18 October 2000.....124

**Figure 38** Regression equation between MODIS fire scar size (km<sup>2</sup>) and collocated Landsat ETM+ fire size for an observation period in September 2001. Only fires smaller than < 4 km<sup>2</sup> are shown with confidence limits at 95% depicted as dotted lines. The regression is shown as a solid line (R<sup>2</sup>=0.98; P<0.001) and shows that fires ≤ 2 km<sup>2</sup> are hardly detected with 500m MODIS data. These areas are shown as data points on the x-axis, at y=0. ....126

**Figure 39** Fire remote sensing and its means to achieve fire management objectives. The positions of Landsat ETM+, MODIS and ASTER are shown (as ellipse circles) with regard to their spatial, spectral and temporal revisit cycles. The level and value of fire information increases considerable more with the temporal revisit cycle of a satellite. The cost arrow implies the lower costs of Landsat ETM+ or ASTER satellite data as compared with hyperspectral (very narrow bandwidth) airborne remote sensing data.....130

## LIST OF TABLES

### SECTION 1: INTRODUCTION

<b>Table 1</b> Examples of current and planned remote sensing systems with fire monitoring capabilities.....	10
<b>Table 2</b> Self-calibrated and literature regression equations used to gain a spatial estimate with the disc pasture meter (DPM) for the KNP and Madikwe sampling sites. ....	22
<b>Table 3</b> Allometry reports for common woody biomass species, parameters required, regression equations and regression squared multiples ( $R^2$ ).....	23
<b>Table 4</b> Summary table showing MODIS and Landsat ETM+ satellite data acquisitions (date) for the study period. ....	26

### SECTION 2: MAIN RESULTS

#### 2.2 Characterizing the surface heterogeneity of fire effects using multi-temporal reflective wavelength data

<b>Table 5</b> Dates of prescribed fires lit at the Madikwe Game Reserve and Kruger National Park, Landsat ETM+ data characteristics, and AERONET aerosol optical thickness (AOT), water volume and air mass measurements made at Skukuza, Kruger National Park (* = AERONET data linearly interpolated from June 12 <sup>th</sup> measurements made 6:55 GMT and 12:55 GMT to 7:40 GMT) .....	45
--	----

#### 2.4 Improved fire emissions estimates from Kruger National Park (KNP) using satellite derived biomass and fire estimates and Airborne Emission Factor (EF) data

<b>Table 6</b> Field sampling and characterization sites descriptions.....	90
<b>Table 7</b> Initial emission ratios (ER) and emission factors (EF, g/kg) for fires investigated by the AFTIR on the University of Washington's (UW) Convair-580 aircraft covering a transect of ~100 km in the KNP area during the SAFARI 2000 intensive research campaign. ....	96
<b>Table 8</b> Range (minimum and maximum), variations ( $1\sigma$ ) and percent differences of emissions derived by using the AFTIR measurements and Landsat ETM+ fuel modeled estimates. ....	105
<b>Table 9</b> Total emission estimates [t] and emissions per unit surface area [ $g/m^2$ ] for September 2001 over the Kruger National Park (KNP), covering an area of 8020km <sup>2</sup> . As a	

comparison cumulative emissions [t] are shown for all fires proceeding the observation period from June to August 2001. .... 107

## 2.5 The relevance of remote sensing burned area information for future fire management policies in the Kruger National Park (KNP)

**Table 10** Spectral, spatial and temporal characteristics as well as practical considerations compared for Landsat ETM+ and MODIS satellite data. The Visible bands are assigned to the visible color sequence (Red, Green and Blue)..... 117

## **APPENDIX**

**Table 11** Example of a biomass sampling protocol measured before a prescribed burn on a late winter annual site in the Kruger National Park..... 157

**Table 12** Examples of field parameters measured on prescribed burn sites in the KNP and Madikwe during the SAFARI-2000 campaign (R= biomass according to RUTHERFORD; S= biomass according to NETSHILUVHI & SCHOLES; CC\_S= combustion completeness using wood mass according to NETSHILUVHI & SCHOLES (2001). .... 158

## **LIST OF MAPS**

### **SECTION 1: INTRODUCTION**

**Map 1** Study sites on 1 kilometre resolution NOAA/AVHRR composite map also showing positions and location of the Landsat ETM+ imagery acquisitions used in this study. The location of the KNP (A) and Madikwe Game Reserve (B) is superimposed in beige. The Unmfolozi/Hluhluwe site is shown as a point C ..... 12

**Map 2** Underlying bedrock – soils..... 14

**Map 3** KNP Vegetation Types (derived from GERTENBACH, 1983)..... 15

### **SECTION 2: RESULTS**

## 2.5 The relevance of remote sensing burned area information for future fire management policies in the Kruger National Park (KNP)

**Map 4** Proposed Fire Management Units in the KNP and Pristine Wilderness Areas ..... 119

## **Section 1: Introduction**

Recent global satellite analyses of biomass burning have shown that the largest number of detected fires was found in Africa (DYWER *et al.*, 2000). African biomass burning accounts for about 35% of the global total (LOBERT *et al.*, 1999). In particular Southern Africa is subjected to some of the most extensive biomass burning in the world (CRUTZEN AND ANDREAE, 1990).

Biomass burning emits a large variety of gaseous and particulate compounds with significance to atmospheric and biogeochemical cycles. Satellite fire mapping methods that accurately and automatically characterize the sub-pixel area burnt and vegetation fuel consumption rates over coherent larger areas is still constrained (BARBOSA *et al.*, 1999a; SCHOLLES AND ANDREAE, 2000a). The extent of biomass burning and regional fire emissions is essential for understanding and predicting environmental impacts.

Fires in Southern Africa occur mainly due to natural causes (such as caused by lightning) and anthropogenic causes, primarily due to arson or land management. People have always exercised significant control over fire regimes in Southern Africa since at least the Holocene (ROY *et al.*, 2002a; BOND, 1997a). Fire properties are characterized by the aboveground fuel biomass (available for burning), the timing of burning and burning severity which is largely controlled by the anthropogenic and micro-meteorological fire conditions.

In the Kruger National Park (KNP) on the north-eastern border of South Africa fire has always been an important management factor since 1912. Currently managers in the Kruger National Park are in the process of building one of the most comprehensive fire records for any ecosystem anywhere in the world (VAN WILGEN *et al.*, 2002). KNP fire management is increasingly geared towards ecosystem management with an integrated approach that considers arson fires alongside with lightning and management fires (BIGGS, 2002).

Fire activity results in two primary signatures that can be detected via remote sensing. Active fires are detectable because high temperature sources emit a strong radiative signature in the visible and infrared regions of the electromagnetic spectrum. The second fire signature is that of the burn scar left by the passage of the fire, much darker in the visible and near infrared wavelengths than the surrounding still-vegetated areas because of the removal of vegetation and the layer of ash resulting from the burning. Fire properties information on the distribution of active fires, fire scar heterogeneity and aerial extent can be provided from the daily orbiting

MODerate resolution Imaging Spectroradiometer (MODIS) onboard the Terra satellite platform (KAUFMAN *et al.*, 1998a; JUSTICE AND KORONTZI, 2000a; JUSTICE *et al.*, 2002a). Terra, the flagship platform of NASA's Earth Observing System (EOS), was launched in February 2000 and has since begun collecting what will ultimately become part of a new 18 year data set cycle (KAUFMAN *et al.*, 1998b). The 500-meter resolution reflective bands are explicitly designed to include fire characteristics that will provide unique capability over existing satellite sensors in terms of active fire monitoring (KAUFMAN AND JUSTICE, 1998a; JUSTICE *et al.*, 2002b). Daytime and nighttime active fire information will be provided accurately in the near term (JUSTICE *et al.*, 2002c) in selected spatial summaries and temporal composites. Burn scar information is important for many users, such as emission scientists and resource managers interested in the extent of burning over time and space. MODIS also offers good spatial (at 250-meter resolution in some visible bands) and radiometric capabilities for burn scar detection (KAUFMAN AND JUSTICE, 1998b). An extensive MODIS burn scar product field validation campaign for representative sites over Southern Africa is currently underway. The Skukuza site in the KNP is used to collect field and higher-resolution satellite data to validate automated well-defined time-series MODIS burn scar information. Many of the MODIS land products are currently still being refined (ROY *et al.*, 2002b).

## 1.1 Determinants of fires in Southern Africa

### 1.1.1 Regional fire patterns

The main determinant of fire within a particular vegetation type is the availability of biomass fuel in net production mass, fuel packaging and attributes. Plant materials consisting of small particles sizes with a large area to volume ratio (such as fine and thin fuels) are most flammable (Luke and McArthur, 1978), because they lose water more rapidly and have a high ratio of fuel to air. Leaves with highly flammable oil and waxes contents are not profound in South African savannas (except Mopane shrubland savannas that constitute a small section of the central KNP). Apart from chemical or morphological biomass fuel properties, the quality of fuels that determines flammability is dependant on the fibre and moisture content of individual fuels (BOND, 1997b). The fuel accumulation and net production is largely determined by the climate (rainfall) and soil attributes such as the percent sand contents and the rain use efficiency (RUE) (kg/ha/mm).

Climate is a second most important fire determinant. Annual precipitation rates can be used to

calculate the annual primary production rates of grass, wood, fractional annual wood increment, and leaf and twig production in semi-arid savannas (SCHOLES AND LANDMANN, forthcoming). The rainfall amount, relative humidity and temperature affects the moisture content of fuels and hence ignition potential. The strongly seasonal water availability in Southern African savannas leads to the accumulation of fine and dry easily-ignited fuels during the dry season, and fire frequencies range from every year in moist savannas to once every ten or more years in arid savannas (SCHOLES, 1997a).

Figure 1 summarizes the main structural and floristic savanna types and the prevalence of available soil nutrients, precipitation that determine fire frequencies and distributions on a regional level in Southern Africa. Figure 1 also shows the close relationship between soil properties and savanna species level composition. The relationship between the herbaceous layer primary productions is linearly correlated to the annual rainfall up to about 900mm per annum. In arid areas with average precipitations  $\approx 550 \text{ mm yr}^{-1}$  and erratic rainfall, fires are limited to the high rainfall years when grass fuels are sufficient to carry a fire. In mesic savanna sites, fire frequencies are more limited by the ignition events than by biomass fuel loads (BOND, 1997c).

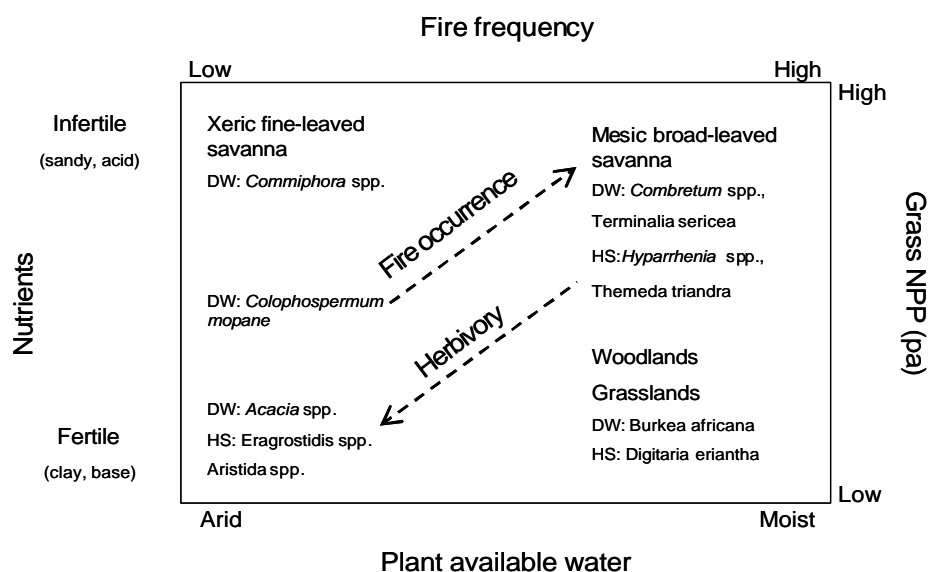


**Figure 1:** Physiological relationship between environmental factors, floristic, structural vegetation characteristics and fire frequency distributions and herbivory in Southern Africa.

Herbivory pressures especially from ‘megaherbivores’ such as elephants, reduce the fuel load through grazing and browsing (FROST, 1999). Areas with abundant palatable grasses are mostly found on clay (based) soils and are hence particularly prone to high grazing pressures

(Figure 1). Figure 1 does not consider fuel biomass decay over longer periods and fuel accumulations as these factors are primarily closely related to the precipitation variability.

### 1.1.2 Landscape and landform fire patterns

The KNP ecosystem is a function of climate, soil, vegetation and animals that forms an interacting unit. At a scale of several hundred meters or kilometres there is a spatial organisation of trees and herbaceous layers from the ridge crest to the valley plains. This vegetation pattern known as Catena is typical in semi-arid savanna landscapes supported by granite parent material (*e.g.* parts of the KNP). The transport of fine soil particles and ions from ridge crests to the valleys under the influence of water movement and gravity establishes a toposequence of soils and associated vegetation (shown in Figure 2) (MILNE, 1936; SCHOLES 1997b).

Different expositions of the slope from the crest through the mid slope, to the toe slope until the valley is reached (sodic site and riparian fringe site) support different savanna communities and tree cover density distributions; fine-leaved savanna types are found on clay soil valley bottoms, while broad-leaved trees are usually supported by the sandy soil sites, such as the crest or scarps. The tree and grass ratio is further determined by the nutrient distribution, shading of trees, water seepage along the slope (SCHOLES, 1997c) as well as soil respiration (PRASAD *et al.*, 2002). The site specific spatial organisation of soil nutrients and other factors of savanna heterogeneity along the slope in Figure 2 are primarily related to the amount of primary production of biomass fuels available for burning. The larger tree canopy cover in broadleaved savannas may result in increased leaf and wood (bark and debris) litter fall resulting in larger biomass fuels amounts to accumulate. Fuel moisture in foliage, wood or grass biomass determines flammability. Increased fuel moisture may be prevalent in seepage grasslands and riparian fringe vegetation causing lower flammability in these fuels.

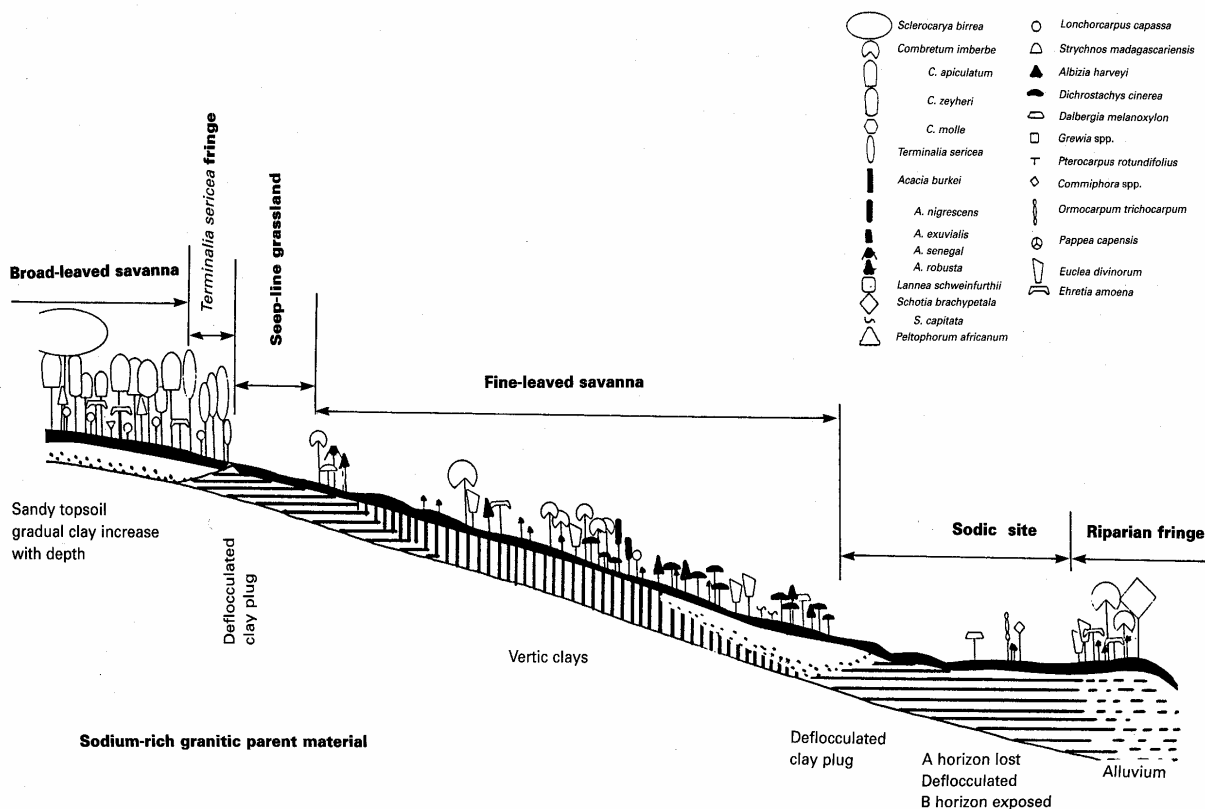


**Figure 2:** A Catena profile for a slope typically found on granite and undulating areas in semi-arid savanna landforms. Dominant tree species are shown on corresponding soils. Broad-leaved sites on the scarp or crest slope (left in the diagram) produce more biomass fuels than fine-leaved savanna sites on the mid-slope (from SCHOLES, 1997).

Monitoring the determinants of fires such as the *before fire* status of fuel types continuously and on a landscape scale is mandatory in methods that aim to characterize the area burnt, combustion efficiency and hence emissions (LEVINE, 1996a). There is currently little progress done in standard primary production models that quantify and stratify the above ground fuels into separate components or entities with different fuel biomass properties (SCHOLES AND LANDMANN, forthcoming).

## 1.2 Science rational for remote sensing fire information

MODIS fire information can provide important input into monitoring the location and timely extent of biomass burning and the fire effects on the ecosystem, atmosphere and the climatic cycles. The need for fire information is articulated by programs such as the International Geosphere-Biosphere Program on behalf of the scientific community to the Committee on

Earth Observing Systems (CEOS) and by the fire component of the Global Observation of Forest Cover (GOFC) initiative (JUSTICE *et al.*, 1999a). Explicitly fire information on severity and combustion completeness over phenological diverse landscape with known detection accuracies is increasingly required by research programs (JUSTICE *et al.*, 1999b; JUSTICE AND KORONTZI, 2000b). The Intergovernmental Panel on Climate Change (IPCC) for instance requires research programs to provide technical and scientific sound information of human-induced climate change in relation to greenhouse gas emission inventory studies, potential impacts of climate change and options for adaptations and mitigation (BRAATZ *et al.*, 1995). Wildfire emissions inventory information is needed for each country to assess the mitigation options.

### 1.2.1 Fire regimes as sources or sink

Each vegetation system has a fire regime that controls the fire severity, fire type, the fire return sequence and ultimately the variety of greenhouse gases releases into the atmosphere. The fire severity determines the part of the available biomass that is combusted, this in turn being controlled by the fire behavior and the vegetation state that is fuel mass, fuel moisture content and fuel compaction (TROLLOPE AND TANTON, 1986a). Under different climate change scenarios, i.e. increased temperatures and drought frequencies, the physical state of the vegetation and thus the fire severity and frequency may change. The fire regime is also changed through management practices for instance to exclude fire from savanna systems for several years. This could prompt savanna systems to become net uptake greenhouse gas sinks, since less frequented fire favor the woody savanna component and biomass fuels are allowed to accumulate (TROLLOPE, 1992). If savanna vegetation is allowed to regrow after annual fire cycles, the CO<sub>2</sub> emissions are neutral. All other gas emissions are net emissions. Presently there is great uncertainty in the magnitude of such sources and sinks of fire greenhouse gases (KAUFMAN AND JUSTICE, 1998c). Satellite remote sensing fire information coupled with vegetation carbon storage information over larger areas has the potential to give some information as to the carbon sources or sink potentials in local fire regimes (MICHALEK *et al.*, 2000).

### 1.2.2. Atmospheric chemistry effects

At regional and local scales MODIS information on the area burnt and active fire energy emissions can feed trace gas and emissions studies and help to analyze the knock on effects of these on the atmospheric composition and chemistry (JUSTICE AND KORONTZI, 2000c;

SCHOLES *et al.*, 1996a; LEVINE, 1996b; CRUTZEN AND ANDREAE, 1990b). Study estimates have shown that annual biomass burning may be directly associated with 38% of the ozone in the troposphere, 32% of the global carbon monoxide; more than 20% of the world's hydrogen, nonmethane hydrocarbons, methyl chloride and oxides of nitrogen; and approximately 39% of the particulate organic carbon (LEVINE, 1996c; KAUFMAN AND JUSTICE, 1998d). However there are notable differences in emission estimates. CO<sub>2</sub> emissions estimates vary by the factor of 2.6 between BARBOSA *et al.* (1999b) and HAO *et al.* (1990a) and there is a 5-fold difference between SCHOLES *et al.* (1996b) and HAO *et al.* (1990b), mostly derived from burned area estimates at one to five km resolutions. The reporting of long-term, accurate and validated emissions data sets with satellite data is increasingly becoming important to research programs.

It is recognized that chemical reactions of gases, gas depositions and organic and graphitic carbon reactions with solar radiation and cloud formation effects may also occur downwind of fires and/or quantified in models. These 'offset' fire implications are not discussed here.

### 1.2.3. Ecosystem effects

Fire has several indirect or direct effects on ecosystems. Firstly, after fire cessation, the decreased surface albedo and increasing solar radiation reaching the soil layer can increase the amount of absorbed energy, thereby increasing the surface soil temperature. Changes in the biological activity in soils due to biomass burning (and the resultant soil temperature increase) may impact the CO<sub>2</sub> budget on a local scale and CO<sub>2</sub> releases through soil respiration on a burnt area are thus elevated (SCHOLES AND ANDREAE, 2000b).

Secondly the removal of vegetation due to fire results in increased surface run-off and reduces plant evapo-transpiration. This may lead to increased surface run-off and soil erosion in fire subsequent precipitation and river sedimentation, especially in tropical and subtropical areas. The lower rates of evapo-transpiration result in lower moisture amounts being transported back to the atmosphere and may decrease precipitation rates (KAUFMAN AND JUSTICE, 1998e). On a regional scale areas that are affected by frequent and high intense fires may cause 'top kill' in woody species and hence favor the grass savanna component (TROLLOPE AND TANTON, 1986ba). Grass savannas generally have lower evapotranspiration rates than woody savannas, especially over several decades (see also 1.2.1).

## 1.3 The heritage of fire remote sensing

### 1.3.1 Past, current and future fire detection sensors

The remote sensing of active fires and fire scar mapping has a long heritage. Coarse orbiting satellite data on the detection of active fires on global and continental scales in the thermal and middle infrared (mid-IR) regions of the electromagnetic spectrum has primarily been acquired by the National Oceanic and Atmospheric Administration (NOAA) Advanced Along Track Scanning Radiometer (AVHRR) (MATSON AND DOZIER, 1981; MUIRHEAD AND CRACKNELL, 1984; GIGLIO *et al.*, 1999; KAUFMAN *et al.*, 1998c), the European Space Agency (ESA) Along Track Scanning Radiometer (ATSR) and from the National Aeronautics and Space Administration (NASA) MODerate resolution Imaging Spectroradiometer (MODIS) instrument. The Defense Mapping Satellite Program (DMSP) is a polar orbiting meteorological sensor that currently provides important night time visible (0.4-1.1  $\mu\text{m}$ ) (in a low light mode in the visible operated routinely at night) and infrared (8-13  $\mu\text{m}$ ) spectral capabilities at coarse resolution (Table 1). Due to its sensitivity to light sources it is particularly useful to identify fires in remote areas of Africa where few city light are visible (CAHOON *et al.*, 1992). Recent work has also shown the potential of Geostationary Operational Environmental Satellite (GOES) meteorological satellites to monitor biomass burning such using the on board Visible Infrared Spin Scan Radiometer and Atmospheric Sounder (VAS). The VAS utilizes the visible regions, the shortwave infrared (SWIR) as well as the longwave infrared (TIR) to detect active fires currently in North and South America, taking a snapshot every 0.5 hours (Table 1). Active fire monitoring has made considerable progress and is due to be implemented as operational products (STROPPIANA *et al.*, 2000b, JUSTICE AND KORNOTZI, 2000d). However, active fire data sets may not provide reliable information on the extent and timing of burning as clouds may preclude hotspot detection and because the satellite may not overpass when burning occurs (JUSTICE *et al.*, 2002d)

Burned area satellite monitoring is less automated (FLASSE *et al.*, 2002), yet the fire-affected area shows a time persistency and hence received considerable attention has been given to regional and continental burned area mapping methods (ROY *et al.* 2003, forthcoming). There is considerable heritage to map burn scars with time series composite AVHRR data mostly using vegetation indices (FREDERICKSEN *et al.*, 1990; KASISCHKE AND FRENCH, 1995; BARBOSA *et al.*, 1999c). The considerable decrease in the vegetation index after fire (magnitude of change) is mostly empirically defined. These burn scar detection efforts have mainly concentrated on a defined temporal window, fail to account for variations in the signal

variation over time as a function of sun-target-sensor geometries (ROY *et al.*, 2002c) and are not rigorously validated with independent *in situ* data sets. Validated time-series (multi-temporal) burned area data sets using 500-meter resolution MODIS and 1 km ATSR data over larger regions will be available in the near-term (ROY *et al.*, 1999, ROY *et al.*, 2002d; ARINO AND ROSAZ, 1999). Current and planned fire remote sensing sensors and their spectral and spatial domain, organised according to burn scar and active fire capabilities, are summarized in Table 1.

There is a need to render operational burn scar monitoring with these sensors, assess how the different fire information can be augmented to contribution to operational fire scar monitoring and deliver fire information products that are extensively validated. The fire products could be combined with *in-situ* data sets on combustion completeness, modelled fuel information and locally determined fire emission factors that input emission estimates (JUSTICE AND KORONTZI, 2000d).

Current sensors	Spatial resolution	Temporal resolution	Waveband regions	Swath width (km)
<b>Active fire</b>				
NOAA/AVHRR <sup>a</sup>	1100m	< 1 day	5 bands: red, NIR, MIR, 2xTIR	2700
MODIS	1000m	< 1 day	36 bands [visible to infrared]	2330
GOES/VAS	900m 6.9km to 13.8km 13.8km	30 mins	12 bands: visible to infrared, water vapour, CO <sub>2</sub> , H <sub>2</sub> O, N <sub>2</sub> O	North and South America
DMSP/OLS	550-2700m	= 1 day (night time)	blue, green and red channel, infrared (2 <sup>nd</sup> channel)	3000
TRMM	4300m	< 1 day	5 bands: green, red, NIR, MIR, 2 xTIR	750
ATSR	1000m	35 day	4 bands: MIR, 3xTIR	555
METEOSAT	2.4-5km	30 mins	Visible, infrared, water vapor 12 bands	3000
<b>Burned area</b>				
MODIS	250m 500m 1000m	< 1 day	36 bands [visible to infrared]	2330
NOAA/AVHRR <sup>a</sup>	1100m	< 1 day	5 bands: red, NIR, MIR, 2xTIR	2700
Envisat <sup>e</sup>	30-1000	1-35 days	~22 bands [visible to infrared] and radar	100-1250
SeaWiFS	1100m	1 day	8 bands: blue, green, red	1502
ATSR2	1000m	35 day	7 bands: green, red, NIR, MIR, 2xTIR	555
SPOT-Vegetation	1150m	26 days	4 bands: blue, red, NIR & SMIR	2250
Landsat <sup>b</sup>	30m, 60-120m 15m	16 days	7 bands: blue, green, red, NIR, SMIR, LMIR & TIR Panchromatic: 1 band: visible/NIR	175 by 180
ASTER <sup>c</sup>	15-90m	1 day	14 bands: green, red, NIR, MIR, TIR	60
SPOT	10m 20m	26 days or less	green, red, NIR & SMIR Panchromatic	60
IRS	23m 5.8m	24 days	green, red, NIR, SWIR Panchromatic/visible	70-810
ERS/SAR	12.5-30m	26 days	Radar	Variable
IKONOS	4m	2.9-1.5 days	blue, green, red, VNIR Panchromatic: visible	11
	1m			
<b>Planned</b>				
NPP VIIRS	active fire and burned area			
Vegetation Canopy Lidar	vegetation entities and aboveground biomass			
EO-1	hyperspectral resolution data			
AATSR <sup>d</sup>	fires and burn scar			
Others:	Fuego, InSAR, Global Imager (GLI), DLR-BIRD, Radarsat-2, ALOS			

<sup>a</sup> 10.5-11.5 $\mu$ m for NOAA-6, -8, -10; 11.5- 12.5 $\mu$ m not on NOAA-6, -8, -10

<sup>b</sup> Landsat-7 specifications

<sup>c</sup> pointer instrument (back and nadir view) on the EOS-Terra platform

<sup>e</sup> Envisat: successor to the ERS programme

<sup>d</sup> successor of ATSR

**Table 1:** Examples of current and planned remote sensing systems with fire monitoring capabilities.

### 1.3.2 Current MODIS status

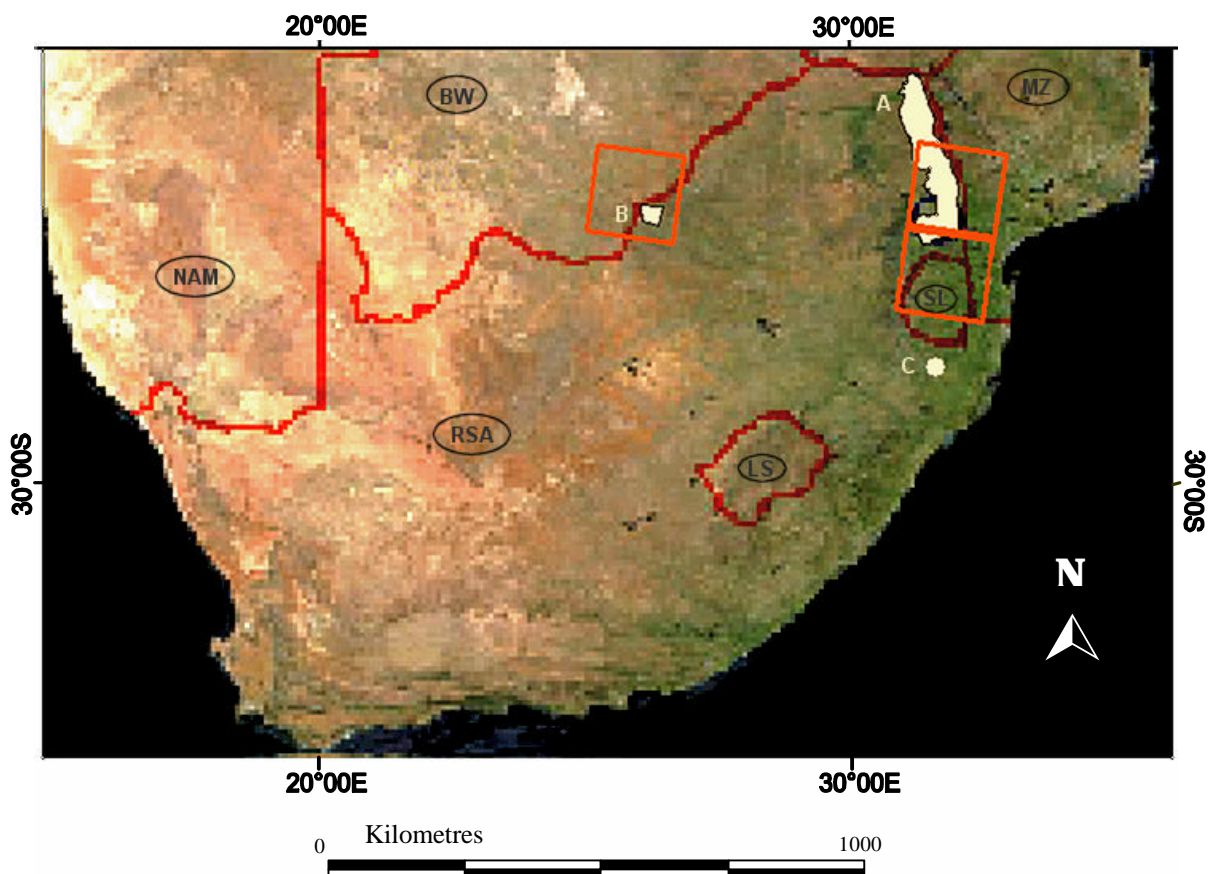
MODIS provides good band-to-band registration (0.1 of a pixel), improved scene to scene registration and good locational accuracies. The  $11\mu\text{m}$  and  $4\mu\text{m}$  (1 km) fire channels saturate at 400 degrees Kelvin and are increasing sensitive to the magnitude of fire energy. The  $0.86\mu\text{m}$  centred band at 250 meter resolution, the  $2.1\mu\text{m}$  and the  $1.6\mu\text{m}$  centred 500 meter resolution reflective bands provide good burn scar detection capabilities. With the launch of the second Earth Observation System (EOS) Aqua (former Terra-pm) satellite platform in 2001, MODIS detection is possible for all global areas above 30 degrees latitude at four times daily (BARNES *et al.*, 1998a).

MODIS surface reflection data tiles captured during the SAFARI 2000 intensive campaign in 2000 were not comprehensively corrected for atmospheric contamination and contained calibration artefacts. MODIS data up to November 2000 is currently mostly available as a beta-version. The data sets are presently being refined and corrected from the beta-versions to a scientific usable and validated higher-order quality level (preliminary or validated maturity level code). The active fire detection algorithm is up to date under-performing (JUSTICE *et al.*, 2002e) and the cloud mask algorithm is known to be falsely labelling some fires and desert regions as clouds (ACKERMAN *et al.*, 1998). Preliminary version MODIS land product tiles were available for the 2001 period. The preliminary maturity level data is usable for scientific work. Additional final consent for the scientific use of preliminary data, however, should be given by the MODIS Land discipline leader. Only cloud free MODIS data tiles captured during the 2001 burning season that were also determined from visible quality assessments to be good quality were used in this study.

The placements of the reflective MODIS bands (bands 1-7) are derived so as to correspond to the Landsat Enhanced Thematic Mapper (ETM+) and Landsat Thematic Mapper (TM) instruments (see Table 1, page 141 gives a complete overview of MODIS and Landsat ETM+ spectral and spatial configurations). MODIS also acquires data in the same orbit as Landsat (BARNES *et al.*, 1998b). Due to the mentioned MODIS quality constraints and the availability of higher-resolution Landsat ETM+ data sets over the Skukuza and other fire sites in South Africa, mostly Landsat ETM+ data is used in this study to achieve the objectives listed below.

## 1.4 Study sites

Time-series composite NOAA/AVHRR 1 kilometre resolution data from Southern Africa is used as a baseline image in Map 1 (below) to display the sampling sites and the location/positions of the Landsat ETM+ acquisitions used in this study. The KNP Skukuza site is the main area of investigation (denoted as A in Map 1). The other sampling sites (from Map 1) in the Madikwe Game Reserve (750 km<sup>2</sup>), denoted as B, and the Umfolozi/Hluhluwe Game Reserve, denoted as C, were supplementary included in the study to create statistically coherent fuel biomass and fire data sets over a variety of savanna types in South Africa. Field data from Madikwe (B) was particularly useful since all corresponding Landsat ETM+ satellite data was consistently cloud free.



**Map 1:** Study sites on 1 kilometre resolution NOAA/AVHRR composite map also showing positions and location of the Landsat ETM+ imagery acquisitions used in this study. The location of the KNP (A) and Madikwe Game Reserve (B) is superimposed in beige. The Umfolozi/Hluhluwe site is shown as a point C.

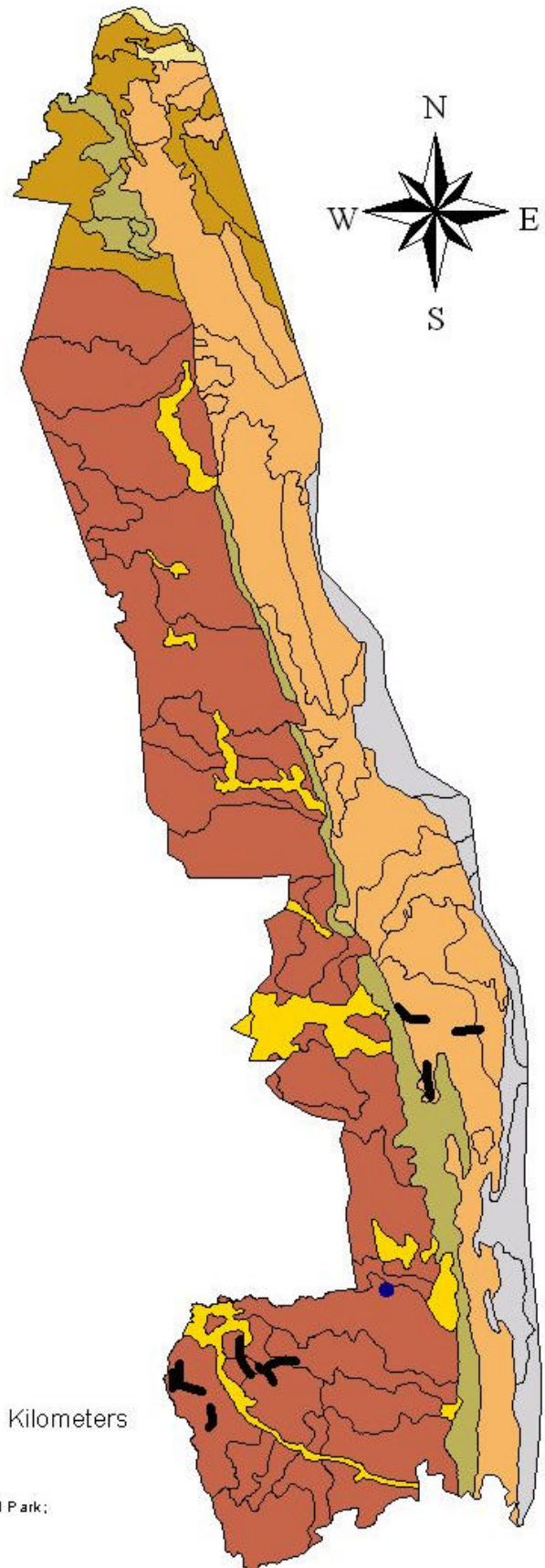
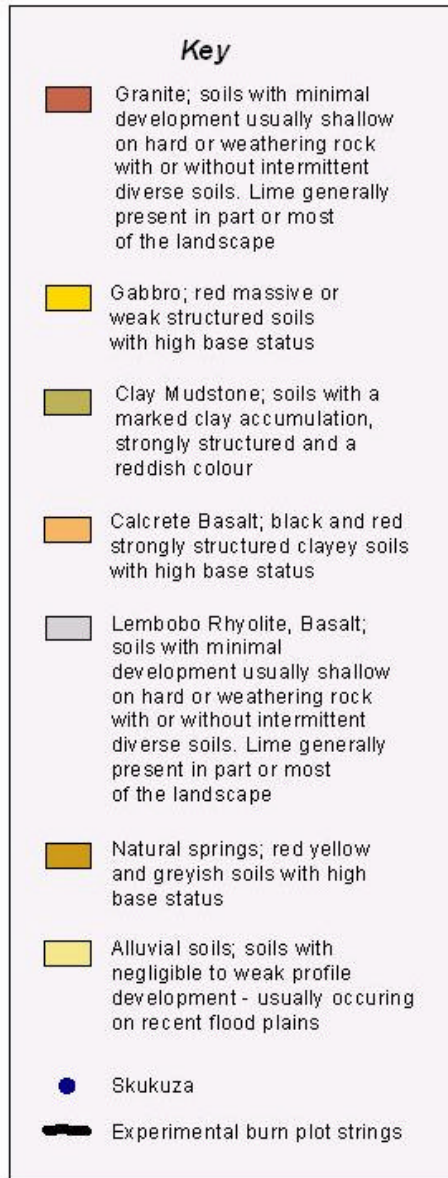
The Kruger National Park (KNP) study site is a primary natural ecosystem with an established natural fire and biogeochemical cycle system. The underlying regional and landscape features that determine fire regimes in the KNP are illustrated in Figure 1 and 2. The KNP landscape has a spatial and temporal dimension. Map 2 below shows the spatial distribution of the major soil types from underlying bed rock in the KNP. The soil map is shown since soil fertility largely determines the succession of biomass fuel entities and herbivore grazing in the KNP. Infertile soils are usually found on granite base rock that mostly consists of light element silicon and aluminium. Soils on basic indigenous rocks produce fertile clay soils, usually found in the centre and northern part of the KNP (BARTON *et al.*, 1986) or on the toe and valley area of the Catena (Figure 2). Climate is the second most important factor determining the ecological potential. Rainfall patterns determine the net primary production of grass and wood (Figure 1). Moreover the Rain Use Efficiency (RUE) of grass determines ecosystem vegetation, which is also dependant on the prevalence of the tree (wood) component in savannas as well as the clay and sandy particle contents in established soils (SCHOLES AND LANDMANN, forthcoming). The Skukuza climate region is in the Lowveld Bushveld region, which receives moderate summer precipitation (500-700mm per annum). Over the past 90 years up to 2001 the average rainfall (monthly and seasonal) stayed fairly constant (KRUGER *et al.*, 2002).

Map 3 shows the KNP vegetation types according to dominant tree species derived from GERTENBACH (1983a). The vegetation landscapes, their plant foliage characteristics and morphology are determined by the underlying mixtures of sandy and clay soils from underlying bed rock (Map 2), the water availability and topography. Fine-leaved savannas such as the *Acacia spp.* dominated shrublands and thickets in the centre of the park were found to have lower tree canopy cover densities (a lesser surface area to woody cover volume ratio) and less surface litter biomass fuel loads. Shrubland vegetation is more compact, contains less moisture than woodland vegetation (*e.g. Combretum spp.* and *Terminalia spp.* dominated landscapes in Map 3) and there is an indication that shrubland fuels are more aged than mature woody or grass biomass fuel components. Shrubland savannas may produce more flammable fuels, capable of sustaining extreme fire intensities, *i.e.* fire rate of spreads ( $\text{m min}^{-1}$ ) (FERNANDES, 2001). The experimental burn plot strings which were field sampled and satellite analysed in this study are shown in Map 2 and Map 3. Sampling was always performed on several prescribed burn plots on respective experimental burn plot strings and within three savanna vegetation types according to GERTENBACH (1983b) (Map 3).

Madikwe Game Reserve (Map 1) has variable soil types from black clays to sandy loam. The Madikwe reserve is dominated by semi-arid shrubland savanna with patches of *Acacia spp.* and *Boscia sp.* dominated undifferentiated woody savannas (KRAUS AND SAMIMI, 2001).

**Map 2:**

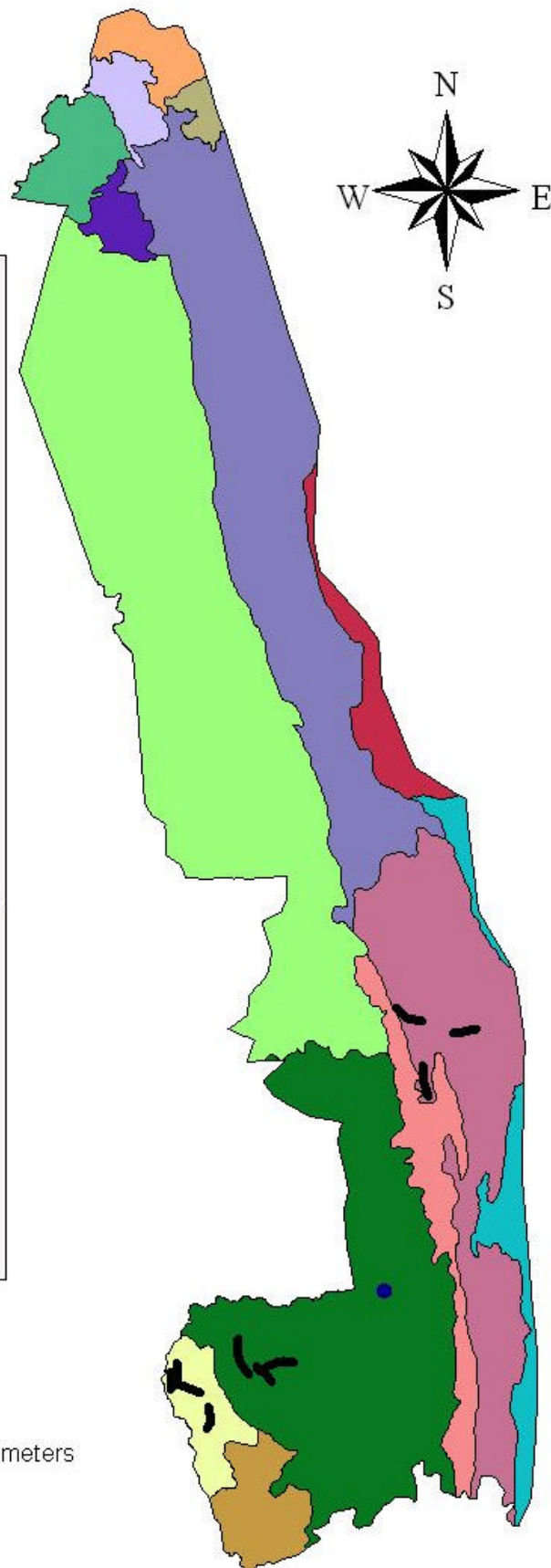
**Underlying bedrock - soils**



Sources: Scientific Services, Skukuza, Kruger National Park; ARC, Institute for Soil, Climate and Water, Pretoria

**Map 3:**

**KNP Vegetation Types**  
(derived from GERTENBACH, 1983)



30 0 30 60 Kilometers

Source: Scientific Services, Skukuza, Kruger National Park

## 1.5 Satellite data corrections

The multi-sensor and multi-temporal data sets in this work prerequisites good scene-to-scene geolocation and atmospheric correction. The geolocation method used is described in each manuscript section. The MOD09 (level 2G) MODIS surface reflectance data sets used in this study are already corrected for atmospheric gases, aerosols, and thin cirrus cloud contamination. The MOD09 correction is applied routinely to MODIS top of the atmosphere (TOA) level 1b input data and cloud free pixels in the seven reflective bands (centred at: 0.64 $\mu\text{m}$ , 0.858 $\mu\text{m}$ , 0.47 $\mu\text{m}$ , 0.55 $\mu\text{m}$ , 1.24 $\mu\text{m}$ , 1.64 $\mu\text{m}$  and 2.2 $\mu\text{m}$ ). To render inter-comparability between MODIS surface reflectance products, Landsat and the ground reflective measurements, the radiometrically and geometrically corrected (Level-1G) Landsat ETM Landsat ETM+ data tiles were calibrated to surface reflectance  $\rho_s$  (section 1.5.1 below).

### 1.5.1 Landsat ETM+ calibration to reflectance

The following equation was used to calibrate the level 1G digital numbers (DN) to absolute radiances (Watts/ (m<sup>2</sup> \* sr\*  $\mu\text{m}$ ))

$$\text{Radiances} = (((L_{\text{min}} - (-1)) / (L_{\text{max}} - 1)) * (DN - 1)) - 1 \quad (1)$$

The  $L_{\text{min}}$  and  $L_{\text{max}}$  are the spectral radiances for each band at the digital numbers 1 or 255 respectively. These have to be extracted for each band gain (High or Low) respectively. The gain values change as the detector loses responsivity and are issued as Calibration Parameter Files (CPF's) updated for distinctive image acquisition time frames (the CPF files were queried at: <http://landsat7.usgs.gov/cpf/cpf.php>). DN is the digital number (unitless).

To account for some in-between scene variations the radiance data was converted to planetary or top-of the atmosphere  $\rho_{\text{TOA}}$  or planetary reflectance (unitless) using the following formula

$$\rho_{\text{TOA}} = \frac{\rho * L_{\lambda} * d^2}{ESUN_{\lambda} * \cos \theta_s} \quad (2)$$

where  $L_{\lambda}$  is the spectral radiance at the sensors aperture,  $d$  is the earth-sun distance in astronomical units,  $ESUN_{\lambda}$  is the mean solar exoatmospheric irradiances (w/(m<sup>2</sup>\* $\mu\text{m}$ )) and  $\theta_s$  is the solar zenith angle in degrees (90° - solar elevation angle). This information as well as the earth-sun astronomical units, the bands spectral radiances ranges and the solar spectral irradiances are found on the Landsat-7 science user's handbook website. ([http://ltpwww.gsfc.nasa.gov/IAS/handbook/handbook\\_html/chapter11.html#section11.3](http://ltpwww.gsfc.nasa.gov/IAS/handbook/handbook_html/chapter11.html#section11.3)).

### 1.5.2 Landsat ETM+ atmospheric correction

As part of the calibration the Landsat ETM+ data sets were corrected to surface reflectance by applying correction factors from the 6S radiative transfer code (VERMOTE *et al.*, 1997a; 2002) (see Table 1, page 55). The transfer code uses an atmospheric point spread model (PSF) combined with optical depth data from AERONET network data collected for the time of the overpass and site specific elevation (m) (HOLBEN *et al.*, 1998). The TOA reflectance in reflective bands is affected by of H<sub>2</sub>O tropospheric aerosol scattering, Rayleigh scattering, ozone and stratospheric aerosol particle scattering and (upward and downward) scattering by primarily CO<sub>2</sub> molecules between the surface of the earth and the stratosphere (VERMOTE *et al.*, 1997b). Given the atmospheric optical properties of each band used (ETM+ bands one to seven: 0.47µm-2.2µm), the aerosol loading data from the AERONET estimates, site elevation above sea level (m), solar zenith angle and Julian day of each respective acquisition, the equation coefficients ( $x_a$  and  $x_b$ ) and atmospheric correction factors ( $x_c$ ) could be derived. These were substituted as follows

$$y = (?_{TOA} * x_a) - x_b \quad (3)$$

$$?_s = \frac{y}{(1 + (y * x_c))} \quad (4)$$

where  $x_a$  and  $x_c$  are the multiply coefficient,  $x_b$  is the subtraction coefficient applied,  $y$  is the atmospheric correction term and  $?_s$  is the surface reflectance.

Results obtained using site specific parameters as demonstrated above are quite accurate (VERMOTE AND VERMEULEN, 1999a).

Figure 3 (a and b) illustrates the difference between a subset enlarged image in reflectance  $?_{TOA}$  (Figure a) and the same enlarged subset corrected for atmospheric gaseous absorption and aerosol perturbations. The subset image shows an older fire scar in the southern KNP (Figure 3). The Landsat ETM+ image in Figure 3 was captured on the 15<sup>th</sup> of August 2000 and displayed as a Red, Green and Blue band combination.

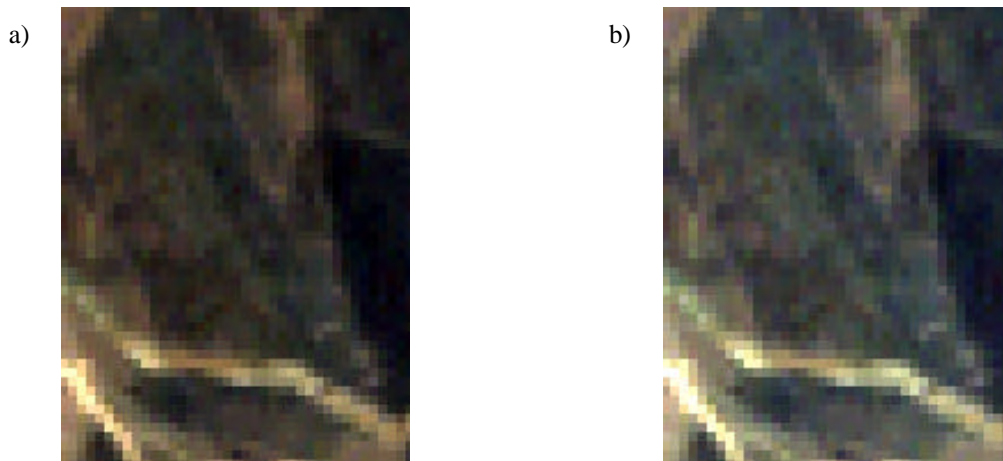


**Figure 3:** Comparison of a fire-affected area in Landsat ETM+ imagery as a red, green blue (visible) band composite over the KNP uncorrected for atmospheric effect in (a) and the same area corrected for atmospheric effect in (b). No image enhancements were applied.

The effect of atmospheric correction is slightly apparent in the higher visibility of lighter and green shades (*i.e.* increased heterogeneity) on the older fire scar in Figure 3b. The proportion (transmittance) effect change (absolute) in (for instance) the Normalized Differential Vegetation Index (NDVI) between the pre corrected and the post-corrected imagery showed an *increase* of 0.078 in the corrected data and over inherent woodland savanna. Over an area of maximum NDVI greenness (irrigated plantation on the KNP border) the atmospherically corrected data exhibited an increase of 0.03. The NDVI measures the spectral contrast between the Red portion and the near infrared portion of the electromagnetic spectrum and is sensitive to plant chlorophyll content (GOWARD *et al.*, 1990; GITELSON AND KAUFMAN, 1998). Sites with exposed soils such as dry perennial river beds exhibited a reflective increase of 9 to 13% in the corrected image using the 0.84 $\mu$ m near infrared ETM+ band. Similar magnitudes of reflective change have been noted by VERMOTE AND VERMEULEN (1998b) in MODIS pre and post atmospheric corrected imagery.

## 1.6 Objectives and study outline

This study *primarily* aims to:

- Reliable and quantitatively map the fire-affected area that is:
  - the fraction of fuel biomass consumed or combustion completeness
  - derive new methods to infer fire severity from high-resolution satellite data
- Validate and calibrate 500-m resolution MODIS fire information using *in situ* field data and Landsat ETM+ data over Skukuza
- Improve emissions estimates for the KNP-area.

- Investigate these results to corroborate/improve fire management policies in the KNP.

These objectives will be met by characterizing the biophysical properties of fire scars, vegetation fuels and emission factors at the KNP site. New mathematical regressions, applicable to optical sensors in reflective bands, and simple differential spectral ratios are derived.

The mentioned primary and secondary objectives are discussed separately in each manuscript chapter (listed below from 1 to 6) and can be read as such (Results-Section II).

The sequences of the manuscripts are the working steps to synthesize the research objectives. The first manuscript (1) is a methodology paper on aboveground fuel biomass sampling techniques, as accurate knowledge on biomass available for burning is a prerequisite for all other working steps (2-5). Manuscripts (2) and (3) are the key research components of the study synthesis. Implications of deriving biophysical fire properties in the Skukuza-area using satellite data are made in (2) and (3). These fire properties, *i.e.* combustion completeness (CC), fire intensity and fire severity are integral and dealt with in subsequent work (4) and (5). Findings from (2) and (3) have relevance for MODIS validation and calibration strategies, limits of burned area detectability and future fire product use. In manuscript (4) the key research findings and methods in (1) to (3) are utilized by demonstrating how these can accurately feed, improve and comprehend local emissions models. Manuscript (5) illustrates the utility of some of the above findings to feed KNP research agendas and makes some simple fire mapping propositions for fire and resource managers in protected areas.

The objectives of each respective manuscript chapter and contributions from co-authors are listed below; each manuscript is currently being submitted for publication:

#### 1. Fuel sampling protocol for Southern Africa

**-Objectives:** improve field fuel biomass sampling techniques that are efficient and accurate in southern African savannas.

**-Co-author contributions:** relevance of field sampling results from Zambia to the proposed sampling techniques (C. Hely), and suggestions on the presentation of results for application studies (G. Gerold).

#### (2) Characterizing the surface heterogeneity of fire effects using multi-temporal reflective wavelength data.

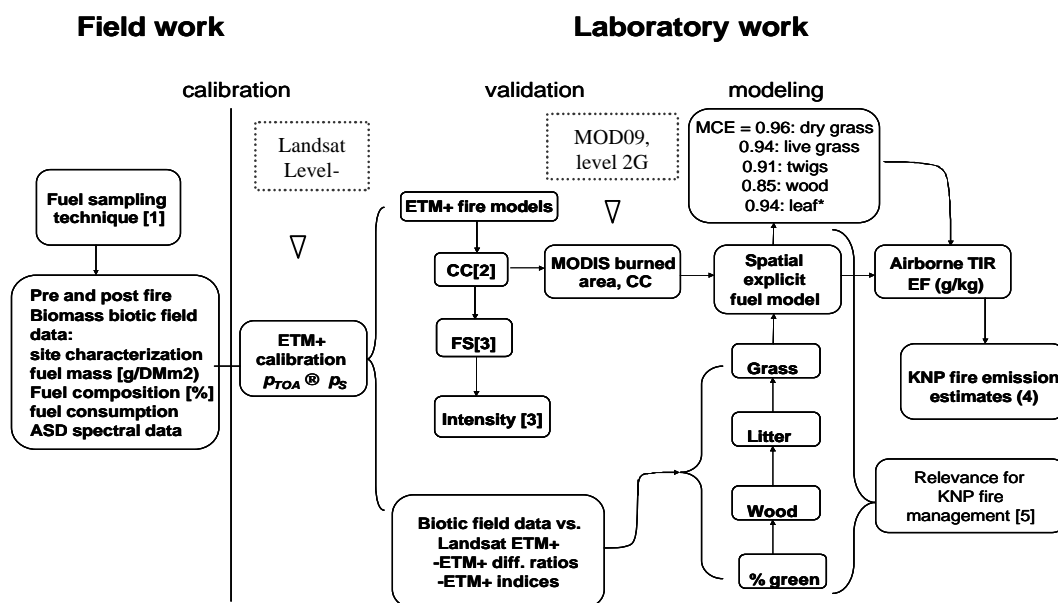
**-Objectives:** characterizing combustion and completeness and area fraction burnt on fire-affected areas in South African savannas using high-resolution (multi-temporal) Landsat ETM+ satellite data.

- Co-author contribution:** illustration of theoretical models on the fraction burnt and combustion completeness using physical properties of burn scars in the KNP (D. Roy).
- (3) Estimating fire intensity and fire severity from remote sensing fire information on experimental burn plots in the KNP.
- Objectives:** deriving a technique to map fire intensity and fire severity with higher-resolution (multi-temporal) satellite data.
- (4) Improved fire emissions estimates from Kruger National Park (KNP) using satellite derived biomass and fire estimates and Airborne Emission Factor (EF) data.
- Objectives:** couple multi-sensor remote sensing data with modelled and well parameterized fuel biomass data (*i.e.* the tree, grass and litter ratio) and *in situ* emission factors (EF) to estimate and improve local fire emissions. Secondary aim is to test the sensitivity of some gaseous compound emissions to the fuel mixture and the combustion efficiency thereof.
- Co-author contributions:** emission ratios (ER) and emission factors (EF,  $\text{g/kg}^{-1}$ ) sampling results from the Airborne Fourier Transform Infrared Spectroscopy (AFTIR) over the KNP-area (B. Yokelson) mounted on the University of Washington's Convair-580 aircraft (P. Hobbs).
- (5) The relevance of remote sensing burnt area information for future fire management policies in the Kruger National Park (KNP)
- Objectives:** collate the new research findings in (1) to (4) and quantitatively investigate the accuracy and suitability of current remote sensing tools to corroborate the fire research agendas, objectives and future strategies of the KNP fire management policies.
- Co-author contribution:** discussion input as to the set up and relevance of the Integrated KNP fire management plan (N. Govender).

Implications and future relevance of the primary objectives are summed-up in the overall conclusion (Section III).

## 1.7 Overview of materials used and methods

This section gives a broader overview of the study synthesis methodology and materials used. The prime strategy of this thesis is to exploit the synergy between field work and laboratory research work, *i.e.* validating some of the findings/data directly at the KNP Skukuza and other prescribed burn sites. Figure 4 gives an overview of the methodology used to collate the information data levels and achieve the study objectives. Field work was primarily performed during the intensive SAFARI field campaign in 2000. Subsequently in 2001 and 2002 the field data was investigated in the laboratory for its use to validate and derive remote sensing fire and fuel biomass information. Three working levels are created: *calibration* of biomass grass fuel loads for the disc pasture meter as well as Landsat ETM+ satellite data calibration (see 1.5). Secondly *validation* of moderate resolution (MODIS) fire information and Landsat ETM+ fire data using *in situ* fuel biomass and field spectral measurements and finally satellite *modeling* of fuel biomass and emission parameters was undertaken for the KNP-area. The individual manuscript chapters are numerated in Figure 4 (as above from [1] to [5]).



\*MCE= Modified Combustion Efficiencies for biomass components (WARD *et al.*,

**Figure 4:** Summary methodology diagram showing field and laboratory study components and working steps as flow arrows or lines. Key issues addressed in each manuscript paper are shown as numbers: manuscript paper one [fuel sampling technique], manuscript paper two [CC= Combustion completeness], manuscript three [FS= Fire severity], manuscript four [KNP emission estimates], and manuscript paper five [relevance of fire information for KNP fire management policies]. The ASD (Analytical Spectral Devise) refers to spectral reflectance measurements recorded on fire-affected areas using a hand-held ASD radiometer.

### 1.7.1 Field sampling

Aboveground biomass was sampled at over 36 (120m by 120m) sampling frames on prescribed burn plots within several savanna types in South African National and private parks (see map 1). **Grass** and herbaceous species mass was determined by measuring the compaction height (cm) of the disc pasture meter (DPM) systematically within the sampling frame (see Section 2). The disc meter permits fast and accurate (provided it is calibrated) sampling over large areas where biomass fuel variability is an important factor, so overcoming the labor-intensive problems associated with clipping and weighting samples (STOCKS *et al.*, 1996). The DPM consists of a circular aluminium disc fitted with a measuring rod, and the standing crop of grass fuel, including possible other herbaceous species, is estimated by relating the settling height of the quantity of grass material holding it perpendicular above the ground. The disc meter equations were calibrated with DPM corresponding grass clippings that were also sampled systematically within a 120 meter sampling frame in fifteen 50 cm by 50 cm quadrats. Grass was ambient air dried, weighted, expressed to the nearest gram (*e.g.* gDM/m<sup>2</sup>) and correlated to the settling height of the disc meter recorded within each respective quadrat. The derived and reference grass regression equations are shown below in Table 2.

Area	Regression	Squared multiple	Significance
Madikwe	$y = 0.0395x + 0.0108$	$R^2 = 0.90$	$P < 0.0001$
KNP <sup>1</sup>	$y = -3019 + (2260 * vx)$	$R^2 = 0.95$	$P < 0.0001$
KNP	$y = 0.0035x^2 - 0.5231x + 28.494$	$R^2 = 0.74$	$P < 0.0001$

<sup>1</sup>TROLLOPE AND POTGIETER (1986)

**Table 2:** Self-calibrated and literature regression equations used to gain a spatial estimate with the disc pasture meter (DPM) for the KNP and Madikwe sampling sites.

**Wood mass** and tree foliage mass (*e.g.* gDM/m<sup>2</sup>) was determined within three randomly selected 10 meter by 10 meter plots on the sampling frame. The height of all woody material, number of stems, basal perimeter (cm) of stems and species composition was recorded in each plot. The wood mass for dominant species was calculated using allometry reports from NETSHILUVHI & SCHOLES (2001) and RUTHERFORD (1979; 1982), using mostly the basal perimeter of dominant shrub and tree species as input parameter.

Table 3 below depicts all allometry equations used for wood and foliage estimates sampled on the burn plots, as well as their relevant sources or references

Reference/source	Biomass species	Parameters*	Regression	Squared multiple (R <sup>2</sup> )
Rutherford (1979), Botanical Review	Shrubs (combined species), <i>P. malvaceus</i> , <i>M. ferruginea</i> )	stem diameter larger 2 cm only	$\ln(\text{total mass in g}) = 3,580 + 2,853 \ln(\text{stem diameter larger than 2 cm})$	
Rutherford (1982), <i>B. africana</i> , <i>O. pulchra</i>	<i>T. sericea</i>	$y = \text{total biomass}$ , $x = \ln[(\text{stem diameter})^2 * \text{height}]$ (cm)	$\ln Y = -10,5573 + 1,2018x$	R <sup>2</sup> = 0,99; P = 0,001
	<i>C. zeyheri</i>	$y = \text{total biomass}$ , $x = \ln[(\text{stem diameter})^2 * \text{height}]$ (cm)	$\ln Y = -10,3373 + 1,2018x$	
	Combined species	$y = \text{total biomass}$ , $x = \ln[(\text{stem diameter})^2 * \text{height}]$ (cm)	$\ln Y = -8,5997 + 1,472x$	
Netshiluvhi & Scholes [2001]: wood biomass allometry reports	<i>A. gerardii</i>	M = kg, C = cm	$\log_{10}M = 2,633(\log_{10}(C)) - 2,580$	R <sup>2</sup> = 0,99
	<i>A. nigrescens</i>	D = cm, M = kg	$\ln M = 1,2723 \ln(D2) - 3,613$	R <sup>2</sup> = 0,94
	<i>C. apiculatum</i>	D = mm, M = kg	$\ln M = 1,4015 \ln(D2) - 9,527$	R <sup>2</sup> = 0,98
	<i>C. collinum</i>	M = kg, C = cm	$\log_{10}M = 2,365(\log_{10}(C)) - 2,319$	R <sup>2</sup> = 0,98
	<i>C. zeyheri</i>	M = g, d = cm, h = m	$\log_{10}M = 2,7710(\log_{10}(d)) + 1,3013$	R <sup>2</sup> = 0,98
	Combined <i>Acacia</i>	M = kg, d = mm, h = mm	$\ln(M * 10000) = 1,0432 \ln(D2H) - 5,6181$	R <sup>2</sup> = 0,96
	Combined <i>Euclea</i>	M = kg, d = mm, h = mm	$\ln(M * 10000) = 0,9107 \ln(D2H) - 3,6075$	R <sup>2</sup> = 0,96
	<i>D. cinera</i>	D = cm, M = kg	$\log_{10}M = 2,521(\log_{10}(C)) - 2,460$	R <sup>2</sup> = 0,96
	<i>G. bicolor</i>	D = mm, M = kg	$\ln M = 1,278 \ln(D2) - 3,04$	R <sup>2</sup> = 0,56
	<i>S. birrea</i>	D = mm, M = kg	$\ln M = 1,3086 \ln(D2) - 9,5446$	R <sup>2</sup> = 0,98
<i>T. sericea</i>	M = kg, D/H = cm	$\ln(M) = 0,7846 * \ln(D2H) - 6,8060$	R <sup>2</sup> = 0,98	
Netshiluvhi & Scholes [2001]: leaf biomass allometry reports	<i>A. gerardii</i>	C = cm, L = kg	$\log_{10}L = 2,075(\log_{10}(C)) - 2,938$	
	<i>C. apiculatum</i>	d = cm, L = kg	$L = 0,0109 d^2 + 0,0520$	
	Combined <i>Acacia</i>	L = kg, d/h = mm	$\ln(L * 10000) = 0,8244 \ln(d2h) - 4,8895$	
	<i>G. bicolor</i>	d = cm, L = kg	$L = 0,0066 d^2 + 0,0019$	
	<i>S. birrea</i>	d = cm, L = kg	$L = 0,0074 d^2 + 0,0038$	

\* C, D, d = basal stem diameter; M and L = wood/leaf mass; H and h = height of tree/shrub

**Table 3:** Allometry reports for common woody biomass species, parameters required, regression equations and regression squared multiples (R<sup>2</sup>).

To validate some of the Landsat ETM+ sub-pixel information in the satellite modeling results (section 2), landscape components were identified as a percent fraction of the whole land cover. The following ‘pure’ landscape features were estimated for the 120 meter sampling

frame

[in %]: fraction of landscape covered by grass, fraction of landscape covered by wood and percent green of trees in their respective height classes, fractional bare soil coverage and fraction of landscape covered by rock outcrops. When dealing with such mosaic landscapes (*i.e.* savannas) in remote sensing, visible interpretation to identify training data sets using several observers on the ground is secure (SETTLE AND CAMPBELL, 1998).

Apart from the fractional surface predictions soil color, soil sand contents, tree cover density using a spherical densiometer (LEMON, 1957); land form and average slope in degrees was estimated. Table X in the appendix gives an overview of important parameters determined for coherent analyses. Most of these parameters were analysed as indicators of the net primary production (NPP) of surface fuels that is to parameterize the Landsat ETM+ derived biomass fuel regression and fire characterization models. Not all the plots measured were however considered/analysed since some concurrent satellite imagery was cloud contaminated. Soil color using the Munsell color scale was determined before and shortly after the cessation of the burn (MUNSELL COLOR CO, 1971).

All of the prescribed burn sites listed in Table X were subsequently burnt and analysed for active fire recordings. During the active fire phase temperature, relative humidity and wind speed were recorded at half-hour intervals. Wind direction and speed was measured with hand held anemometers. Flame height and flame length was recorded with nine 3.5 meter tall steel rods that were placed within the 120m sampling frame. A diesel trenched string was suspended in a taut fashion from the metal rod at 30 cm above the ground and after fire cessation the ‘burn off’ length was recorded to estimate the flame height and length. The rate of fire spread ( $\text{m s}^{-1}$ ) was measured by taking time measurements between two steel rods that were known to be at a specific distance from one another. The active fire measurements, however, were not further investigated due to the calibration artefacts in the concurrent ‘beta version’ MODIS and MODIS airborne simulator (MAS) data (see 1.3.2) (ROY *et al.*, 2002e). Section 2 covers other aspects of the biomass fuel sampling design, methods used, results, possible error sources and results. In Section 2 the ASD spectral measurements taken on fire-affected areas and of ash and vegetation are discussed.

### 1.7.2 Statistical methods and satellite data

Analyses of hypothetical relationships between the fraction of a pixel burnt, the combustion completeness (CC), and reflection change as a function of the above fire effects at different wavelengths (and waveband combinations) were modelled (see first manuscript [1] in Section 2). To illustrate the ‘theory’ implied models on CC, fraction burnt, fire severity and fire

intensity, simple non-linear and linear regressions are analysed using the field collected data and satellite reflectance. Analyses of variances, multi-variant regression determinants, prediction and confidence intervals are investigated for regression model accuracies and prediction suitability. Each of these methods are implied, discussed and/or illustrated in the respective manuscript chapters (Section 2).

This study uses an approach that endeavours to continuously model the land-cover with satellite data, using the mentioned regression derived models at sub-pixel level, rather than thematically classifying satellite data pixels into homogeneous and ordinal parcels or entities. Classification approaches in fuel and fire models have inherently substantial errors and variations in each processing step (*e.g.* HELY *et al.*, 2002; HOROWITZ *et al.*, 2002) and hence the final estimate has a broad range of uncertainty (SCHOLES *et al.*, 1996c).

### 1.7.3 Satellite data

Multi-temporal data sets were used to account for the continuously changing effects in fire-affected areas, and to be able to define changes between imagery more accurately. Landsat ETM+ imagery was selectively requested (depending on cloud cover) for the southern and central KNP-area (ETM+ path 168, row 077 to row 078), Madikwe (path 172, row 068) and Umfolozi-Hluhluwe Game Reserve (path 168, row 80) (Map 1). Only the reflective bands were considered. Table 4 gives an overview of the Landsat ETM+ and MODIS data sets used, their acquisition date and area. The surface reflectance MODIS (MOD09) imagery granules cover both the KNP and the Madikwe sites respectively. The MODIS data is an earth-gridded geophysical parameter product (level 2G) in HDF format with global attribute and scientific datasets (SDS) appended. Table I (page 141 in Section 2) gives the spectral and spatial waveband properties of the reflective MODIS and Landsat ETM+ bands in detail.

Sensor		Landsat ETM+			MODIS	
Area	Madikwe	Madikwe	Skukuza	Umfolozi/Hluhluwe	KNP-Madikwe	
ETM+ path/row	171/077	172/077	168/077-078	167/080	MOD09GQAK <sup>a</sup>	MOD09GHK <sup>b</sup>
2000		11-Aug	15-Aug	08-Aug		
	20-Aug	27-Aug	31-Aug			
			18-Oct			
2001			18-Aug		03-Sep	18-Aug
			03-Sep		05-Sep	03-Sep
					07-Sep	
					13-Sep	
					15-Sep	
					18-Sep	
					22-Sep	
					23-Sep	
					24-Sep	
					04-Oct	

<sup>a</sup> Two bands: 0.64 $\mu$ m , 0.858 $\mu$ m (at 250-meter resolution)

<sup>b</sup> Seven bands: 0.64 $\mu$ m, 0.858 $\mu$ m, 0.47 $\mu$ m, 0.55 $\mu$ m, 1.24 $\mu$ m, 1.64 $\mu$ m, 2.2 $\mu$ m (at 500-meter resolution)

**Table 4:** Summary table showing MODIS and Landsat ETM+ satellite data acquisitions (date) for the study period.

## **Section 2: Main Results**

### **2.1 Fuel sampling protocol for Southern Africa**

BY Tobias Landmann <sup>\*</sup>, C. Hely <sup>\*\*</sup>, G. Gerold <sup>\*</sup>  
(*submitted* to the Journal of Basic Applied Ecology)

#### **2.1.1 Background**

The most important factors affecting fire intensity (kW/m) and fuel consumption rates is the aboveground biomass fuel load (kg/ha), biomass fuel moisture and climate parameters (Trollope, 1992). Unlike climate parameters fuel is a potentially measurable variable at the time of combustion.

Biomass fuel status monitoring provides important information for understanding fire behavior, including ignition, growth and rate of spread (Cheney and Sullivan, 1997) and biomass fuel load is a large uncertainty for some molecular species in emissions estimates (Justice and Korontzi, 2001). Pre burn fuel mass is a denominator and numerator value in the combustion completeness equation and hence needs to be quantified most accurately. Methods to quantify fuel in combustion completeness equations remain outstanding issues and knowledge on the spatial heterogeneity of fire behavior in this respect is little (Frost and Robertson, 1987).

The fuel protocol will give the complete fuel information and characterization for studies pertaining to risk or hazard assessments, emissions and fire behavior modeling as well as land management purposes. The woody savanna fuel component has seldom been measured in studies pertaining to fire in African savannas (Shea *et al*, 1996b). Previous studies in Southern African savannas on fire effect and biomass combustion factors concentrated mainly on the grass sward (Trollope *et al*, 1986,1996; Stocks *et al*, 1996) and aboveground flora/or fauna material below 2,5m (Shea *et al*, 1996c) as fuel source. There is no known common sampling strategy for flammable foliage and total biomass that would contribute to total fuel load and therefore studies on combustion completeness and fire severity.

---

\* Department of Landscape Ecology, University of Goettingen, Goldschmidtstr. 5, 37077 Göttingen, Germany.  
fax (49) 551-3912139, e-mail tlandmann@csir.co.za; ggerold@gwdg.de

\*\* Department of Environmental Sciences, University of Virginia, VA 22903 Charlottesville, USA.  
fax (1) 434-9822137, e-mail Christelle\_Hely@maddux.evsc.virginia.edu; ch8se@virginia.edu

\*\*\* CSIR Environmentek, Bering Naude ave., 0184 Brummeria, Pretoria, South Africa.  
fax (27) 12-8412345, e-mail bscholes@csir.co.za

The overall accuracy target is aimed to be  $\pm 10\%$  error of the total fuel load, this being based on 15 half meter quadrants on a designated plot and using equal intervals along sampling transects. Grass is the most important savanna fuel and is hence measured using a two-way approach with most precision. Biomass is referred to as being all living plant matter, while we use the term fuel to describe all aboveground fuel biomass available for burning.

## 2.1.2 Sampling strategy

### 2.1.2.1 Site set up

The sampling site should have a minimum size of 120m x 120m. A 120m x 120m site dimension is efficient since it affords a manageable size for field measurement, while allowing a large number of different sites to be examined, and was sufficiently large to minimize potential problems with most high-resolution satellite instruments (such as Landsat and Aster) navigation. It is also a manageable size for prescribed burn experiments and measuring fire behavior. The site should be set up using a compass with the starting point facing north, taking the GPS position in degrees and decimal minutes on the SW corner (see Figure 5).

Use a road or self-made firebreak as a plot circumference or reference line and pace out the quadrats using the compass as a direction guide. On areas with persistent heterogeneous topography, a triangular sampling grid with equal intervals would better to account for slope effect.

### 2.1.2.2 Description of site

Note the sampling date and if possible record the fire history of the plot with the date of the last burn that is burning treatment if you are working on an experimental burn plot.

Estimate the average height of tree stand and percentage of green leaf. The green leaf component is not highly flammable and therefore a visual inspection would suffice here.

The following other ancillary data is needed to validate the mentioned fuel load models:

- land use type, i.e. reserve, intensively or extensively stocked.
- percentage of sand, loam and clay soil content and where possible determine the profile depth.

- land-form shape, that is crest, scarp, mid-slope, toe slope or valley.

An example protocol to estimate pre fire fuel in the Kruger National Park (KNP) area is shown in the appendix (Table 5).

### 2.1.2.3 Fuel sampling and tree cover density

Sampling is done systematically within the 120m frame changing direction at every clipping point that is every 30m (Figure 5). If combustion completeness (CC) from the burn has to be calculated, some precautions have to be taken in order to set up and mark properly the areas that will be undisturbed before the fire. In the undisturbed area, sample again after the burn.

Use a spherical densiometer to read the tree cover density at every 50cm by 50cm clipping point, i.e. 15 times within the sampling frame, sum the scores and multiply by 1.04 to get percentage tree cover for the whole area. If you do not have a densiometer, the tree cover density can be estimated by using a 100 meter line or measuring tape stretched tightly above the ground along the diagonal directional of the plot. Count the number of woody material intersections and height and average the tree cover for the sampling area.

Grass, wood and litter (leaf, dead grass) must be collected in a bag, transported and weighted.

**Grass and forbes.** A two-step approach is recommended to sample grass. Firstly grass can be clipped at ground level within the 50cm by 50cm sampling points and secondly the clipped quadrants can be used to calibrate a disk pasture meter (DPM), which is then used to obtain a good spatial estimate.

For the disc pasture meter: let the metal plate settle on the grass sword and take the centimeter reading holding the iron rod that perpendicular on the ground. For the standard disk, the quadrature should be 50 cm in diameter, which means that it samples 0.2 m<sup>2</sup> (Bransby and Tainton, 1977). Using your own regression with the amount of grass clipped for the disc settling height or an equation already derived for a savanna biome, estimate the spatial grass amount in t/ha (see calculations). Before you clip make a visual estimate of the mass fraction of the material that is still green and also make sure that all logs and other shrubs [not forbes] are removed as they may falsify the grass compaction height. If the disc meter is available, measure standing grass height between sampling quadrants repeat every 6 meters along the sampling grid (this will amount to 75 disc readings in the sampling area).

**Leaf and wood litter.** In the same quadrat all fallen litter, leaves and fallen grass from ripe and senescent grass must be collected and put in a large bag [and store separately]. Also pick up all woody material (dead wood and twigs) that have a basal diameter smaller or equal to 1.5cm and store these in the bag.

It is advisable to pick up all litter and wood before clipping the grass and to carefully determine which forbes and grasses are rooted inside the 50cm quadrat.

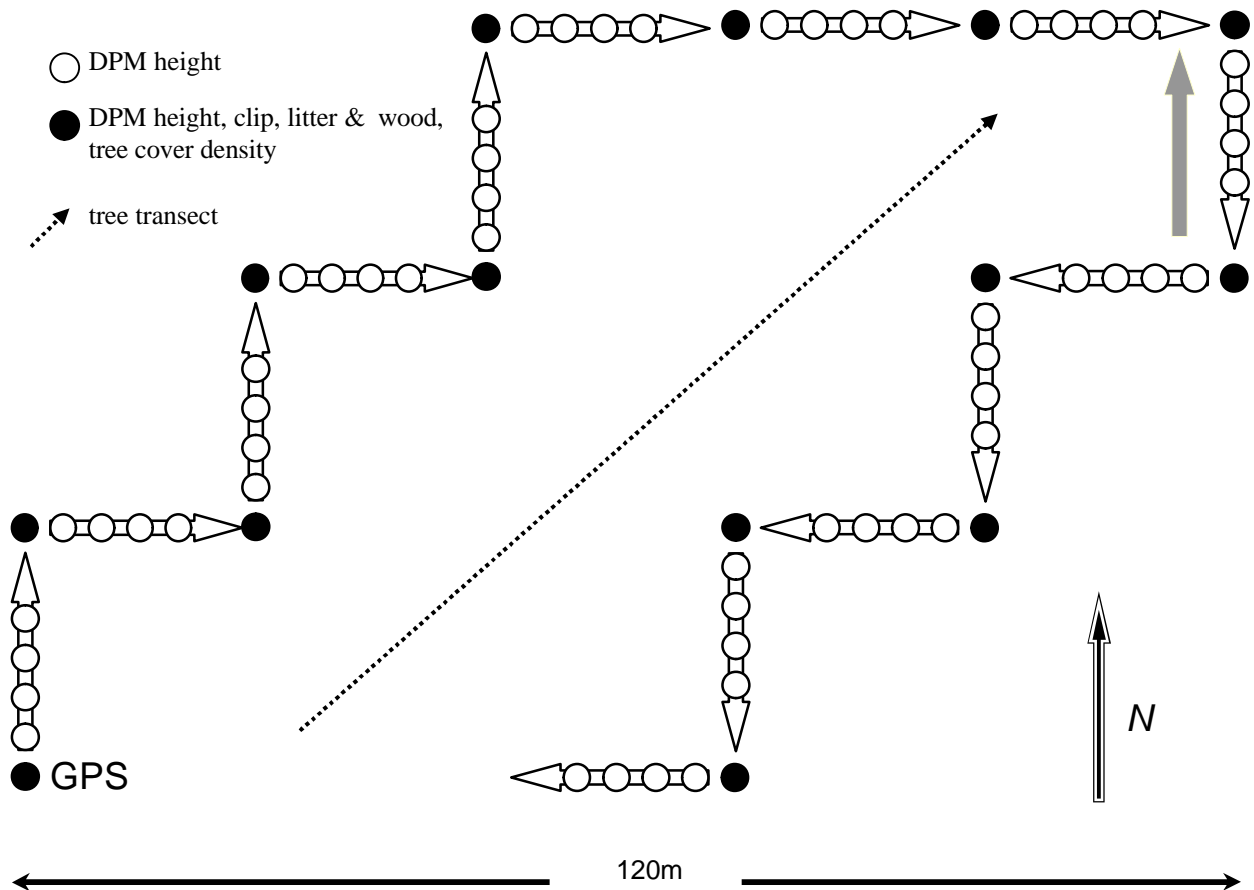


**Figure 5:** Effective sampling design position showing the 15 sampling quadrats, the woody fuel transect and possible sequence to record disc meter heights.

## 2.1.3 Calculations

### 2.1.3.1 Tree cover density

#### i. Spherical densiometer method

Hold the spherical densiometer at chest level, facing north and count the number of squares that are totally filled with canopy wood with 4, those that are between half and three quarters with 3, between a quarter and a half with 2, less than a quarter with 1 and no canopy in square with 0. Sum the scores at each clipping sampling point, that is 15 per sampling area, and multiply by 1.04 (Lemmon, 1957).

#### ii. Transect method

Set up a 100-meter long tape or line along the diagonal of the plot and taking the GPS position of one end. Walk along this line and record the length of each canopy cover segment for woody species taller than 2m that crosses the line. Sum the lengths. Precision can be increased by repeating the measurement along another line still representative of the site and by averaging the total lengths.

### 2.1.3.2 Fuels

Collected grass, fine wood, and litter have to be oven dried at 60 degrees C for at least 24 hours and each fuel type sample has to be weighed as dry matter in grams. Alternatively samples can be ambient air dried in a ventilated open area for at least 4 days.

Calculate the average fuel amount per unit surface area (on a dry matter bases) per site for each fuel type, i.e. grass, litter, and woody material ( $\text{Kg/m}^2$ ) [see table 5 in the appendix].

When calibrating the DPM settling height, a linear regression relating grass mass per unit surface area and settling height must be derived using the 15 sampling points in the grid [also calculate the average standard deviation and the confidence level]. If a calibrated regression is available, the DPM readings can be used to average grass mass in kg/ha for the whole sampling grid.

Trollope and Potgieter (1986) derived a regression relating the disc meter height to herbaceous mass for the Kruger Park biome using 75 samples. Other areas where the disc meter is calibrated are the Zululand plain lands (Brockett *et al*, 1992), the Eastern Cape Thornveld (Trollope *et al*, 1983), both in South Africa, the Lewa Wildlife Conservancy in East Africa (Trollope *et al*, 1998) and the Etosha National Park (Namibia).

### 2.1.3.3 Combustion completeness

Combustion completeness is calculated by subtracting the residual biomass per unit surface area from the before-burn biomass measurements according to the following equation:

$$CC = \left( \frac{Preburn_{load} - Postburn_{load}}{Preburn_{load}} \right)$$

Use the same sampling design to measure *post-burn* DPM residual **grass** sward (where grass has not been burnt). If no disc meter is available, clip any grass material that is left standing on the 50cm plots that you flagged approximately next to where you sampled the pre-burn grass. Use the mean mass of these clippings or the regression to get post-fire grass mass.

Estimate the combustion completeness (%) of the total of shrub wood and leaf material that is burned, only taking shrubs into account that are smaller than 2m in height, i.e. those that are in the flaming zone.

**Litter and woody** debris can also be sampled in the post-burn sampling plots. The assumption is that the adjacent quadrats are similar to the pre-fire quadrats. To measure fine wood material residual in woodland areas, resample the same line intercept [marked before the fire]. Because some burn treatments or burnt areas are more complete than others, it would suffice to estimate fraction area burnt percentage as a surrogate of combustion completeness, e.g. on prescribed burn sites. However, by using this visual approximation [except in sites that are 100% burned without residuals], the accuracy attributed to the fuel load sampling is depreciated.

## 2.1.4 Discussion

### 2.1.4.1 Error thresholds

The choice of 15 sampling points is to reach a maximum error threshold of approximately 10% of the mean in a relative homogeneous site. The error calculation is a relation between the standard deviation and the square root of the number of samples; thereby the accuracy would increase with more [n] numbers of sampling points (Sokal and Rohlf, 2000). This would amount to an overall accuracy  $\pm 0.4$  t/ha for a plot having a mean fuel mass of  $\pm 4$  t/ha.

Using the DPM the number of samples should be 75 to reach an error threshold of approximately 10% of the mean. From studies in the KNP and the Zululand plains, the accuracy of the disc meter decreased as the mean disk height increased (Bailey *et al*, 1993). In medium KNP fuels, i.e. in disc meter heights between 9cm and 13cm, a confidence level of 95% was reached, using between 80 and 100 [n] numbers of samples for the regression.

If a DPM grass regression model for a biome is not precise enough alternative models should be developed and tested within the limits of precision deemed and specific to the sampling area. However, if available, the DPM would provide a better representative and effective fuel measure for grass heterogeneity.

Due to the spatial variability when adding wood mass using allometry equations for individual species and projecting these to the whole sampling area, assumption of accuracies have to be made.

#### 2.1.4.2 General relevance

The entire protocol has been tested in the Kruger National Park (KNP) and Madikwe Game Reserve in South Africa using the DPM with calibration regressions available. Parts of it have been applied in Zambia (Mongu and Kasama regions) and in the Etosha National Park in Namibia, here using grass clippings to calculate grass mass per surface area (Alleaume *et al*, 2002, *submitted*; Hely *et al*, *in press*, 2001b). The different alternatives to estimate tree cover density, grass and other fuels are not being compared to one another in this protocol.

The line intercept method (van Wagner, 1968) is usually used in measuring woody debris in forested area. Consequently, in woody savanna like Miombo Woodlands the line intercept method should be used to determine the woody fuel component instead of the clipping method. It has been effectively used in Zambian and Namibian sites where the tree cover canopy was higher than 30% but no effort has yet been made to determine accuracies of different sampling methods mentioned.

This protocol should be appended using allometry equations to account for the shrub and tree biomass component. For this one can use the transect method to determine number of trees and shrubs, their height (m), basal diameter (cm) and number of stems. All fallen dead wood material larger than the sampled 1,5cm diameter is not accounted for because large wood rarely burns in Southern African savannas.

### 2.1.5 Application of this protocol to the SAFARI sites

Results from the SAFARI 2000 campaign in 2000 to validate and calibrate spatial fuel and CC models from satellite data such as Landsat Enhanced Thematic Mapper (ETM+) (Goward *et al*, 2001) can be accurately derived using this protocol.

For instance, grass and wood mass (t/ha) sampled at the South African SAFARI sites correlated significantly ( $R^2=0.62$ ;  $n=21$ ) (figure 6) to (30-meter) high-resolution Landsat ETM+ data, using collocated Landsat ETM+ adapted tasseled cap at-sensor reflectance index data (see Huang *et al*, 2001). We used percent fractional cover of woody species in their respective height classes as a multiplicative of wood mass (t/ha) from the sampling area to calculate woody material (t/ha) smaller than 2 meter (figure 6), that is the wood fraction that is most profoundly exposed to fire. Accurate spatial information on fire fuel mass is required to support fire policies reliant on decisions whether or not to apply control burns to reduce the risks of massive lightning or other fires. The new KNP integrated fire management plan of 2002 is exemplary for such a decision support fire policy (Biggs, 2002).

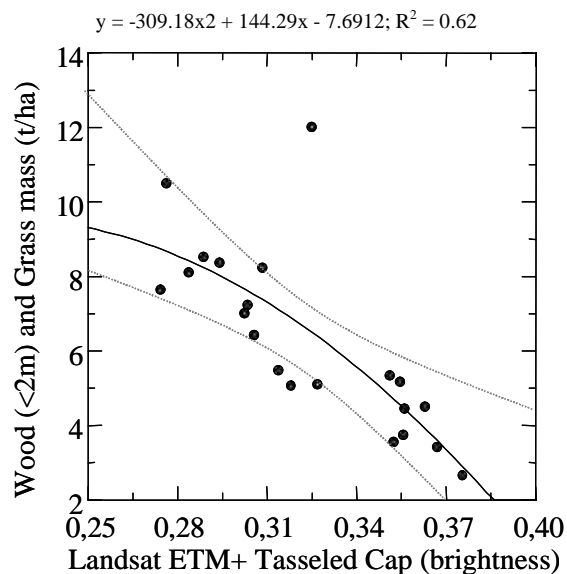


**Figure 6:** The non-linear relationship (black line) using 95% confidence intervals (grey line) wood and grass biomass fuel (t/ha) and Landsat ETM+ tasseled cap brightness index data. In this example from prescribed burn sites in the Kruger National Park, the below 2 meter wood portion was calculated using allometry equations according to Netshiluvhi and Scholes (2001) and grass was accounted for by disc pasture meter heights.

To spatially extract combustion completeness (CC), a simple non-linear regression between Landsat ETM+ surface reflection, using band 4 (0.78-0.9  $\mu\text{m}$ ), and field determined biomass fuel within the flaming zone (<2m in height) consumed by the fire (figure 7) was established ( $R^2=0.64$ ;  $n=20$ ). The measurements were taken on SAFARI 2000 burn sites in the Kruger National Park (open tree and woodland savanna) and Madikwe Game Reserve (open tree savanna). This regression model can effectively be applied to extrapolate CC site data to a landscape level as a continuous measurement, bearing in mind the spatial and spectral variation of the remote sensing instrument as a function of varying topography, land cover and vegetation status, and sun illuminous effects. For example, selected imagery compares different locations and seasons as continuous measurement of burn patchiness: homogeneous burn patterns occur late in the dry season and usually indicate high fire intensity, whilst more patchy fire patterns are found earlier in the season (Flasse *et al*, 2002).

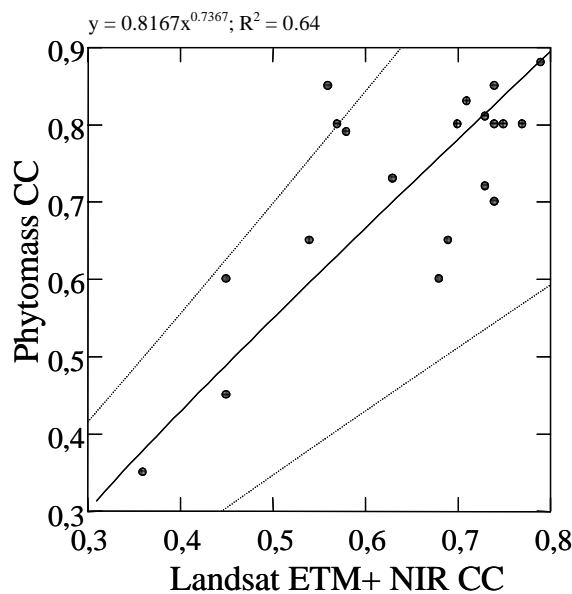


**Figure 7:** The non-linear relationship using 95% confidence limits between field combustion completeness (CC) from pre and post-burn biomass fuel measurements and site corresponding Landsat ETM+ reflectance CC from pre and post fire ETM+ imagery using ETM+ band 4 (0.78-0.9  $\mu\text{m}$ ).

The protocol data and resulting regression CC models can be extrapolated to landscape scales with, for instance, 250-meter resolution satellite data from the Moderate Resolution Imaging Spectroradiometer (MODIS), below for an arid-savanna SAFARI site in Namibia (Figure 8).

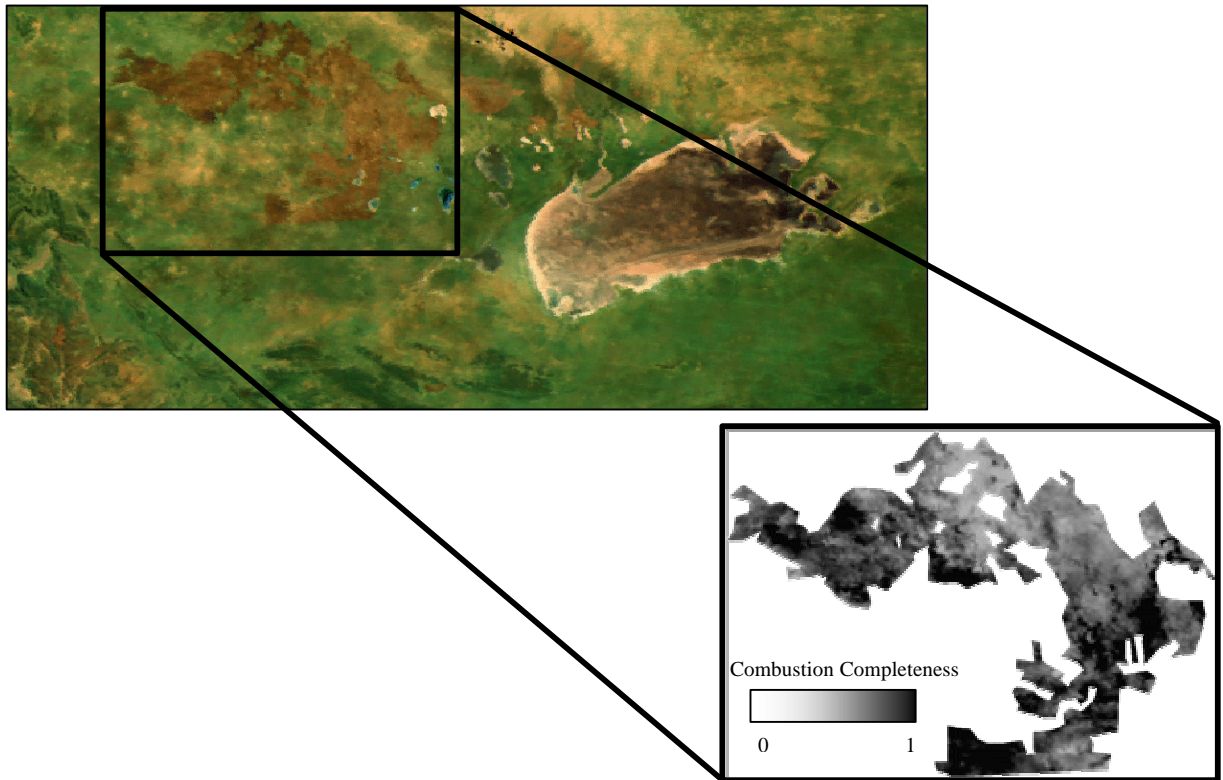


**Figure 8:** The upper image from MODIS shows a wildfire that burned over a 12-day period in September 2000. The fire destroyed approximately 3065 km<sup>2</sup> in an area (rectangle) to the east of the Etosha National Park pan, Namibia. Based on methods presented in the protocol, the lower rectangle relating combustion completeness to tree cover and fuel loads has been produced (from Alleaume *et al*, 2002, *submitted*).

Fire combustion completeness from satellite data may be directly related to measurements [using either field or remote sensing] of fire intensity (kW/m) and vegetation species ‘topkill’ (Trollope & Tainton, 1986), thus helping to assess specific park management policies that (say) target to enhance biodiversity by removing morbid vegetation or bush encroachment. Relating these issues in satellite data models remain outstanding and need further future attention.

## 2.1.6 Practical considerations

A whole working day is required for 2 people to complete this sampling grid.

Instruments needed:

- a GPS with sufficient battery power
- a compass
- a measuring tape of at least 30m
- a 50cm by 50cm frame
- a battery-powered electronic field balance or manual scale
- other items: clipper, gloves, bags (potato or paper bag) and a permanent marker pen

Optional:

-a disc pasture meter (DPM)

- a spherical densiometer or alternatively a 100m tape line
- a 50cm by 50cm frame
- a battery-powered electronic field balance or manual scale other items: clipper, gloves, bags (potato or paper bag) and a permanent marker pen

## 2.1.7 Summary

A methodology technical guideline to establish the pre and post burn aboveground biomass fuel mass and composition per unit surface area (in t/ha) is derived. The objective is to account for biomass fuel heterogeneity on a pre-burn area and to help bundle the different approaches previously used to measure the fuel component in Southern African savannas. Semi-arid savannas have less fuel moisture in the woody component than moist savannas. This protocol aims to quantify the actual mass consumed based on dry matter weight of the different fuel components.

As savanna fires are mainly surface fires, the assumption is that mature trees and shrubs are almost never burnt in Southern African savannas (Scholes *et al*, 1996). The fuel sampling strategy focuses primarily on ground surface fuel and stratifies into woody material smaller than 1.5 cm in diameter, grass and litter. Previous studies done by Shea *et al* (1996a) in South Africa indicate that 42 to 84% of woody debris having a diameter of 0 – 0.64 cm was consumed by fire, but <50% of the wood being 0.64 to 2.54 cm in diameter was burnt.

In addition to this, the protocol provides *in situ* site fuel characterization and land cover data, to integrate those data into higher order model outputs and in doing so to validate spatial fuel

models. Hely *et al* (2002a, *in press*) is currently deriving fuel prediction models for Southern Africa as part of the Southern African Fire-Atmosphere Research Initiative (SAFARI) 2000 project. Sampled site fuel characterization such as total foliage and wood and shrub mass, height and percentage of canopy cover can be purposefully correlated and extrapolated to low or even moderate resolution remote sensing instruments (e.g. SPOT, Landsat, Aster or MODIS).

Results can be integrated to model regional fire biomass emissions to predict associated environmental impacts and for studies on combustion completeness and fire behavior.

**Key words:** biomass site characterization, combustion completeness, fuel modeling

## 2.2 Characterizing the surface heterogeneity of fire effects using multi-temporal reflective wavelength data

D. P. Roy<sup>1</sup> and T.Landmann<sup>2</sup>

<sup>1</sup> Department of Geography, University of Maryland, College Park, and NASA Goddard Space, Flight Center, Code 922 (B32), Greenbelt, MD 20771, USA

<sup>2</sup> CSIR Environmentek, Meiring Naude avenue, Pretoria, South Africa, and Department of Landscape Ecology, University of Göttingen, Germany  
(International Journal of Remote Sensing- *in press*)

### 2.2.1 Introduction

Satellite remote sensing is an effective tool in continuous monitoring of biomass burning over large areas. In the last decade various methodologies have been proposed to map the spatial extent of biomass burning using remotely sensed data. Although these methods have provided useful information, their detection capabilities remain unclear, particularly with respect to the heterogeneity of the fire-affected area. To first-order, the heterogeneity of fire-affected areas may be considered in terms of the spatial distribution of the burned components and the degree, i.e., completeness, of combustion. These parameters are important for understanding the effect of fire on vegetation structure and ecosystem processes (Knapp and Seastedt 1986, Trollope and Tainton 1986), and are important for estimating the amount of biomass burned and so for estimating trace gas and particulate emissions required to understand release of carbon and greenhouse gasses to the atmosphere (Levine 1996; Barbosa *et al.* 1999). Fire deposits charcoal and ash, removes vegetation, and alters the vegetation structure. The remotely sensed signature of fire-affected areas may vary as a function of surface property variations, including vegetation composition, structure and soil background, and the fire behavior. The fire behavior controls the severity of fire effects including the degree and parts of the vegetation structure that are burned (ground cover, canopy cover, woody components etc.) and the amount and reflectance of deposited charcoal and ash. The combustion completeness is a commonly used term and is defined as the fraction of fuel exposed to the fire which actually burns (Shea *et al.* 1996, Scholes *et al.* 1996). Factors including the micrometeorological conditions (wind velocity, relative humidity, etc.) and the fuel type,

mass, compaction, and fuel moisture, may influence fire behavior and so the combustion completeness and determine burned-unburned patchiness at the scales of meters (Stocks *et al.* 1996, Ward *et al.* 1996). Soil, rock surfaces and green or wet vegetation may not burn at any scale (Scholes *et al.* 1996). Temporally, the remotely sensed signature of fire-affected areas may change depending on the degree of vegetation regrowth/recovery and the degree of charcoal and ash dissipation by the elements (Langaas 1995, Trigg and Flasse 2000).

Despite the different factors that determine the remotely sensed signature of fire-affected areas, methodologies to map their spatial extent have been developed for a number of remote sensing systems. Algorithms that use multi-temporal satellite data to take advantage of the temporal persistency of fire effects have received considerable attention for regional to continental scale mapping (e.g., Barbosa *et al.* 1999, Fraser *et al.* 2000, Roy *et al.* 2002). These methodologies have relied on classification or thresholding techniques to label remotely sensed observations as burned or unburned. In general, the accuracy of the data products produced by these algorithms has been inferred in a validation context by statistical comparison with independently collected data. However, no algorithm, or validation results, has been presented quantifying the expected detection capabilities with respect to the completeness of combustion or the spatial burn heterogeneity within the sensed observations. This may be due to the empirical nature of the algorithms and difficulties in collecting sufficiently representative independent data. However, this poses a potential limitation on the appropriate use of these data. No methodology to map combustion completeness using remote sensing has been demonstrated, although multi-temporal high spatial resolution satellite data have been used to map ordinal classes of parameters that are related to combustion completeness, such as fire intensity and severity (e.g., Michalek *et al.* 2000, Rogan and Yool 2001, Miller and Yool, 2002).

This paper examines the relationship between the change in reflectance caused by the action of fire and the heterogeneity of fire effects. The possibility of deriving the combustion completeness and the fraction of the remotely sensed observation (pixel) that burned is investigated and implications for algorithms that examine change in reflectance to map fire-affected areas are considered. A simple reflectance model parameterized for the combustion completeness and the fraction of the remotely sensed observation that burned is used to investigate the influence of these parameters. Extensive field and satellite observations made before and after prescribed fires during the intensive SAFARI-2000 dry season campaign

(Swap *et al.* 2002) on different semi-arid savanna types in the Kruger National Park and the Madikwe Game Reserve, South Africa are presented.

## 2.2.2 Modeling

The ability to differentiate between burned and unburned remotely sensed observations depends on the spatial distribution and spectral contrast of the burned and unburned components sensed in each observation and on the sensor's geometric and radiometric characteristics (Eva and Lambin 1998a). To examine this in more detail a modeling approach is used so that: (i) a range of model parameter values may be investigated that would be difficult to define using satellite data, (ii) normalization of uncertainties, caused for example by changing sensing and surface conditions, is not required, (iii) the models may be used in a predictive capacity.

In this paper we only model optical remote sensing at reflective wavelengths, noting however that remotely sensed temperature estimates and thermal wavelengths have been used to aid differentiation between burned and unburned vegetation (e.g., Cahoon *et al.* 1994, Eva and Lambin 1998b, Barbosa *et al.* 1999). The noise free optical imaging process may be modeled as the convolution of the scene radiance with the sensor point spread function (PSF). Usually the sensor optics, detector, electronic filters, and sensor motion are modeled as a single acquisition PSF by convolving the individual PSFs of these effects together (Reichenbach *et al.* 1995). The optical image collected at the sensor is digitized and quantized into discrete values for electronic storage and transmission. The measurement made by a detector will be referred to as an observation and the sensed surface dimensions will be referred to as the observation area. Assuming that observations are cloudless, uncontaminated by atmospheric effects, and that there is no significant amount of multiple scattering between the different scene components, then the sensed reflectance can be modeled as [1]. This is the linear mixture model (Settle and Campbell, 1998). In this model the reflectance contributions of the scene components sensed in an observation are directly proportional to their surface areas.

$$\mathbf{x} = \mathbf{M} \mathbf{p} + \mathbf{e} \quad [1]$$

$$\sum p_c = 1 \text{ and } p_c \geq 0 \text{ for all } c$$

where  $\mathbf{x}$  is an  $(n \times 1)$  vector describing the observed multi-spectral signal for  $n$  wavelengths,  $\mathbf{p}$  is a  $(c \times 1)$  vector describing the ground cover proportions of  $c$  scene components,  $\mathbf{M}$  is a  $(n \times c)$  matrix whose columns describe the scene component endmember spectra i.e., the response

received in the absence of noise by an observation composed only of a single scene component, and  $\mathbf{e}$  is an  $(n \times 1)$  vector describing the noise.

We model the effect of fire using two parameters, the combustion completeness and the fraction of the observation area that burn. The combustion completeness is defined [2] as the ratio between the fire fuels consumed and the pre-fire fuel *we said this in the introduction*

$$cc = (b_{t1} - b_{t2}) / b_{t1} \quad [2]$$

$$0 \leq cc \leq 1$$

where  $cc$  is the combustion completeness,  $b_{t1}$  and  $b_{t2}$  are the pre-fire and post-fire fuel loads ( $\text{g/m}^2$ ) respectively. We consider the fraction of the observation area that burns in a spatial two dimensional sense, ignoring the vertical dimension and recognizing that dense tree canopies with high leaf area index may obscure the understory signal (Fuller *et al.* 1997) and so obscure understory burns (Thompson 1993).

The most simple case to model is where the same proportions of the different scene components burn and where the completely burned scene components ( $cc=1$ ) have the same endmember spectra. We assume no noise. In this case the observed burned reflectance for a given wavelength, assuming linear mixing [1], is modeled as [3].

$$x = (1-f) \rho_u + f(1-cc) \rho_u + cc f \rho_b \quad [3]$$

$$0 \leq f \leq 1 \text{ and } 0 \leq cc \leq 1$$

where  $x$  is the observed reflectance,  $cc$  is the combustion completeness,  $f$  is the fraction of the observation area that burned,  $\rho_u$  and  $\rho_b$  are the unburned and completely burned ( $cc=1$ ) endmembers respectively (i.e., the reflectances measured if the observation area contained only the unburned and completely burned material respectively).

### 2.2.3 Study area

Field work was performed in South Africa, in the Kruger National Park (KNP), located along the Mozambican border, and approximately 900 km west in the Madikwe Game Reserve (MGR). Both the KNP and the MGR are within unperturbed savanna ecosystems where inherent soil properties, precipitation, and plant and animal competition regulate biomass available for burning. In South Africa most burning occurs in the dry season, from approximately June to October, when the vegetation fuel (litter, grass, fine leaves and

branches) is dry and senescent. Field work was performed in the 2000 dry season at the locations of prescribed surface fires. The prescribed fires were primarily head fires started from line ignitions aligned along the perimeters of demarked areas and along road and seepage lines.

The KNP is characterized by predominantly weathered granite derived soils with coarse and fine sandy loam, undulating topography (slope between 2 and 5 degrees), and precipitation ranging from 500mm to 900mm per annum (Shea *et al.* 1996). Experimental plots have been purposefully burned in the KNP every 1 to 3 years since 1954 (Biggs and Potgieter 1999). We examined prescribed fires lit on experimental plots near Pretoriuskop, in the south west of the park, and near Satara, in the center of the park. The Pretoriuskop plots are in parkland Sourveld savanna (Gertenbach 1983) with dominant *Combretum collinum/C zeyheri*, *Terminalia sericea* tree species, Sicklebush (*Dichrostachys cineria*) and *Acacia* shrub species, and tall growing *Hyperthelia dissoluta* grasses (Shea *et al.* 1996, Trollope and Potgieter 1986). The plots near Satara are in less wooded Marula Knobthorn savanna (Gertenbach 1983) with *Sclerocarya caffra* (Marula) and *Acacia* tree species and shorter growing grasses such as *Aristida* (Trollope and Potgieter 1986). All of the KNP plots had relatively small amounts of exposed soil (less than approximately 5% by surface area). The prescribed fires consumed the majority of the litter and much of the grass, shrub and tree canopy material below approximately 2 meters. Trees taller than 2m were moderately scorched. Some large fallen wood litter (diameter > 1.5cm) was left unburned at the Pretoriuskop plots. Prior to the fires the vegetation in the different Pretoriuskop plots were observed to be approximately 30-60% green and the Satara plots approximately 10-15% green.

The MGR is composed of savanna parklands (Thorn Bushveld) (Cole 1986) with *Boscia* tree species and dominantly *Arcacia* shrub species and a mix of tall grass species such as *Hyperthelia* as well as short *Aristida* and *Eragrostis* grass species (Scholes 1997). Soils are derived from weathered granite with black turfs and sandy loams, and precipitation ranges from 400mm to 500mm per annum (Schulze 1997). Prescribed fires lit on relatively flat valley plains (slope < 4 degrees) to counteract bush encroachment were examined. As at KNP the MGR prescribed fires consumed the majority of the litter and most of the standing grass. There were slightly more exposed soil surfaces (approximately 5-10% surface area), less standing grass, and a higher shrub density than at the KNP. More shrub material was combusted than at KNP resulting in spatially more patchy burns. Soil color variability was

much higher at MGR than at KNP. Prior to the fires the MGR vegetation was more senescent than at the KNP plots and was observed to be approximately 5-15% green.

## 2.2.4 Satellite data

Radiometrically and geometrically corrected (Level-1G) Landsat ETM+ data acquired shortly before and after the prescribed fires at KNP and MGR were obtained (Table 5). The Landsat data were acquired within 8 days of the different prescribed fires except the pre-fire KNP Pretoriuskop Landsat data which were acquired two months before the fires due to persistent cloud cover. The Landsat ETM+ data were converted from digital counts to at-sensor radiance using Landsat calibration coefficients and then converted to at-sensor reflectance. In this study only the Landsat 30m reflective bands were considered. The shorter wavelength Landsat bands were strongly contaminated by smoke aerosols because of the large amount of biomass burning in the region. Consequently, the at-sensor reflectance data were atmospherically corrected to surface reflectance using the 6S radiative transfer code (Vermote *et al.* 1997). The 6S code was run using Aerosol Robotic Network (AERONET) (Holben *et al.* 1998) aerosol optical depth, water volume and air mass measurements, summarized in Table 5, and assuming KNP and MGR elevations of 400m and 900m respectively. The AERONET data were measured at Skukuza, in the KNP, on the same dates and at approximately the same times as the Landsat overpasses. Although the geolocation accuracy of the Landsat data was high, it was necessary to manually coregister the different dates to improve their coregistration to less than one 30m Landsat pixel. This was achieved by applying integer pixel translational offsets found using ground control points.

**Table 5:** Dates of prescribed fires lit at the Madikwe Game Reserve and Kruger National Park, Landsat ETM+ data characteristics, and AERONET aerosol optical thickness (AOT), water volume and air mass measurements made at Skukuza, Kruger National Park (\* = AERONET data linearly interpolated from June 12<sup>th</sup> measurements made 6:55 GMT and 12:55 GMT to 7:40 GMT).

	Madikwe Game Reserve		Kruger National Park		
Date of prescribed fire 2000	August 18 and August 20		August 14 (Pretoriuskop fires) August 22 (Satara fires)		
ETM acquisition date 2000	August 11	August 27	June 12	August 15	August 31
ETM path/row	172/077	172/077	168/077	168/077	168/077
ETM sun elevation angle (degrees)	38.1	42.6	32.7	39.2	43.9
ETM cloud cover (%)	0	0	34	49	0
ETM overpass time (GMT)	8:05	8:05	7:40	7:40	7:40
AERONET time (GMT)	8:06	8:03	6:55 and 12:55	8:29	7:40
AOT 1020 nm	0.08	0.11	0.12*	0.03	0.13
AOT 870 nm	0.10	0.15	0.13*	0.03	0.17
AOT 670nm	0.16	0.23	0.20*	0.04	0.27
AOT 500 nm	0.27	0.37	0.35*	0.05	0.45
AOT 440 nm	0.33	0.43	0.42*	0.05	0.54
AOT 380 nm	0.42	0.54	0.54*	0.08	0.68
AOT 340 nm	0.50	0.61	0.62*	0.09	0.78
Water (cm)	2.08	2.70	2.77*	2.09	1.57
Air Mass (unitless)	1.51	1.40	2.34*	1.40	1.46

## 2.2.5 Field measurements

Field measurements were made at different sites located within areas burned by the MGR and KNP prescribed fires. The field measurements were used to estimate the site-level combustion completeness and the proportion of the site area that burned. In addition, samples of ash and non-photosynthetic vegetation fuel were collected for spectral analysis. Combustion completeness was calculated from [2] as the proportion of the total pre-fire fuel load (standing grass, standing woody vegetation, and litter) that burned. Estimates of the proportion of the site area that burned were made as part of the field sampling. The measurements were made before and after the fires in 120m x 120m sites that were judged from extensive pre-fire field inspection and examination of the Landsat ETM+ data to have homogenous vegetation. A 120m x 120m site dimension was used as it afforded a manageable size for field measurement, while allowing a large number of different sites to be examined, and was sufficiently large to minimize potential problems with Landsat ETM+ navigation. Data collected during the prescribed burning, including type of fire (head or back fire), length of the flaming front and fire climate parameters (relative humidity and wind velocity), are not reported here but were used in conjunction with visual observations to reject inadequately burned sites. The results from 20 sites (13 KNP and 7 MGR), that were judged from field inspection to have all their litter biomass completely burned, are presented in this paper. It is recognized that some sites may have contained residual uncombusted litter biomass but in general all surface fine fuels were removed by fire. Shea *et al.* (1996) noted that 96 percent of all litter is typically combusted by surface fires in the KNP.

### 2.2.5.1 Pre-fire field measurements

The standing grass fuel load was estimated in two steps. A disc pasture meter, developed by Bransby and Tainton (1977), was used to measure the settling height of the standing grass every 6m along transects spaced 30m apart within the 120m x 120m site. Secondly, standing grass was clipped in 50cm square quadrats located every 30m along the same transects. The clippings were dried and weighed and used to calibrate the disc pasture meter using a transformed linear regression relating the disc meter settling height [cm] to the grass biomass [g] (Trollope and Potgieter 1986). The grass fuel load [ $\text{g/m}^2$ ] was estimated using the regression equation for the site. Litter material (leaf and woody material such as dead wood and twigs less than 1.5cm in diameter) were collected within the same 50cm quadrats. The

litter material was subsequently, dried and weighed, and used to estimate the site litter fuel load [ $\text{g}/\text{m}^2$ ].

The standing woody vegetation (i.e., trees and shrubs) could not be measured by destructive sampling. Consequently, the woody fuel load was estimated using published allometry equations applied to individual measurements of tree and shrub height [m], number of stems, and basal diameter [cm] in three 10m x 10m plots located randomly across the site. The mean of the three plot estimates was taken as the site-level standing woody fuel load [ $\text{g}/\text{m}^2$ ]. Up to 21 allometry equations were used. It is recognized that uncertainties may be introduced by this approach depending on the measurement accuracy and the degree that the allometry equations for individual species were representative of the site's woody vegetation. Allometry equations published by Netshiluvhi and Scholes (2001) derived by sampling KNP vegetation in the dry season were used.

#### 2.2.5.2 Post-fire measurements

The post-fire grass fuel load was estimated using the disc pasture meter only in areas where unburned and partially burned grasses were left standing. The litter fuel load was not measured (only sites judged from field inspection to have all their litter biomass completely burned were considered). The percentage of woody standing biomass left after the fire in the three 10m x 10m plots was estimated visually. Visual estimates were made below the maximum flame scorch height (approximately 2.5m). The post-fire woody fuel load [ $\text{g}/\text{m}^2$ ] was derived by subtracting this percentage from the pre-fire estimate.

Ash samples were collected at each site after the prescribed fires had cooled. Fires of different temperatures are known to produce ash of different shades, with hot fires producing white ash and cool fires producing blacker ash (Stronach and McNaughton 1989). Representative black and white ash samples were collected for subsequent spectral analysis. Estimates of the proportion of the site area that burned were made as part of the field sampling. The 50cm square quadrats located every 30m along transects spaced 30m apart were examined. If a quadrat contained less than 50% unburned material, it was considered unburned. Quadrats were unburned because of heterogeneity of the vegetation fuel and fire behavior, or because they contained bare soil.

## 2.2.6 Reflectance spectra results

The reflectance spectra of black and white ash and non-photosynthetically or 'brown' vegetation fuel samples were measured using an Analytical Spectral Devices (ASD) radiometer. The 'brown' vegetation fuel material was composed of equal parts of the dried grass clippings and litter. Samples from the KNP and MGR sites were measured separately. The measurements were made in the spectral range 400nm to 2500nm with the ASD radiometer aligned perpendicular to the samples to simulate nadir remote sensing and under diffuse laboratory illumination conditions. The measured spectra are shown in Figure 17. Dry long grass spectra collected from the Pierre shale, Canon City, Colorado, provided by the USGS Digital Spectral Library (Clark *et al.* 1993) are also shown.

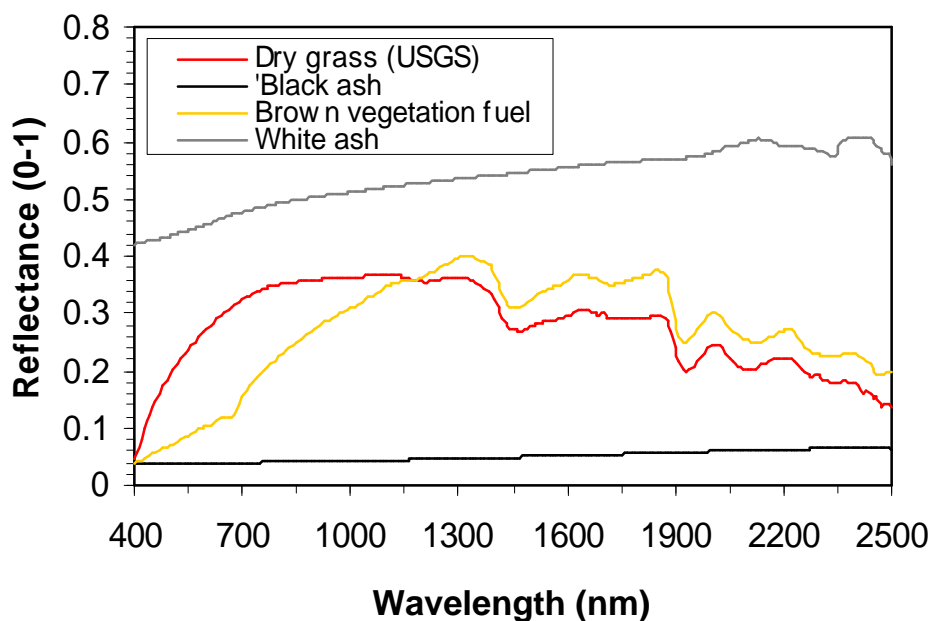


**Figure 17** Reflectance spectra of black and white ash and non-photosynthetically active 'brown' vegetation fuel samples made using an ASD radiometer. The samples collected from the Kruger National Park (KNP) and the Madikwe Game Reserve (MGR), South Africa.

The most obvious spectral change evident in Figure 17 is the decrease in reflectance from unburned 'brown' vegetation fuel to black ash over all but the shortest wavelengths of the 400-2500 nm region. The white ash samples have higher reflectance than the black ash and are higher than both the 'brown' vegetation fuel and the USGS dry long grass spectra. This illustrates an important issue. Fires that are sufficiently hot to produce white ash may not be

detected using methods that expect a drop in reflectance associated with biomass burning. Similarly, methodologies to relate change in reflectance to fire properties, such as combustion completeness, may be biased significantly by the presence of white ash.

### 2.2.7 Illustrative modeling results

The non-photosynthetically active 'brown' vegetation fuel and black ash reflectance measurements illustrated in figure 17 were used as unburned and burned endmembers in [3] to model the relationship between observed reflectance, combustion completeness ( $cc$ ), and the fraction of the observation area that burned ( $f$ ). Figure 18 shows modeled reflectance values over the full range of  $cc$  and  $f$  using the average of the KNP and MGR 'brown' fuel vegetation and black ash ASD reflectance measurements at 1240nm. The 1240nm wavelength has been shown to provide good burned-unburned discrimination in field measurements made in Namibia (Trigg and Flasse 2000), and by empirical examination of MODIS surface reflectance data over most of southern Africa (Roy *et al.* 2002). The reflectance decreases as either  $f$  or  $cc$  increases. The decrease in reflectance is linear as a function of either  $cc$  or  $f$  holding the other fixed. Figure 18 illustrates that there are infinity of  $cc$  and  $f$  combinations that may produce the same observed decrease in reflectance after a fire. This implies that methodologies that attempt to retrieve  $cc$  or  $f$  will not work reliably without knowledge of one of these parameters. This is illustrated using the Landsat ETM+ data and field measurements in the following section.

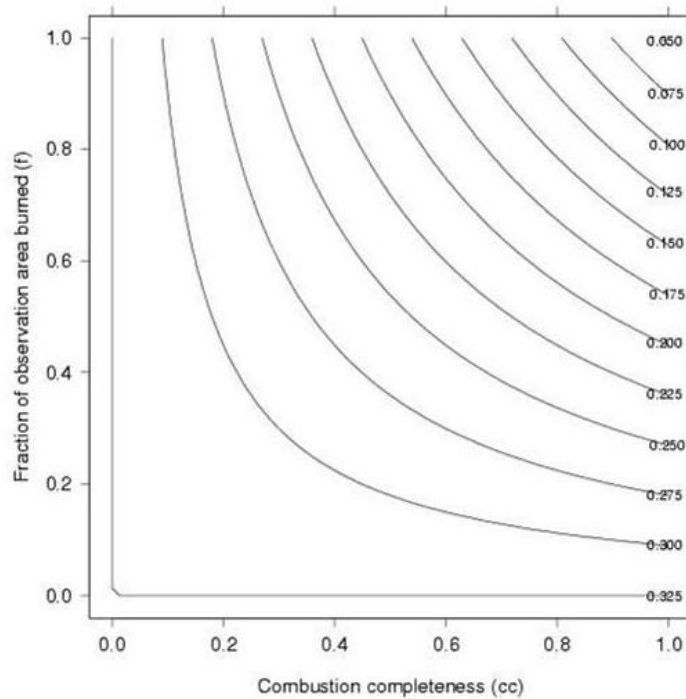


**Figure 18** Modeled reflectances for a hypothetical observation sensed over a fire-affected area with different combustion completeness and fraction of the observation area that burned. Reflectances modeled using the average of the KNP and MGR 'brown' fuel vegetation and black ash 1240nm ASD reflectance measurements ( $r_u = 0.325$  and  $r_b = 0.046$ ).

Spectral indices are used by many remote sensing applications and have been widely used to map the spatial extent of fire-affected areas. This is primarily because spectral indices have attractive properties, such as normalizing certain illumination and topographic variations, and because alternative more physically based approaches, for example, based upon inverting models against reflectance measurements are significantly less easy to implement (Verstraete and Pinty 1996, McDonald *et al.* 1998). Figure 11 shows modeled reflectance plotted as a function of  $f$  for fixed  $cc$  using average KNP and MGR 'brown' vegetation fuel and black ash ASD reflectance measurements at 1240nm and 2130nm. The 2130nm wavelength is less sensitive to burning than 1240nm (the reflectance gradient is smaller) which has been observed previously (Trigg and Flasse 2000, Roy *et al.* 2002). Figure 12 shows a spectral index computed as the difference between the 2130nm and 1240nm reflectance divided by their sum. This ratio spectral index is illustrated because it appears to provide good burned-unburned discrimination using MODIS data. We note that similar indices have been found to provide good burned-unburned discrimination using Landsat TM band 4 (760-900 nm) and band 7 (2080-2350nm) (Lopez Garcia and Caselles 1991) and using AVHRR band 1 (580-

680nm) and the reflective component of the middle-infrared AVHRR band 3 (3550-3930nm) (Pereira 1999, Roy *et al.* 1999). The spectral index values were computed using the reflectance data illustrated in Figure 11. Unlike the reflectance data, the spectral index values decrease in a non-linear manner with respect to  $f$  (or to  $cc$ ). This implies that ratio type spectral indices may be sensitive in a non-linear manner to the size and combustion completeness of the fire. Consequently they may provide variable detection capabilities when used to map fire-affected areas or to extract fire properties.

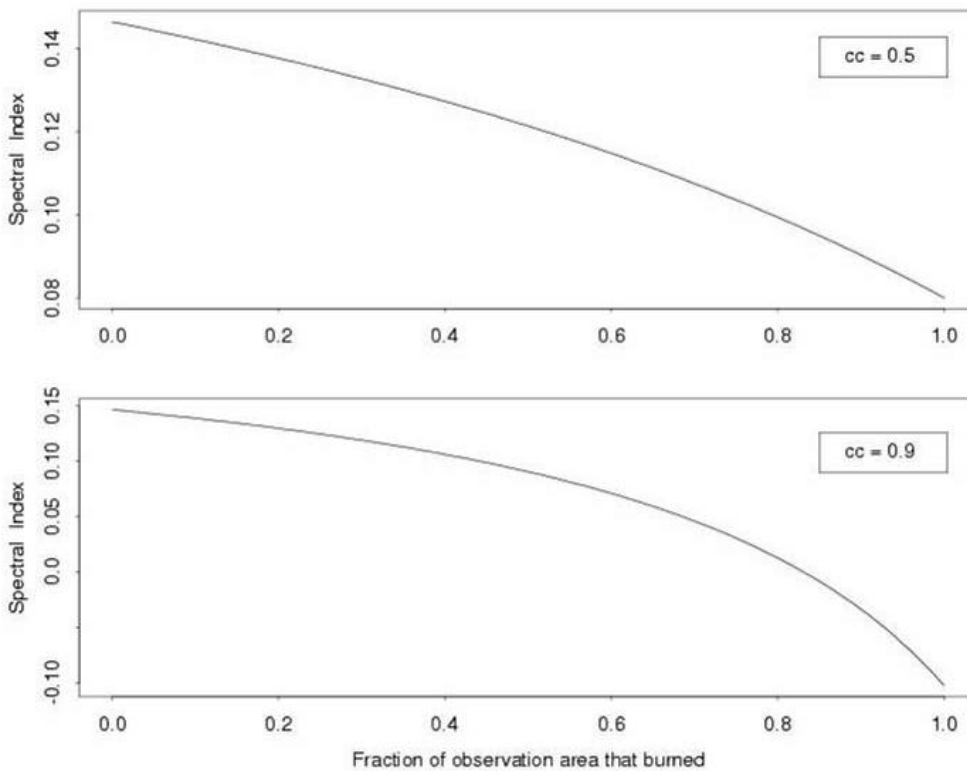


**Figure 11** Modeled reflectances for a hypothetical observation sensed over a fire-affected area with combustion completeness = 0.5 (top) and combustion completeness = 0.9 (bottom) plotted as a function of the fraction of the observation area that burned. Reflectances modeled at 1240nm (solid line) and 2130nm (dashed line) using the average of the KNP and MGR 'brown' fuel vegetation and black ash ASD reflectance measurements at these wavelengths (1240nm:  $r_u = 0.325$  and  $r_b = 0.046$ ; 2130nm:  $r_u = 0.242$  and  $r_b = 0.074$ ).

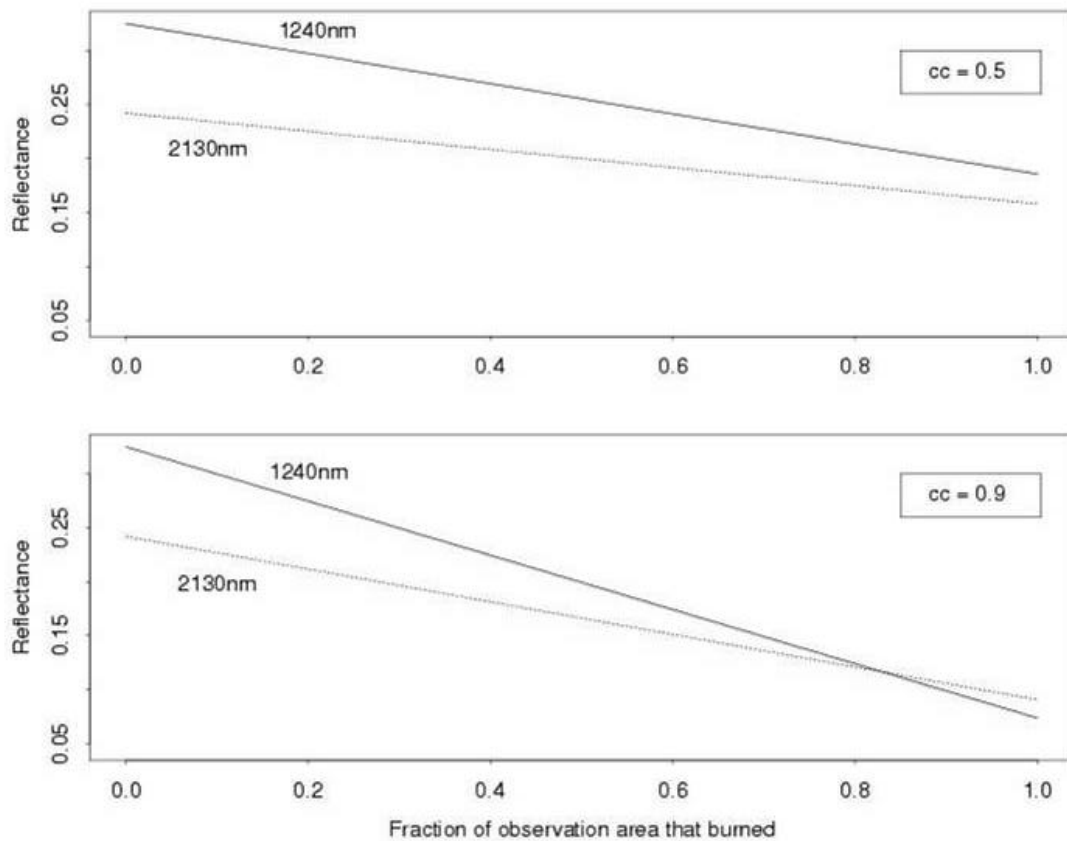


**Figure 12** Modeled spectral index values for a hypothetical observation sensed over a fire-affected area with combustion completeness = 0.5 (top) and combustion completeness = 0.9 (bottom) plotted as a function of the fraction of the observation area that burned. Spectral index values computed as  $(r_{1240\text{nm}} - r_{2130\text{nm}}) / (r_{1240\text{nm}} + r_{2130\text{nm}})$  using the reflectance data illustrated in Figure 11.

In biomass burning mapping approaches the definition of the magnitude of spectral change associated with the conversion of vegetation to burned vegetation is critical. Figure 13 illustrates the change in reflectance for two fires modeled using different products of  $f$  and  $cc$ , illustrating a small and/or incomplete burn ( $f*cc = 0.25$ ) and a larger and/or more complete burn ( $f*cc = 0.5$ ). The change in reflectance is plotted as a function of the pre-fire reflectance to simulate different types of surface. Thresholds based on relative rather than absolute changes have been suggested as being useful to account for variability of spectral values due to biome type, soil characteristics etc. (Eva and Lambin 1998a). Accordingly, both the absolute change in reflectance (Figure 13a) and the relative change in reflectance (Figure 13b) are shown (solid lines). These reflectance data were modeled using the average of the KNP and MGR black ash 1240nm ASD reflectance measurements. Figure 13 illustrates that burns with the same  $f$  and  $cc$  product exhibit reflectance changes that depend on the pre-fire

reflectance. Evidently, burns on highly reflective surfaces (e.g., dry senescent grass) are more likely to be detected than burns occurring on less reflective surfaces (e.g., certain dense forest covers) and larger/completer burns are more likely to be detected than small/incomplete burns. A reason for dry senescent vegetation being most discriminate from ash reflection may be that with increasing wavelengths in the mid-IR the signal is more insensitive for water moisture in vegetation (Trigg 1999; Stroppiana *et al.*, 2002).

For example, in figure 13a an absolute reflectance threshold more negative than -0.15 will fail to detect the small/incomplete burn and will only detect the larger/completer burn if the pre-fire reflectance is greater than 0.4. The relative change in reflectance shown in figure 13b is non-linearly dependent on the pre-fire reflectance. This non-linearity is most pronounced when the pre-fire reflectance is low, implying caution in the application of relative reflectance thresholds for detection of burning over dark (low reflectance) surfaces.

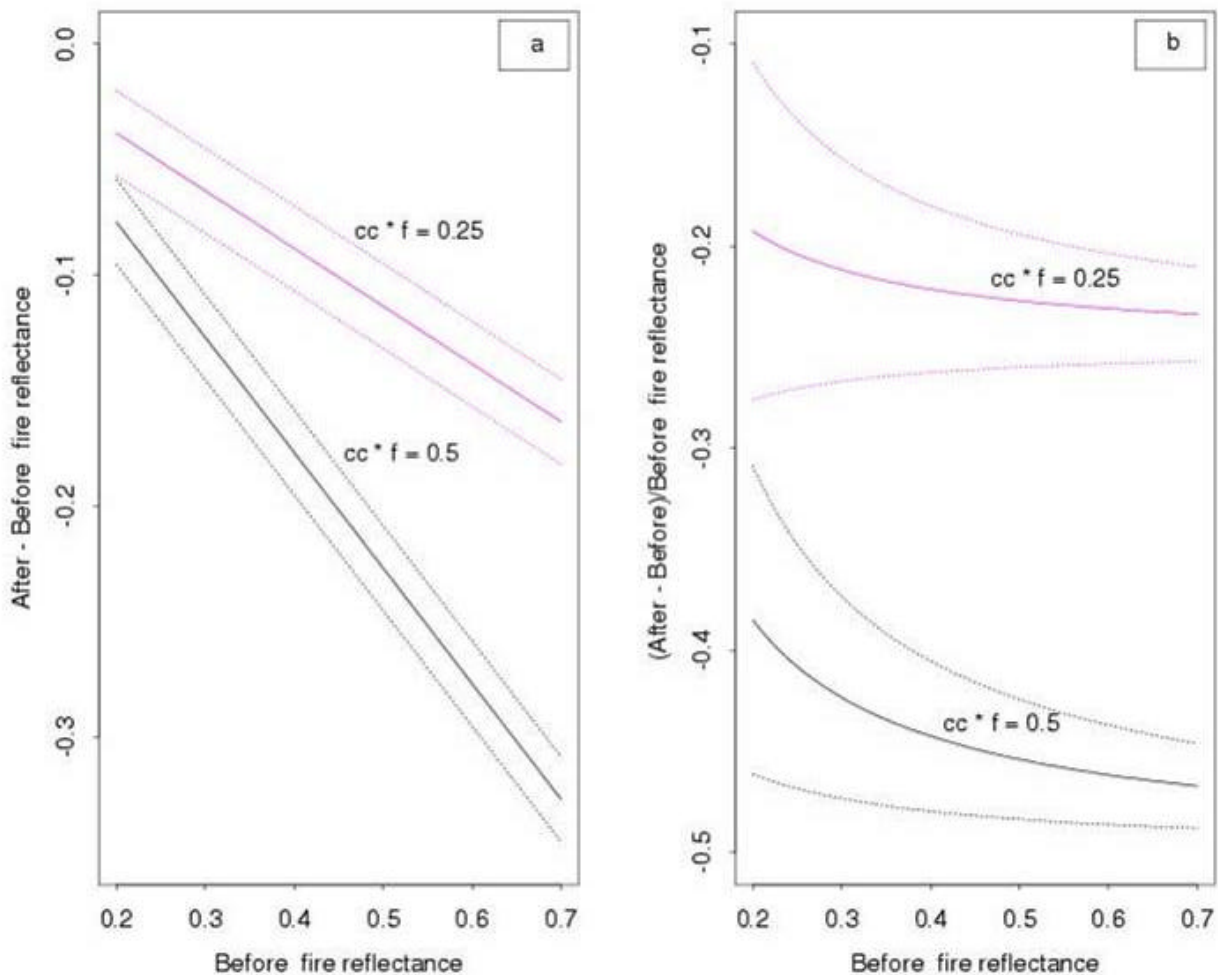


**Figure 13** Modeled absolute (left) and relative (right) change in reflectance for a hypothetical observation sensed over of fire-effected areas with different combustion completeness ( $cc$ ) and fractions of the observation area that burned ( $f$ ), illustrating a small and/or incomplete fire ( $f*cc = 0.25$ ) and a larger and/or more complete fire ( $f*cc = 0.5$ ). Reflectances modeled using

the average of the KNP and MGR 'brown' fuel vegetation and black ash 1240nm ASD reflectance measurements ( $r_u = 0.325$  and  $r_b = 0.046$ ). The dashed line shows modeled  $1\sigma$  errors computed assuming normally distributed 1240nm reflectance errors with a mean value of zero and  $1\sigma = 0.013$ .

Remote sensing data are noisy, due to the sensing system optics and electronics, the effect of the atmosphere, and data processing. The impact of noise is illustrated by the dashed lines in Figure 13 which show the  $\pm 1\sigma$  (one standard deviation) error computed analytically from [3] using standard propagation of variance formula (Cooper 1987) and assuming that the before and after fire reflectance values are independent. A reflectance error with a mean value of zero and  $1\sigma = 0.013$  is modeled corresponding approximately to the MODIS 1240nm band land surface reflectance error inferred from preliminary validation of the MODIS land surface reflectance product (Vermote *et al.* 2002). The modelled error in the absolute change in reflectance is 0.018 ( $1\sigma$ ) and is independent of the pre-fire reflectance (Figure 13a). The modeled error in the relative change in reflectance decreases as the pre-fire reflectance increases (Figure 13b), reinforcing the earlier observation concerning caution in the application of relative thresholds for detection of burning over dark surfaces. Noise imposes a lower limit on change detection capabilities. Figure 14 shows modeled absolute change in reflectance over the full range of  $cc$  and  $f$  using the MGR and KNP 'brown' fuel vegetation and black ash 1240nm ASD reflectance measurements. Given the assumptions implicit to this modeling then the illustrated  $cc$  and  $f$  values with absolute reflectance changes more negative than -0.018 are not expected to be detected reliably using MODIS 1240nm land surface reflectance data. The model results illustrated in Figure 14 indicate that burns with  $cc*f$  less than 0.08 and less than 0.05 will not be detected reliably at the MGR and KNP sites respectively. Larger and/or more complete burns will fail to be detected at the MGR site than at the KNP site because the spectral contrast between the brown vegetation fuel and black ash samples collected at the MGR is smaller than at KNP. Clearly, other unmodeled factors, such as the reduction in spectral contrast since the time of fire and ash reflectance, will also impact detection capabilities.

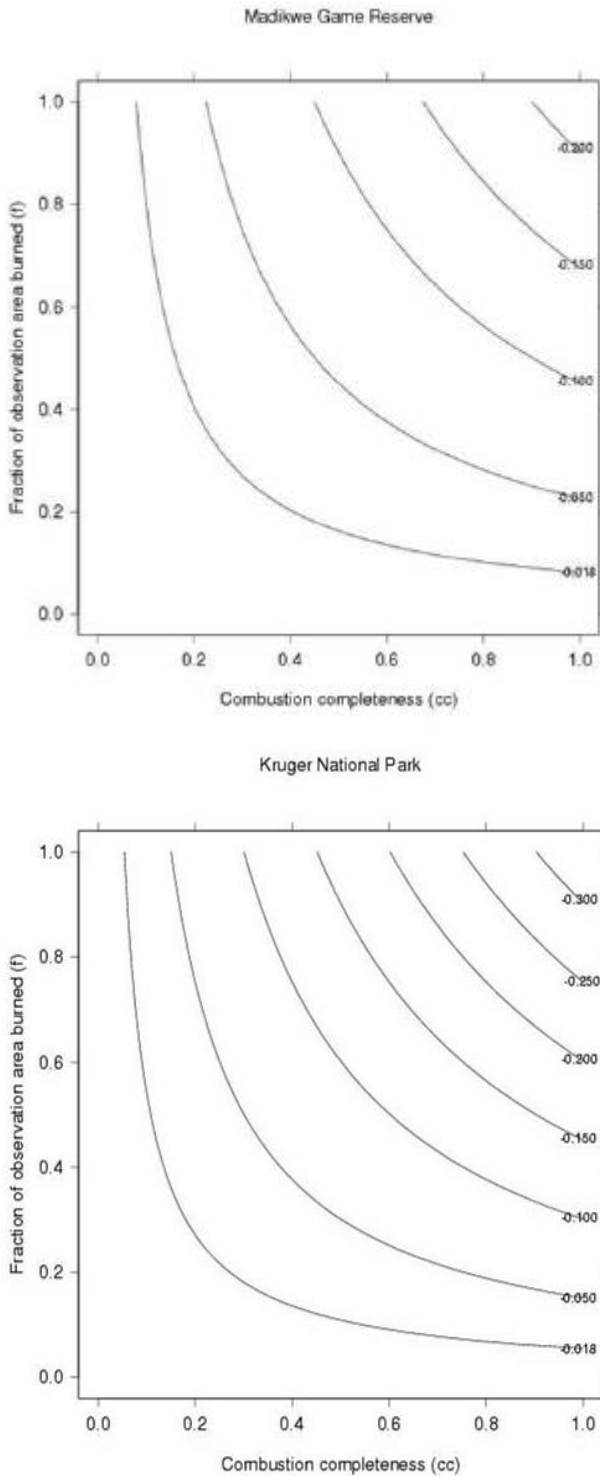


**Figure 14** Modeled absolute change (after - before fire) reflectance for a hypothetical observation sensed over a fire-affected area with different combustion completeness and fractions of the observation area that burned. Model results shown separately for the MGR 'brown' fuel vegetation and black ash 1240nm ASD reflectance measurements ( $r_u = 0.269$  and  $r_b = 0.047$ ) and the KNP 'brown' fuel vegetation and black ash 1240nm ASD reflectance measurements ( $r_u = 0.378$  and  $r_b = 0.046$ ).

## 2.2.8 Comparison of Landsat ETM+ reflectance and ground measurements

Figure 15 illustrates the Landsat ETM+ surface reflectance data for the 13 KNP and 7 MGR sites before and after the prescribed fires. The mean of the cloud-free 30m pixel reflectance values corresponding to each 120 x 120 m site are shown. In general burning reduces the mean surface reflectance, although for ETM+ bands 1, 2, 3 and 7 the differences between the mean unburned and burned reflectance values are small, which is expected from previous studies in African savannas (Landmann 1999). Some of the KNP sites have higher post-fire than pre-fire ETM+ band 1 (450-515 nm) reflectance which is probably due to inadequate aerosol correction of the shortest ETM+ wavelength band associated with the use of interpolated AERONET data (Table 5). The pre-fire ETM+ band 4 (750-900nm) KNP reflectance values are considerably higher than the MGR values because the KNP vegetation are less senescent (greener) with a smaller proportion of exposed soil surfaces. The ETM+ band 4 soil reflectance was approximately 0.3 at KNP and varied from approximately 0.2 to 0.3 at the MGR sites (found by examination of visually identified soil pixels).

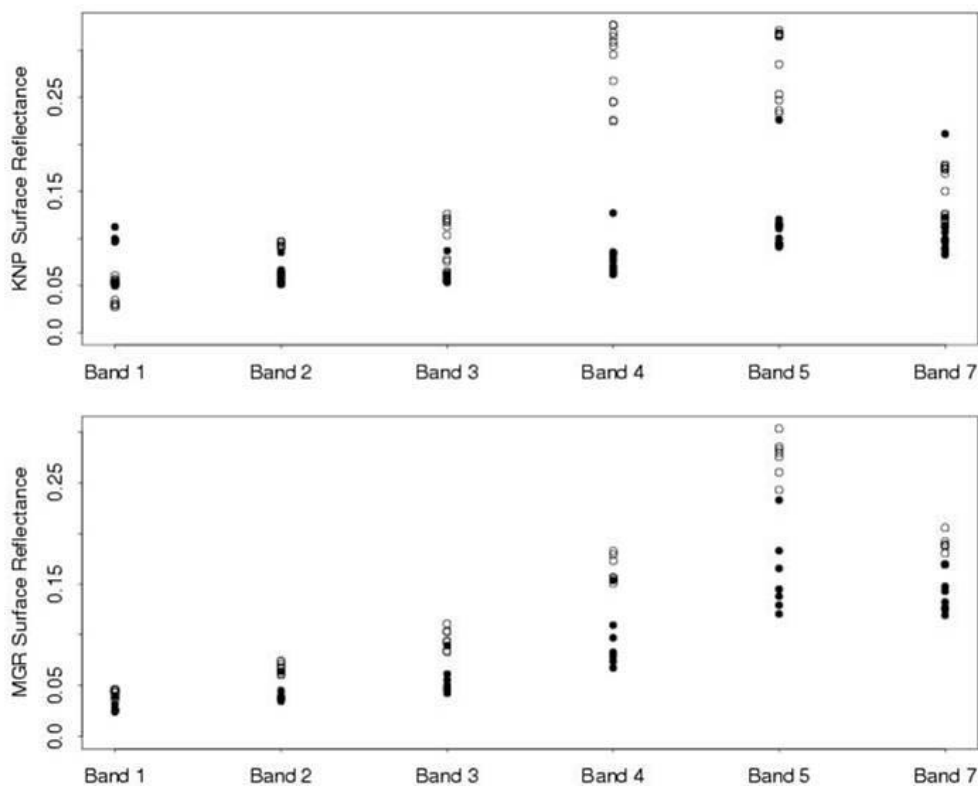


**Figure 15** Landsat ETM+ surface reflectance data acquired before prescribed fires (open circles) and after prescribed fires (closed circles) at 13 sites in the Kruger National Park (KNP) (top) and at 7 sites in the Madikwe Game Reserve (MGR) (bottom). The mean

reflectance of the cloud-free 30m pixels falling within each 120m x 120m site are shown for Landsat bands 1 (450-515nm), 2 (525-605nm), 3 (630-690nm), 4 (750-900nm), 5 (1550-1750nm) and 7 (2090-2350nm).

Figures 8-10 illustrate comparisons of the field-based estimates of site-level combustion completeness ( $cc$ ) and the proportion of the site area that burned ( $f$ ) with the Landsat ETM+ band 4 data acquired before and after the prescribed fires. Figures 8 and 9 show the absolute change in reflectance plotted as a function of  $cc$  and  $f$  respectively for the different 30m pixels (solid dots) at the 13 KNP and 7 MGR sites. Figure 10 shows the absolute change in reflectance plotted as a function of the product of  $cc$  and  $f$ . Simple linear regression fits of these data and the coefficient of determination ( $R^2$ ) (used to indicate goodness of fit) are illustrated (solid lines). All of the illustrated regressions (solid lines) are significant ( $p < 0.001$ ). Simple linear regression fits of the mean of the 30m ETM+ pixel values falling over each site are also shown (dashed lines) with  $R^2$  values shown in the figure legends in parentheses. The regressions computed using the mean rather than the original pixel values produce similar fits but have inflated  $R^2$  values and are significant at lower levels of confidence (which is expected from statistical theory). ETM+ band 4 results are illustrated because they consistently provided higher  $R^2$  values than any other band, with similar results and only slightly lower  $R^2$  values found using ETM+ band 5 (1550-1750 nm). The assumptions implicit to the linear regression analysis are probably not met here, in particular the  $f$  and  $cc$  values cannot be assumed to have negligible error. Consequently, caution must be applied in the interpretation of these results.

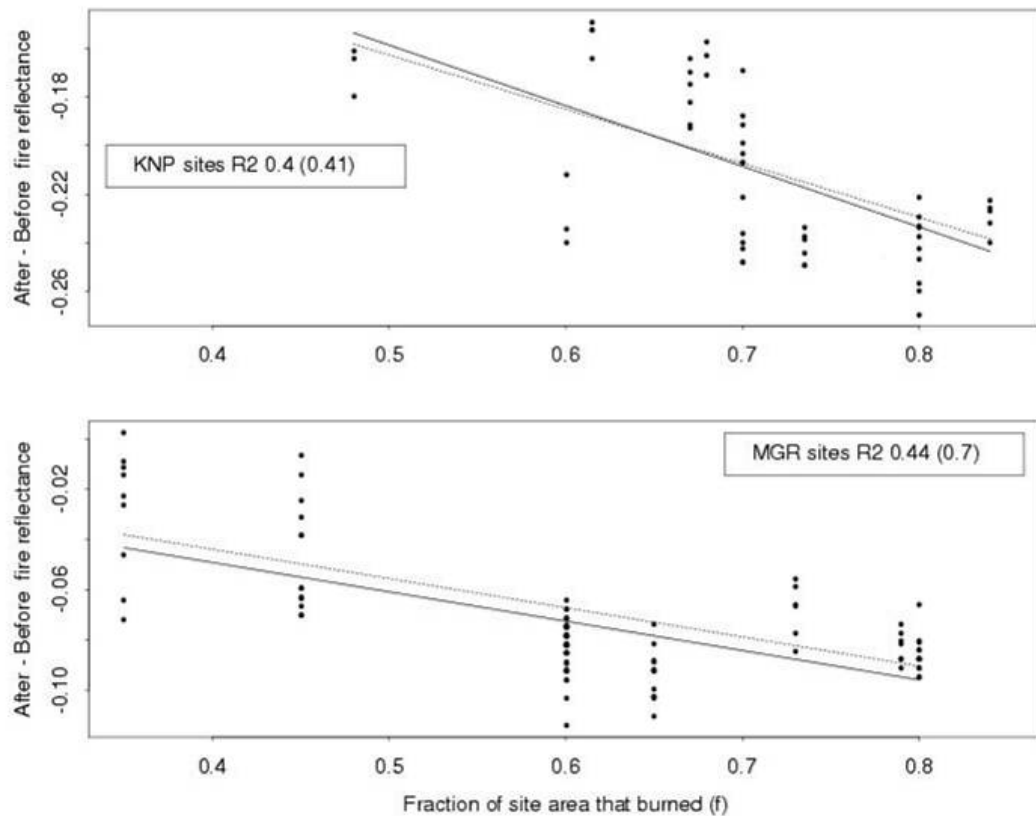


**Figure 16** Change in Landsat ETM+ band 4 surface reflectance data acquired before and after prescribed fires at 13 sites in the Kruger National Park (KNP) (top) and at 7 sites in the Madikwe Game Reserve (MGR) (bottom) plotted as a function of site-level estimates of combustion completeness. The change in reflectance for cloud-free 30m pixels falling within each 120m x 120m site (dots) with simple linear regression fits of these data (solid lines) and regression fits of the mean of the pixel values at each site (dashed lines,  $R^2$  in parentheses) are shown.

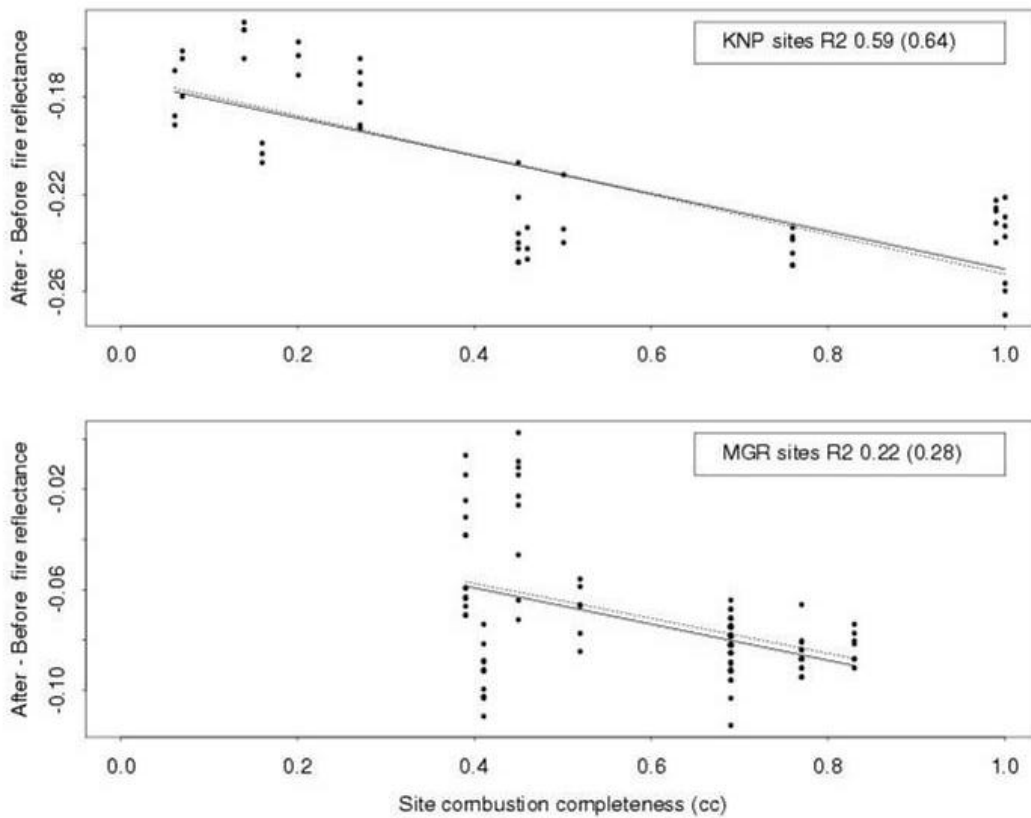


**Figure 17** Change in Landsat ETM+ band 4 surface reflectance data acquired before and after prescribed fires at 13 sites in the Kruger National Park (KNP) (top) and at 7 sites in the Madikwe Game Reserve (MGR) (bottom) plotted as a function of site-level estimates of the fraction of the site area that burned.

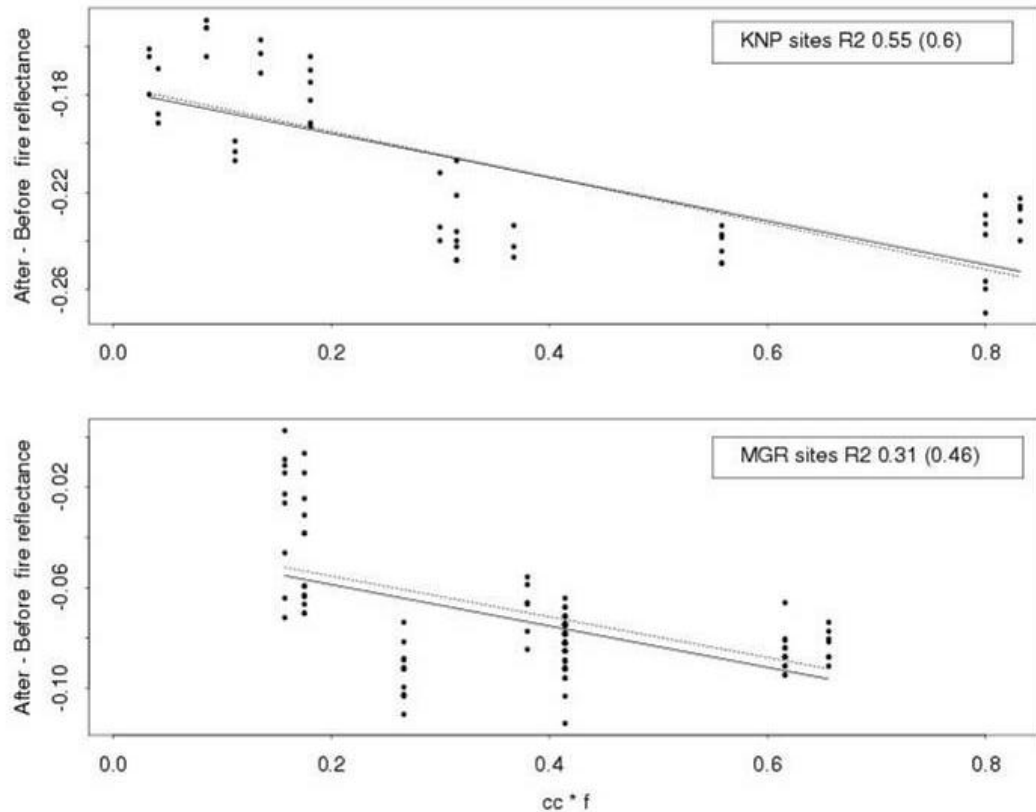


**Figure 18** Change in Landsat ETM+ band 4 surface reflectance data acquired before and after prescribed fires at 13 sites in the Kruger National Park (KNP) (top) and at 7 sites in the Madikwe Game Reserve (MGR) (bottom) plotted as a function of the product of estimates of the fraction of the site area that burned and the site-level combustion completeness.

The changes in ETM+ band 4 reflectance caused by burning are greater for the KNP than the MGR sites (Figures 7-10). This is primarily because the pre-fire reflectance values are higher at KNP than MGR (Figure 15) and not because the KNP sites have higher values of  $cc$  and  $f$  (Figure 18). This underscores the observation made in the previous section that burns on highly reflective surfaces are more likely to be detected than burns occurring on less reflective surfaces. The variation in the change in reflectance at individual sites (Figures 8-10) is no more than approximately 0.04 and 0.06 for the KNP and MGR sites respectively. This variation may be due to noise in the ETM+ surface reflectance data and inadequate coregistration of the different dates. The variation may also be due to spatial differences in the pre-fire state and the homogeneity of fire effects across each site. For example, the variation may be greater at the MGR sites than at KNP because the MGR burns and underlying soil were spatially more heterogeneous. However, we note that the greatest

variations occur for the two MGR sites that have the lowest  $cc$  and  $f$  values ( $cc \cdot f < 0.2$ , Figure 18) and include pixels with small reflectance differences (less than 0.02 magnitude). These reflectance differences are sufficiently small that they may be close to the meaningful change detection limit when noise in the ETM+ surface reflectance data is taken into consideration. Small amounts of highly reflective white ash were observed at most of the sites after the prescribed fires (approximately 10% white to 90% black ash) but we have insufficient data to quantify the likely impact on the results presented here.

Figures 8-10 illustrate that both  $cc$  and  $f$  explain variation in the change in reflectance due to burning. This finding supports the simple modeling results presented in the previous section. At the KNP sites  $R^2$  values of 0.59 and 0.40 are found for  $cc$  and  $f$  respectively. At the MGR sites  $R^2$  values of 0.22 and 0.44 are found for  $cc$  and  $f$  respectively. The relationship between the change in reflectance and  $cc$  is stronger at KNP than at MGR. This may be related to the greater spectral contrast observed between the 'brown' vegetation fuel and black ash samples at KNP than MGR. However, this may also be due to sensitivity of the regression analysis to the relatively small range of  $cc$  values collected at the MGR sites (approximately 0.4 - 0.8) compared to the KNP sites (approximately 0.1 - 1.0) (Figure 16). The MGR data, for the limited range of  $cc$  cases examined, have a stronger relationship between change in reflectance with  $f$  than with  $cc$  (Figure 17). This may be indicative of the spatial heterogeneity in the pre-fire and post-fire reflectance at the MGR sites due to in particular the large soil variability at MGR. In all cases, caution in the interpretation of these results must be exercised, because of the small number and distribution of  $f$  and  $cc$  values relative to their underlying population (Figure 14). In general, although statistically significant, the regression relationships illustrated in Figures 8-10 are not particularly strong. Evidently, if relationships of this nature were used in a predictive capacity, for example to predict  $cc$  and/or  $f$ , then they would need to be applied in a site specific manner.

## 2.2.9 Conclusions

The field and satellite observations and modeling results described in this paper demonstrate that both the combustion completeness ( $cc$ ) and the fraction of the observation area that burns ( $f$ ) influence the change in reflectance that occurs after the passage of fire. Consequently, methodologies that use change in reflectance to retrieve  $f$  or  $cc$ , or related fire properties, may not work reliably without prior knowledge of one of these two parameters. In addition, the

results demonstrate that the change in reflectance observed for fires with the same product of  $cc$  and  $f$  will depend on the pre-fire reflectance. Further, the action of certain high temperature fires is to deposit highly reflective white ash that may increase rather than decrease the reflectance after a fire (Stronach and McNaughton 1989) and so bias methodologies that expect a drop in reflectance associated with burning. As pre-fire reflectance, fire temperature,  $cc$  and  $f$  vary as a function of many factors, empirical relationships made between ground observations of these parameters and changes in reflectance may only be applicable in a local context. For example, fire monitoring and management in protected areas (e.g., Biggs 2002) and local post-fire ecosystem rehabilitation studies (e.g., Miller and Yool, 2002).

The findings described here imply that algorithms developed to make spatially explicit maps of fire-affected areas have variable detection capabilities in space and time. Algorithms may detect burns with different degrees of heterogeneity as the pre-fire reflectance changes (e.g., due to vegetation phenology), as the combustion completeness changes (e.g., due to the seasonally and temporal changes in the fire regime), and as the degree of spatial fragmentation of the burned surface changes. We recognize that detection variability may always be present, especially when classification approaches are used. However, this observation has implications for the utility of such data, and implies that their accuracy should be validated by examination of regions that include representative variations of  $cc$ ,  $f$  and pre-fire reflectance. The model presented in this paper is simple and is probably not representative of most fire-affected surfaces. However, the modeling results show that methods to map fire-affected areas may be less sensitive to noise and provide less variable detection capabilities with respect to  $f$  and  $cc$  by thresholding absolute changes in reflectance, rather than thresholding relative changes in reflectance or ratio type spectral band indices.

Finally, we note that the product of  $f$  and  $cc$  is related to the change in reflectance, and that this product multiplied with the fuel load [ $\text{g}/\text{m}^2$ ] provides an estimate of the biomass fraction burned [ $\text{g}$ ] in a satellite observation. Retrieval of this information by remote sensing would provide a major advance over anecdotal estimates of combustion completeness and assumptions that the entire satellite observation area burned that have been previously used for emissions estimation (e.g., Scholes *et al.* 1996, Barbosa *et al.* 1999). The use of well calibrated, atmospherically corrected, cloud-screened, reflectance data, combined with less empirical mapping approaches, based for example upon inverting bi-directional reflectance models against surface reflectance measurements (Roy *et al.* 2002), may possibly allow the

development of algorithms with known detection limits defined with respect to  $f$  and  $cc$  and the retrieval of the product of  $f$  and  $cc$ . Further work is required in these respects.

## 2.2.10 Summary

The relationship between changes observed in multi-temporal remotely sensed data and disturbance processes are increasingly being studied. The possibility of mapping both the location and degree of change and retrieving information concerning the disturbance process are primary goals. This paper studies changes in reflective wavelength data caused by the action of fire and illustrates, by simple modeling, and with field and satellite observations. Fire heterogeneity information using spatial explicit satellite data sets is an important parameter to input and improve emission models or evaluate the fire effects on biodiversity. Implications and recommendations for the development of methods to retrieve the completeness of combustion and the proportion of the surface area that burned, and methods to map the spatial extent of fire-affected areas with known detection capabilities, using multi-temporal reflective wavelength data are made.



## 2.3 Estimating fire intensity and fire severity from remote sensing information for experimental fires in the Kruger National Park (KNP)

T. Landmann\*

(South African Journal of Science – *in press*)

### 2.3.1 Introduction

Satellite imagery provides rigorous information typically over large or remote areas where direct characterization of fires cannot be feasible measured or observed by the park or resource managers. Remote sensing methods use portions of the electromagnetic (EM) spectrum not visible to the eye to extract a wide range of fire related information.

Regional measurements of fire intensity and fire severity on fire affected areas are seldom measured by fire specialists in the field (FLASSE *et al.*, 2003)

Fire intensity is largely influenced by fire behaviour parameters such as fuel load, fuel moisture, and vegetation compaction and is expressed as either heat energy release per active fire pixel from remote sensing (KAUFMAN AND JUSTICE, 1998) or heat release over time and area/perimeter (kilowatts/meter) as described by flame height, length of flaming front and type of burn. (TROLLOPE, 1992; TROLLOPE AND TANTON, 1996) STRONACH & MCNAUGHTON (1998) associated combustion efficiencies of fires in the Serengeti with different grey values of ash and stipulated this as being retrospective indicators of fire intensity.

Fire severity is dependant on the pre fire vegetation status and the magnitude of conversion from vegetation to ash and charcoal by the heat of the fire. Defining the magnitude of change in reflection from using remote sensing seems increasingly critical in recent multi-temporal methodologies to map fire scars (ROY *et al.*, 2002). Ecologically fire severity is the fire impact that integrates the physical, biological and chemical changes on a site as a result of fire disturbances (ROGAN AND FRANKLIN, 2001). This inevitable entails effect on the rehabilitation

---

\* CSIR Environmentek, Meiring Naude avenue, Pretoria, South Africa, and Department of Landscape Ecology, University of Göttingen, Germany

of individual species; different vegetation components affected by fire and individual species resilience, and the downward fire heat flux and its effect on the soil (TROLLOPE AND TANTON, 1986; ROGAN AND FRANKLIN, 2001; MICHALEK *et al.*, 2000; YOKELSON *et al.*, 1999; VAN DE VIJVER, 1999).

Fire intensity and severity have important consequences for fire regimes of a vegetation biome (*i.e.* fire intensity, frequency of occurrence within a biome, seasons of burns and type of fire). Ultimately changes in fire severity will result in a change in ecological impact within a vegetation biome, thus modifying ecosystem composition and functioning (KAUFMAN AND JUSTICE, 1998; TROLLOPE AND TANTON, 1986; ROGAN AND FRANKLIN, 2001).

Applying regular intense savanna fires, for instance, may result in growth of the grass component and simultaneous suppression of the woody savanna component. High intensity fires will prevent juvenile trees from escaping to a height where the canopy is no longer killed or affected by fire (BOND, 1997). Fire intensity and severity are also important input parameters in emission models that require estimates of the fraction of above-ground fuel that is consumed by the fire (MICHALEK *et al.*, 2000).

Furthermore spatial fire severity and fire intensity information may be required by resource managers in national or private reserves to monitor this component of the fire regime (CHAFFEY AND GRANT, 2000). Areas that require post-fire management for ecological impact analyses can be located and assimilated (CAETANO *et al.*, 1995), while fire reports, made by national park or resource managers, can be corroborated effectively. Using the spatial information the current fire situation of a managed region can be assessed and areas that are deviating from the intended fire policy can be identified from the spatial satellite data.

Recent remote sensing methods to map fire scar severity mainly used high resolution Landsat Thematic Mapper (TM) and Landsat Multiple Spectral Scanner (MSS) satellite data. Most of the studies used Principle Component Analyses (PCA), vegetation indices and trained or untrained classification techniques to map ordinal classes of severity. The remote sensing information was mostly combined with field information on vegetation and soil heat penetration criteria (PATTERSON AND YOOL, 1998; COCHRANE AND SOUZA, 1998; SALVADOR *et al.*, 2000).

In South African national park areas only two studies are known that map fire severity using 30-meter Landsat TM. Thompson (THOMPSON, 1993) investigated the use of single-date Landsat-5 Thematic Mapper Normalized Differential Vegetation Index (NDVI) data in a

once-off study in Hluhluwe-Umfolozi Game Reserve in eastern South Africa. HUDAK (1998) used multi-spectral principle component classification methods to map fire severity in the Madikwe Game Reserve in the north-western part of South Africa. Several recent studies have implied mapping fire severity using multi-temporal Landsat information (MICHALEK *et al.*, 2000; ROGAN AND YOOL, 2001; MILLER AND YOOL, 2002), and only one other study by ROGAN AND FRANKLIN (2001) is known that uses spectral mixing analysis to estimate fire severity at a Landsat sub-pixel scale in southern California.

This paper propagates a new method of calculating fire severity from 30-meter Landsat information using the fire intensity and the respective combustion completeness of a burnt pixel. The prospect of deriving fire intensity from the nature that is colour of the ash is investigated using the sub-pixel Landsat abundances of whiter and completely black ash spectral signatures. The combustion completeness from Landsat ETM+ is investigated as an indicator of fire intensity and as an indicator of the abundance of non-photosynthetic vegetation left on the burnt pixel area. The possibility of using both the combustion completeness and the fire intensity in a burnt pixel for quantitatively mapping fire severity is probed. The sub-pixel information on fire intensity and fire severity are substantiated with field information on the amount of pre-fire fuel phytomass and fractional land cover observations from visual field inspections. Phytomass is herein defined as the above-ground live and dead biomass that is available for burning, sometimes also called biomass fuel. Extensive fieldwork was performed on a section on small seven hectare experimental burn blocks during the Southern African Fire-Atmosphere Research Initiative (SAFARI) 2000 (SWAP *et al.*, 2002) intensive campaign in the KNP.

## 2.3.2 Methodology

### 2.3.2.1 Site description

Six annually burnt experimental burn plots (EBPs) in the southern part of the Kruger National Park (KNP) near Pretoriuskop were investigated. Three experimental burn plots (EBPs) were on the Shabeni set of burn plots; the other three were on the Kambeni set of burn plots. The EBPs are part of the KNP long-term burning experiment initiated in 1954, and each string is located within different savanna types according to GERTENBACH (1983) and each burn plot is about seven hectare in size. Both the Shabeni and the Kambeni burn plots are within the Cluster Leaf/Rock Fig Sour Bushveld savanna type (GERTENBACH, 1983). The park managers set prescribed fires on the EBPs at different intervals and seasons. A complete overview of the

utility of the EBPs is provided by TROLLOPE *et al* (1998). Although the EBPs are designed to be within unperturbed savanna ecosystems, where inherent soil properties, precipitation, and plant and animal competition regulate biomass available for burning (KAUFFMAN *et al.*, 1992), they may be heterogeneous in terms of soil type and plant community distributions (TROLLOPE *et al.*, 1998). A homogeneous vegetated sampling frame was hence chosen on each respective EBP to sample above-ground phytomass in dry matter (DM)  $\text{g/m}^2$ . Bare soil and rock surfaces only make up less than 5 percent of the total land cover on each of the EBPs; the average tree and shrub cover density at the Shabeni and the Kambeni plots was measured at 19 and 29 percent respectively (established from tree canopy cover measurements for the whole burn plot). The slope varies between three to five degrees and precipitation ranges from 500mm to 750mm per annum for this savanna type (GERTENBACH, 1983). The vegetation homogeneity makes the investigations using satellite data more plausible, because less spatial variability in the satellite reflection is accounted for.

### 2.3.2.2 Field data collection

The Kambeni and the Shabeni strings of EBPs were investigated for their aboveground phytomass [ $\text{gDM/m}^2$ ]. The satellite measurement methodology required the incorporation of ground measurements: phytomass information is needed to parameterize the fire intensity and fire severity information from remote sensing. Three burn plots on each string respectively were investigated and fuel sampling was done in a clearly marked 120 meter by 120 meter sampling frame on each EBP.

Pre fire grass fuel was determined in each EBP using the disc pasture meter according to BRANSBY AND TAINTON (1977) and following a prescribed sampling design within the 120 meter frame. Grass was also clipped in 15 quadrats in order to recalibrate the regression equation for the disc pasture meter developed for this savanna biome by TROLLOPE AND POTGIETER (1986). A total for 75 disc meter readings were taken in the sampling frame to get a good spatial estimate. Woody biomass was determined for each EPB using allometry equations according to NETSHILUVHI AND SCHOLE (2001). The input parameters required were basal stem diameters [cm], number of stems and tree and shrub height [m] estimates for individual species. The woody biomass estimates were determined in three randomly selected 10 meter by 10-meter plots within the sampling frame. Tree cover density was estimated within each sampling frame using a spherical densiometer at 16 locations in the frame (LEMMON, 1957). Grass mass and woody mass up to a height of two meter were combined to

give total available phytomass [ $\text{g}/\text{m}^2$ ] as an average for the 120 meter sampling frame on each EBP.

Pre and post fire fractional estimates on the different land cover components found on each of the EBPs were determined using visual inspection. A consistent sampling protocol using three observers was implied on each EBP. The percent cover of bare soil, percent covered by trees/shrubs in different heights, percent green leaf of the respective woody vegetation and percent covered by standing grass were noted. The inferred ground information on land cover proportions fractional land cover can be used to verify ‘training’ pixels of “pure” examples of the different land cover categories estimated from remote sensing (SETTLE AND CAMPBELL, 1998). Primarily the fractional land cover information was used to verify the spectral unmixing calculations.

During burning field notes were taken on the completeness of the individual fires so as to possibly reject an EBP because the area was not combusted homogeneously. Usually experimental block burning results in relatively large and homogeneous burned areas (BROCKETT *et al.*, 2001) which would make them appropriate for scientific analyses. The Shabeni plots were burnt on 13 August 2000, whilst the Kambeni plots were burnt on the morning of 14 August 2000. All burning occurred under similar micrometrological conditions, using perimeter line ignitions along the boundary of the EBP.

Shortly after the fire, samples of pure white ash, representative black ash samples and non-photosynthetic phytomass (senescent grass, twigs, leaves and bark) samples were collected and later analysed in a laboratory using an Analytical Spectral Device (ASD) radiometer. An effort was made to keep black samples, as black as possible, recognising that ashes from savanna phytomass will always contain some white ash component. The white ash was considered to be representative of pure white ash. The spectral endmembers of the respective samples were captured in the reflective domain from  $0.45\mu\text{m}$  to  $2.2\mu\text{m}$ . Endmembers represent the purest “homogeneous” materials from which other materials are created (BOARDMAN AND KRUSE, 1994). The ASD takes reflective measurements of the samples at  $0.1\mu\text{m}$  resolutions, and these can be re-sampled to wavelengths simulating (at-nadir) satellite surface reflection of ash and phytomass in reflective bands.

### 2.3.2.3 Satellite data

In this study full advantage was taken of the 30-meter high-resolution Landsat Enhanced Thematic Mapper (ETM+) satellite data sets captured over the southern KNP in 2000 as part of a project to improve burn scar-mapping capabilities from the MODerate resolution Imaging Spectroradiometer (MODIS). The project aims to identify the limitations of MODIS burned area maps using independent and higher-resolution reference data sets (ROY *et al.*, 2002). MODIS senses the earth's surface in 36 bands spanning the visible (0.415 $\mu\text{m}$ ) to thermal infrared (14.235 $\mu\text{m}$ ) electromagnetic (EM) spectrum at nadir spatial resolutions of 1 km, 500 m and 250 m respectively (BARNES *et al.*, 1998). MODIS provides daily global coverage for all areas above approximately latitudes of 30°.

Landsat ETM+ data is collected on the Landsat-7 platform in a near-polar, near-circular, sun-synchronous orbit, imaging the same point on the Earth's surface every 16 days. Landsat-7 ETM+ data has a spatial resolution of 15m and 30m in the reflective bands and senses the earth in seven spectral bands from the visible (0.479 $\mu\text{m}$ ) to the thermal infrared (2.209 $\mu\text{m}$ ). Two Landsat ETM+ cloud free datasets (ETM+ path 168, row 078) captured over Skukuza (KNP) on 12 June 2000 and on 15 August 2000 were investigated to encompass pre burn phytomass availability, change in reflection between the pre and post-fire image, the combustion completeness and fire severity. The pre and post-fire imagery were manually geometrically 'precision' corrected to improve their co-registration to less than one 30m Landsat pixel. In this study only the reflective bands were investigated (from 0.4  $\mu\text{m}$  to 2.3  $\mu\text{m}$ ). As part of the radiometric calibration process the Landsat data was corrected to surface reflection using an atmospheric model using the 6S radiative transfer code (VERMOTE *et al.*, 2002).

The 6S code was run using Aerosol Robotic Network (AERONET) (HOLBEN *et al.*, 1998) aerosol optical depth, water volume and air mass measurements. Surface reflection is needed to make Landsat comparable to the laboratory ASD reflective information, which emulates at-nadir surface satellite reflectivity.

### 2.3.2.4 Theoretical Approach

#### *Fire intensity*

Landsat ETM+ and corresponding MODIS and grey ash reflection spectra from 0.41 $\mu\text{m}$  to 2.11 $\mu\text{m}$  were simulated using the ASD radiometer reflections from the two different ash

samples taken on the EBP (Figure 19). By dividing the sampled black ash spectra from the ASD measurement by the pure white ash spectral endmember (also called reference endmember), the relative abundance of the pure white ash spectra in the collected black ash was determined at 8.8 percent (HILL, 1990). This was rounded off to 9%. By linearly interpolating between the pure white ash and the black ash curve, it becomes possible to model percent abundances of white ash contents in ‘grey’ ashes at a chosen percent interval (Figure 19). These would simulate, in theory, ‘grey’ ash levels pertaining to emitted energy releases and combustion efficiencies within a scale of meters. The combustion efficiency is the degree of oxidation of the fuel (proportion of carbon oxidized as CO<sub>2</sub>) and decreases with the smoldering rates of combustion (WARD *et al.*, 1996). Figure 19 below also shows the simulated ASD non-photosynthetic vegetation spectra determined with the sampled vegetation on the fire area. The non-photosynthetic vegetation samples were representatives of the constitution of dry leaf material, grass residuals and twig litter sampled on the Kambeni and Shabeni burn scars and subsequently analysed with the ASD in the laboratory.

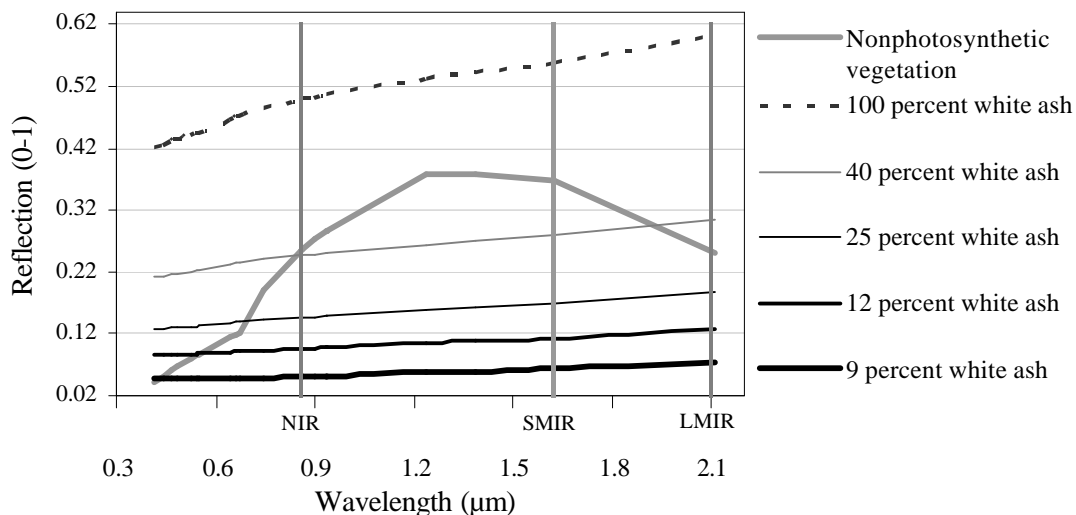


**Figure 19:** Shown are spectral ash reflective curves to simulate different percent white ash contents in ‘greyish’ ash and non-photosynthetic vegetation. The most bottom ash curve has nine percent white ash in it and is the reflection of the black ash as collected in the field. The positions of narrow band Landsat ETM+ near-IR, short mid-IR (SMIR) and long mid-IR (LMIR) bands (and corresponding MODIS centre wavelengths) are marked with the grey vertical lines.

### *Spectral unmixing*

Linear spectral unmixing was performed using Landsat ETM+ per pixel information of the three Kambeni experimental burn plots (EBP). The underlying assumption of spectral unmixing is that each Landsat fire scar pixel is a multivariate product of several spectral (physically pure) components (SETTLE AND CAMPBELL, 1998).

This implies that for a given pixel the multi-spectral signal ( $X$ ) can be described as the linear function of the ground cover proportions from the spectral pure endmembers matrix ( $M_i$ ) for the pixel component  $i$ . The known pixel components are bare soil [a], unburnt vegetation [b], green leaf residues [c], shade [d], and ashes/charcoal [e]. The term  $f$  is the dimension abundance vector (proportion) of the known endmember matrix ( $M$ ) and (?) is the random term used to describe residual atmospheric or other detector instrument noise

$$X = M_a f + M_b f + M_c f + M_d f + M_e f + ? \quad [1]$$

Ideally all endmember abundances ( $M_i f$ ) add up to one (as being  $X$ ) and are between zero and one (ELMORE *et al.*, 2000). Because all fractional abundances are proportions between zero and one, we shall define any abundance of a material as being  $(1-x)$ , whereby  $x$  is always between zero and one. For the linear unmixing, all spectral endmembers abundances ( $M_i$ ) must be known for the pixel for which their abundances ( $M_i f$ ) are calculated. The endmember number can never exceed the number of channels used (SETTLE AND CAMPBELL, 1998). The result from the spectral unmixing are grey scale abundance images for each known endmember.

The success of linear unmixing depends critically on the selection of the endmembers. The endmembers can be extracted from the image itself as being ‘pure’ representatives of a certain landscape feature or pixel component. For this contextual knowledge of the fractal surface component of a certain endmember must be known from ground observations. Alternatively reference endmembers are chosen from reflective laboratory measurements of a particular endmember. The validity of the unmixing result that is the choice of candidate endmembers is assessed by analysing the fraction and the root mean square error (RMS) (ELMORE *et al.*, 2000). Several linear unmixing trial calculations using different endmembers with one another were pre investigated for their validity.

The following endmembers were finally selected: non-photosynthetic vegetation (from the ASD measurements), green vegetation (extracted from the image itself), and the nine percent white in black ash curve as well as the twelve white in black ash curve. The non-photosynthetic vegetation endmember can be termed the brown spectral curve, the nine percent white ash endmember the black ash endmember and the 12 percent white in black ash endmember the grey ash endmember. The resultant abundance image for each endmember showed physically meaningful results (*i.e.* between zero and one) and low RMS values. The

resultant abundances were also verified by the post-burn pixel fractional cover observations derived from the visual inspections made on each of the EBP.

Endmember combinations using the ten and eleven percent white ash in black ash abundance spectra and >12 percent white ash abundances endmember showed abundance results that were negative or >1 as well as higher RMS values. Endmember combinations using the soil endmember together with the brown phytomass endmember; the shadow with the photosynthetic (green) phytomass endmember also showed unmeaning results. This has been previously observed in other studies and may be due to spectral similarities between bare soil surfaces and brown vegetation, similarities or multiple scattering between green and shadow (ROBERTS *et al.*, 1993; HILL, 1990) or spectral confusion between ashes that exhibit similar reflections and/or are linear combinations of each other. A soil and a shadow endmember were hence not included in the final unmixing calculation. From the fractional land cover components shade was calculated to only constitute one percent of the total land cover on and soil eight to nine percent.

### *Combustion Completeness*

Combustion completeness (CC) in African phytomass is mostly defined as the fraction of fuel exposed to the fire which actually burns (SHEA *et al.*, 1996; SCHOLES *et al.*, 1996).

Current experimental work on multi-temporal Landsat ETM+ datasets has shown that ETM+ CC using the SMIR (1.55 $\mu$ m-1.75 $\mu$ m) band is related to the fraction of the vegetation exposed to the fire that is actually burnt (ROY AND LANDMANN, 2003). The following differential index was applied to collocated pre and post fire pixels in Landsat ETM+ data of the EBPs;

$$CC = (p1 - p2) / p1 \quad [2]$$

$$0 \leq CC \leq 1$$

CC is the combustion completeness;  $p1$  and  $p2$  are the pre-fire and post-fire Landsat ETM+ band 5 (SMIR) reflectance values per pixel Landsat ETM+ pixel respectively. Landsat ETM+ band 5 (SMIR) is known to exhibit good capabilities to characterize CC, since the SMIR is most sensitive to reflection (?) change (due to fire) in African savannas and insensitive to smoke aerosols (TRIGG AND FLASSE, 2000). The ETM+ image captured on the 12 June 2000 was used for the pre-burn reflection in [2] and the post-fire imagery was captured on the 15 June 2000.

### *Phytomass modeling*

Average total grass and woody phytomass [gDM/m<sup>2</sup>] estimates for each EBP pixel in the 120 meter sampling area were related to corresponding cloud free Landsat ETM+ tasselled cap (at-sensor) brightness index. The tasselled cap and other indices are commonly being used to estimate non-photosynthetic vegetation mass in African savannas (KRAUS AND SAMIMI, 2002; FRANKLIN AND HIERNAUX, 1991).

The tasselled cap brightness index takes into account local background soil reflection and is sensitive to non-photosynthetic vegetation (HUANG *et al.*, 2001). The regression was significant ( $P < 0.002$ ) and showed a squared multiple of  $R^2 = 0.56$ .

The assumptions implicit to the linear regression analysis are probably not met since we are comparing average phytomass to corresponding reflectance averages per EBP site. Consequently they can only serve as an approximation/estimate of the available surface fuel phytomass. Erroneous results for grass mass would be calculated if areas of high tree cover canopy would not be masked. High tree cover densities and foliage mass 'hide' the underneath grass sward. Since green leaf chlorophyll is very sensitive to the Landsat ETM+ Normalized Differential Vegetation Index (NDVI) (FLASSE *et al.*, 2003), an imperially derived NDVI threshold was used to mask areas of high green chlorophyll.

The pre burn image from 12 June 2000 was cloudy in parts over the Shabeni sites and therefore the Shabeni plots were omitted for further investigations on pre burn fuel mass and combustion completeness. Both combustion completeness (CC) and pre-fire phytomass Landsat information were used as auxiliary indicators of fire intensity and fire severity. Other fire intensity parameters (apart from fuel load) such as micrometeorological conditions at the time of burn, fuel moisture and fuel compaction are unpredictable fire behavior variables that occur at the time of combustion.

## 2.3.3 Results

### 2.3.3.1 Fire intensity

Using the spectral linear unmixing method described relative Landsat ETM+ abundance image channels of black and grey ash, non-photosynthetic (brown) and green vegetation were created. The scatter diagram in Figure 20 shows grey ash abundances per pixel from the linear unmixing result as a function of black ash abundances per pixel. Evidently, Kambeni 7 has

considerable more abundance of black ash, less abundance of grey ash than all other sites and is most distinct from Kambeni 5. Both plots were burnt under the same micrometeorological conditions on the 14 August 2000 and both sites are homogeneous in terms of vegetation distribution. Inherently for linear spectral unmixing the black and grey ash mix directly that is proportional (or linearly) over the whole spectrum used in the unmixing calculation. This is expected since the “shape” of the endmember curves is similar.

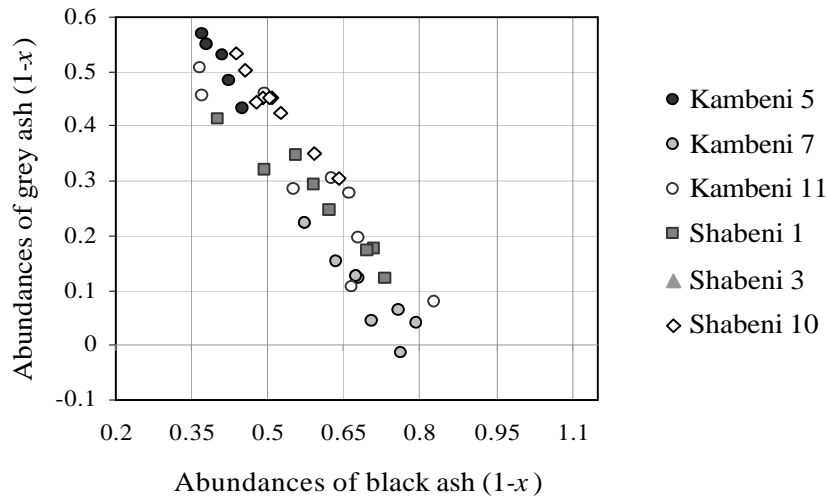


**Figure 20:** Scatter diagram showing the abundance of grey ash ( $1-x$ ) and concurrent black ash ( $1-x$ ) on Experimental Burn Plots (EBP) in the southern KNP. The values represent relative abundances from 0 to 1 ( $1-x$ ) of black and grey ash endmembers.

The modelled Landsat ETM+ grass and woody phytomass in Figure 21 below shows that Landsat estimated pre fire fuel amount is significantly related to the abundance of grey ash ( $1-x$ ) using the spectral unmixing result ( $R^2=0.49$ ;  $P=0.001$ ). No relationship was found between black ash abundances and pre fire phytomass. Since fuel amount is an important determinant of fire intensity (TROLLOPE AND TAINTON, 1986; VAN DE VIJVER, 1999) and more intense fires produce whiter ash (STRONACH AND MCNAUGHTON, 1989), most pixels in Kambeni 5 can be seen to be a high intense burn. Due to the cloud cover in the pre burn imagery the Shabeni plots could not be investigated further. The average standard derivation of individual pixel values using the grey ash abundance image was 10% smaller for Kambeni 5 than for Kambeni 7. This indicates that the proportion of grey ash is greater on Kambeni 5 and probably more distinct from the other landscape components.



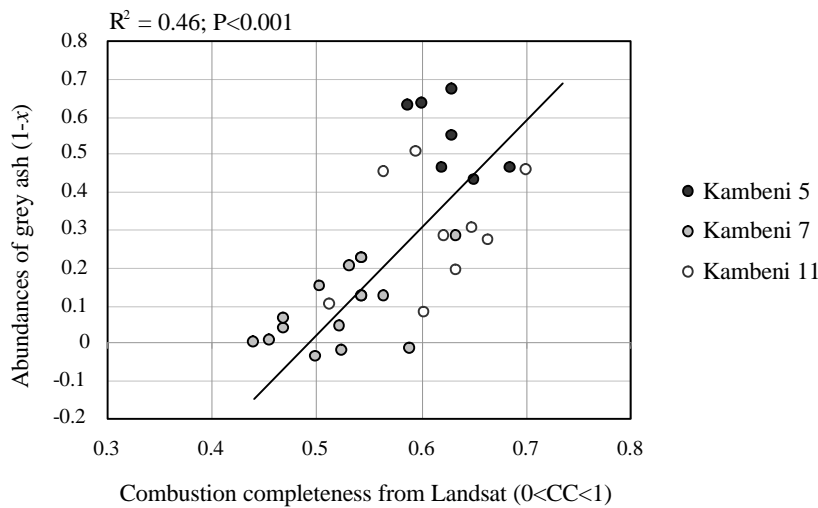


**Figure 22:** Relationship between abundances of grey ash (1-x) from the linear unmixing and Landsat ETM+ combustion completeness (CC) per pixel

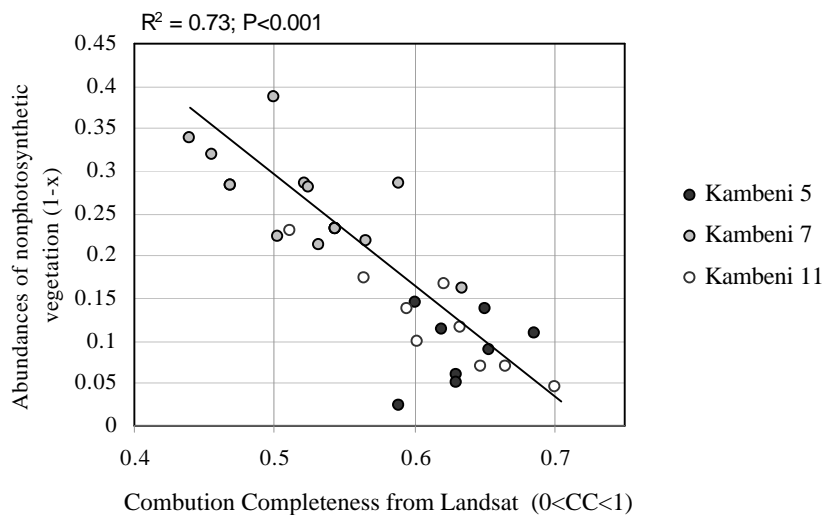


**Figure 23:** Relationship between residual non-photosynthetic (brown) phytomass abundances (1-x) from the linear unmixing and Landsat ETM+ combustion completeness (CC) per fire-affected pixel.

### 2.3.3.2 Fire severity mapping

On a remote sensing scale fire severity is defined as the degree of change caused by the fire event (FLASSE *et al.*, 2003; MICHALEK *et al.*, 2000). Given so, fire severity (*FS*) is a product of the abundance of the grey ash endmember (intensity) from the linear unmixing result  $I_{(1-x)}$  per unit area of the fire (or pixel) and the combustion completeness (*CC*) of that same area unit or pixel:

$$FS = I_{(1-x)} * CC \quad [3]$$

Fire intensity is a fire energy descriptor that describes the nature of the burn and thus largely determines degree of reflection change. Combustion completeness (CC) determines the fraction that burned or the relative fire impact irrespective if the fire was intense or not. CC is largely dependant on the pre burn reflection or vegetation (Figures 3), as this determines the differential ratio in [2].

Therefore as an index combined they would define the magnitude of spectral change induced by converting vegetation to charcoal and ash. Figure 24 below illustrates the magnitude of response of the fire severity index as a non-linear function of reflection change in pre and post-fire pixel values for the Kambeni plots. The ideal non-linear model relationship between fire severity and reflection change is shown (with  $R^2=1$ ). A non-linear response of this index to reflectance change is expected from statistical theory. The amplitude/contrast of fire severity has broader ranges of values than the hypothetical model ( $R^2=0.52$ ;  $P<0.001$ ), i.e. the actual data curve is steeper. This implies that fire severity observed herein is broader defined and is essentially more dependant on fire intensity than on CC, as the CC is determined by the change in reflection (?) due to fire using the SMIR ETM+ band (pre-burn<sub>?</sub> - post-burn<sub>?</sub>). Also from Figure 24, mapping fire severity or extraction of the fire affected area using the change in reflectance between images is not feasible, because fires with the same reflectance change show considerable differences in fire severity. This has implications for fire mapping methods and burn scar product development that quantify fire extent or severity, and rely on the maximum reflectance change between a pre and a post-fire image as a surrogate for fire effect.

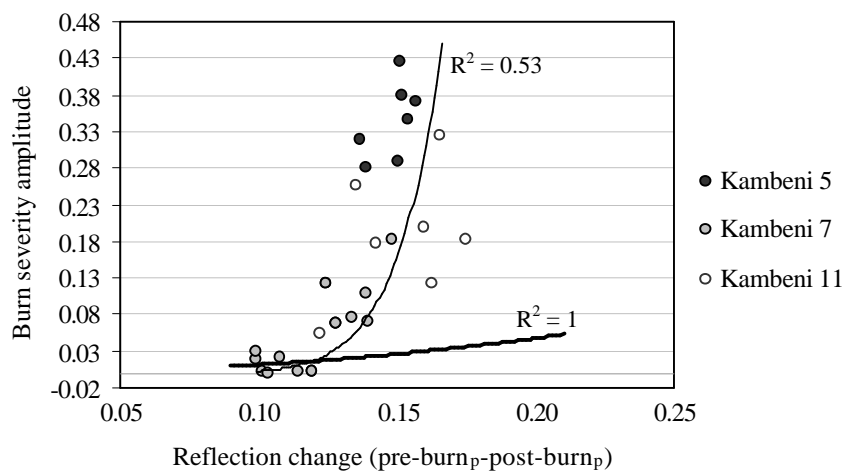


**Figure 24:** The amplitude of fire severity and absolute reflection change (pre-burn<sub>?</sub> – after-burn<sub>?</sub>) in Landsat ETM+ using the SMIR band. The hypothetical model shows ( $R^2=1$ ) a lesser

sensitivity to the burn severity amplitude. The actual data ( $R^2=0.53$ ) is a non-linear function that is most determined by fire intensity than by the change in reflection in between two images. The same reflection change can exhibit different fire severity levels.

The exhibited fire severity levels in Figure 24 can be used to evaluate classes of FS. From the FS levels in Figure 24 and the pre fire fuel measurements we can classify Kambeni 5 as being a severe fire. Most pixels in Kambeni 11 can be classified as being a moderate fire and Kambeni 7 can be classified as a low severity burn. As with the fire intensity value distributions per pixel, the FS variances were considerable larger for the low severity fire (Kambeni 7).

Figure 25 below shows Landsat mapped abundances of grey ashes and fire severity for Kambeni 5 (top row) and Kambeni 7 (lower row) respectively. Brighter shades in pixel values show increasing grey ash abundance and increasing fire severity. The distinctive difference in fire severity between the low and the severe fire becomes apparent. The measures on the scale are unit-less and from zero to one.

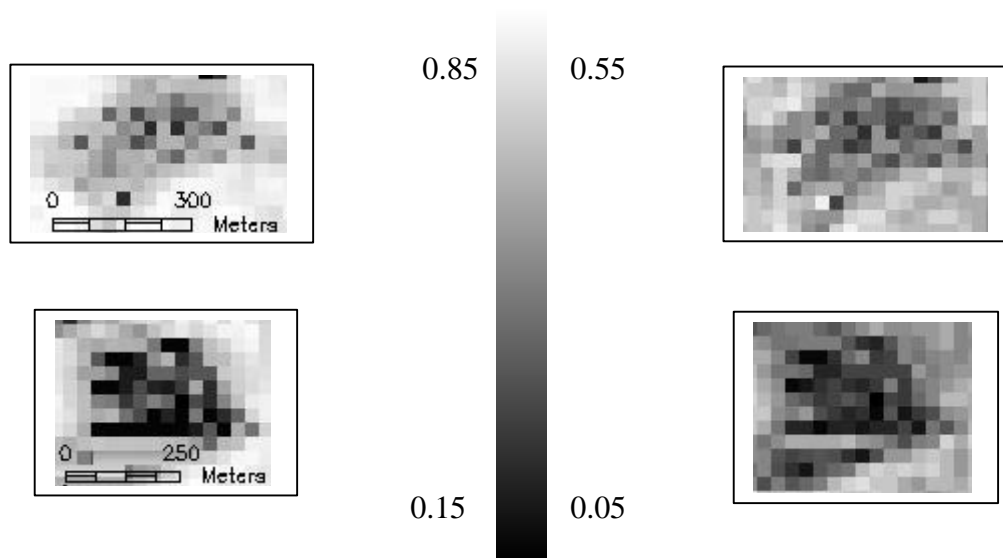


**Figure 25:** The left images show the abundance output band of ‘grey’ ash from the linear unmixing result for Kambeni 5 and Kambeni respectively. The right column shows the fire severity as a product of the abundance of grey ash and combustion completeness. Evidently, Kambeni 5 exhibits brighter that is higher fire severity pixel values than Kambeni 7 (bottom). No image enhancements or stretching was applied.

### 2.3.4 Discussion and conclusion

The fire severity images in Figure 25 (right) show grey values surrounding the perimeter of the burnt area, which are not well separable from the burnt pixels. This underlines that thresholds to extract or characterize the fire-affected area can only be implied when fire severity information is available for the area of interest (*i.e.* the burn scar) from either phytomass field observations or other *in situ* independent high-resolution satellite data. Relative fire induced reflection changes account for local variability in vegetation, soil types and may include field knowledge on land cover proportions. Hence relative reflection changes in methods that aim to quantitatively determine the area burnt are perhaps superior over absolute reflection change threshold methods that are often implied without prior knowledge. This study has illustrated that instead of classifying a candidate pixel as burnt or unburnt an estimate about the nature of the burn and the fire impact (CC) can be made at a sub-pixel scale. The sub-pixel fire information was verified with *in situ* field and the other auxiliary Landsat information stating the precision and accuracy of the linear unmixing method by using the regression coefficients ( $R^2$ ) as accuracy measures. This permits the calculation of several fire severity classes on a site scale.

In this regard it should be noted that characterizing the fire intensity and severity using the presented methods in areas that are not homogeneously vegetated and subjected to low intense, patchy or sub-canopy burns may be problematic. Partly charred residual vegetation is known to reflect similar than brown un-charred vegetation (TRIGG, AND FLASSE, 2000).

Soil surfaces may reflect similar to low intense or older burned areas (TRIGG AND FLASSE, 2000; FLASSE *et al.*, 2003). These problems are particularly pronounced when single date imagery is used for the spectral unmixing and not supplemented with information from a pre-burn image. When calculating fire severity as a product of the abundance of grey ash and CC some spectral confusion between light burns and soil as well as sub canopy fire incompleteness is eliminated. Soil and canopy cover are permanent land cover types and usually not attenuated by change in multi-temporal techniques to map fire scars (PEREIRA *et al.*, 1997). However, multi-temporal fire mapping techniques require the image processor to apply complex methods and algorithms to geo-locate the imagery and correct the data to surface reflection, *i.e.* the same physical units.

The Landsat ETM+ high resolution fire characterization results shown here have implications for validating fire affected areas from moderate to high-resolution sensors, such as MODIS. Validation and calibration of coarse resolution fire information is generally difficult with directly measured field biotic parameters (KAUFMAN AND JUSTICE, 1998). Landsat fire severity information can be used as stepping stone data between fire severity levels from field data and possibly from moderate or high-resolution sensors *e.g.* MODIS. Since MODIS has daily global coverage for all areas above 30 degrees in latitude, it would make a potentially suitable tool to characterize fire scars in particular fire severity, and the accuracies thereof, on a landscape scale. MODIS burned area time-series information for Southern Africa, corrected for sensor viewing angles and surface illuminous variation, is currently being validated with Landsat mapped burned areas and will be available in the near-term (ROY *et al.*, 2002; JUSTICE AND KORONTZI, 2001).

Explicitly future work in high-resolution fire scar characterization should aim to investigate:

- fire induced spatial and temporal changes of fuel phytomass endmembers over time using multi-temporal data sets. Changes in these endmembers due to burning should be spatially quantified at a sub-pixel level. Changes should not be considered as a result of maximum reflection change but rather by the shape of the resulting ash spectra that is as the actual magnitude of fire induced change. Endmembers are suited for change detection studies as they are particularly corrected to the true ‘pure’ surface reflection of a particular material.
- the relationship between active fire temperature and the corresponding spatial distribution of grey and black ash spectral signature. This work postulates that high temperature active fires would produce whiter ash surfaces within a common savanna type. High resolution (hyperspectral) aircraft data flown over a prescribed burn site several times would be an ideal technique to qualitatively investigate this relationship. If a relationship can be found we can use this regression to model/predict fire intensity on fire scars rigorously over larger areas in time-series satellite data sets.
- the relationship between fire severity information using well calibrated multi-temporal high-resolution satellite sensors and MODIS surface reflectance data, using the 250-meter resolution wavelengths. The approach entails (i) using CC calculations from high-resolution pre and post-fire fire data to predict abundances of non-photosynthetic phytomass  $(1-x)$  (*e.g.* Figure 23), (ii) deriving a simple relationship between non-

photosynthetic phytomass ( $1-x$ ) and the abundance of grey ash ( $1-x$ ) (as suggested by the linearity of the unmixing results in Figure 20), (iii) substituting the abundances of non-photosynthetic phytomass ( $1-x$ ) into [3], *i.e.* as a multiplicative of CC information of the same pixel in the high-resolution data, and (iv) deriving a spatial prediction model for fire severity from 250-meter resolution MODIS information using the high-resolution fire severity data.

Finally, inferring fire intensity from the ash colour using satellite data is more efficient than directly measuring fire intensity (temperature, duration or flame features) near the active flame in the field. These measurements require sophisticated instrumentation; active fire behaviour is often unpredictable and varies considerable within short distances.

This work has been carried out as part of the SAFARI initiative. Tanja Kraus contributed greatly with the field work and field data assessment with additional field assistance being provided by the Kruger National Park staff, in particular Andre Potgieter of Scientific Services. Funding for this research came primarily from the Gottlieb Daimler and Karl-Benz Foundation, the University of Göttingen and the National Aeronautics and Space Administration (NASA) Land Use and Land Cover Change (LUCC) program. My sincere gratitude also goes to the Council for Scientific and Industrial Research (CSIR) for hosting the research activities, in particular Dr. Bob Scholes.

### 2.3.5 Summary

Burn severity and fire intensity was quantitatively mapped using a unique linear spectral mixture model to determine sub-pixel abundances of different ashes and combustion completeness measured on the same fire-affected pixels in Landsat data. A new burn severity index (BSI) was derived that is shown to map three categorical classes of burn severity on three experimental burn plots (EBPs) in the southern Kruger National Park (KNP), South Africa. Those pixels which exhibited a greater abundance of white ash were found to be significantly related to the pre-burn above-ground fuel biomass ( $\text{g/m}^2$ ) and an indicator of burn efficiency and fire intensity. Landsat ETM+ combustion completeness was most significantly related to the abundance of post-burn residual non-photosynthetic or 'brown' fuel biomass. For the same reflectance change in pre- and post-fire imagery, a larger magnitude in fire severity was measured on corresponding ETM+ pixels. This implies that

fire severity is more dependent on the colour of the ash than on the magnitude of change in reflectance. Burned area mapping methods that rely on reflectance change in multi-temporal imagery may not reliably characterize burn effects such as fire severity and efficiency in semi-arid savannas.



## 2.4 Improved fire emissions estimates from the Kruger National Park (KNP) using satellite derived biomass and burned area data and *in situ* Airborne Emission Factors (EF)

Tobias Landmann

Council for Scientific and Industrial Research (CSIR), Environmental Technology (Environmentek), Pretoria, South Africa and University of Göttingen, Department of Landscape Ecology, Germany.

Bob Yokelson

University of Montana, Department of Chemistry, Missoula, USA

Peter V. Hobbs

University of Washington, Department of Atmospheric Sciences, Seattle, USA

*(submitted to the Journal of Geophysical Research)*

### 2.4.1 Introduction

African wildfire green house gas (GHG) emissions are a large and constitute the prime source of gas and particulate emissions over Southern Africa [Andreae, 1997; Hao *et al.*, 1996a; Braatz *et al.*, 1995a; Crutzen and Andreae, 1990]. The biomass fuel burnt annually in African savannas is estimated to be 2000 Tg DM $y^{-1}$  (DM= dry matter weight), and the amounts of carbon burnt annually in Africa amount to around 61% of the global annual average carbon burnt [Lacaux *et al.*, 1993a]. Natural and managed biomass burning in savannas release trace gases such as NO, CO<sub>2</sub>, CO, NO<sub>x</sub>, N<sub>2</sub>O, SO<sub>x</sub>, CH<sub>4</sub> and smoke aerosols into the troposphere. Some of these gases are chemically-reactive and strongly influence the formation of ozone; smoke and soot particles affect cloud microphysics and radiative fluxes and can thus be a major concern on regional and global scales [Potter *et al.*, 2001; Kaufman *et al.*, 1998a].

Wildfire emissions models aim to estimate trace gas and particulate emissions to understand release of carbon and greenhouse compound gasses to the atmosphere [Levine, 1996a]. The emission estimates are largely driven by the emission factors (amount of emitted substance

per kg of fuel consumed) as a function of the amount of biomass burnt and the combustion conditions of the fire [Kituyi *et al.*, 2001a; Gupta *et al.*, 2001]. Most atmosphere-biosphere or so called land surface parameterization models are designed to describe the climatically important energy and water exchanges and the carbon dioxide fluxes between the dynamics of the land surface and the atmosphere. There are two types of prevalent biomass emission models. Some models describe use land cover classifications in one single cover type in each grid cell [Zhan *et al.*, 2000a]; alternatively others are based on the understanding of *in situ* site determinants that drive biomass load and vegetation composition in a continuous fashion over the whole region [DeFries *et al.*, 1999a; Scholes *et al.*, 1996a].

African savannas are heterogeneous vegetation complexities where mixtures of trees, shrubs, grasses, soil particles and litter (bark, leaf and twig litter fall) vary in the scale of several square meters [Zhan *et al.*, 2000c]. These complexities may not be captured with some coarse resolution or standard primary production models that quantify the above ground fuels as one component/entity with a single set of properties [Horowitz *et al.*, 2002]. Consequently the biggest uncertainty in current regional and global emissions model estimates for most molecules is still the fire available biomass fuel mass and the amount of fuel actually consumed by the fire [Justice & Korontzi, 2000a; Barbosa *et al.*, 1999b]. Differences are large between existing emissions models [Roy *et al.*, 2002a; DeFries *et al.*, 1999b]. Despite these important repercussions and recently completed regional emission studies it has been difficult to accurately estimate trace gas emissions on a local or regional level [Kituyi *et al.*, 2001b; Barbosa *et al.*, 1999a].

Recently launched satellite systems such as the MODerate resolution Imaging Spectroradiometer (MODIS) can provide data with new spectral combinations and improved spatial resolution have the potential to provide continuous improved estimates of the vegetation properties (tree, grass and shrub ratios), possible aboveground biomass and fire characterization information [Kaufman *et al.*, 1998b; Justice and Korontzi, 2000b]. Due to the large heterogeneity in fuel conditions in southern African ecosystems and the impracticality of taking field measurements in every classified area, satellite data provides the only current effective tool to systematic observe higher temporal fire and vegetation dynamics [Salvador *et al.*, 2000; Roy *et al.*, 2002b], especially in remote areas. The use of remote sensing data in fuel consumption and emission models give confidence of land use change information on a regional to landscape scale over continuous time periods. The use of satellite data in these

models, however, prerequisites sufficient spatial and spectral, radiometric resolution of the sensor, and data is validation for inter-annual variability of the land cover.

Considerable work has been done to integrate remote sensing information into regional emission model estimates. In South American experiments such as the Geosphere-Biosphere Program in 1991 [Levine, 1996b], the SCAR-B (Smoke Clouds Aerosols and Radiation-Brazil) [Kaufman *et al.*, 1998c], the Experiment for Regional Sources and Sinks of Oxidants (EXPRESSO) [Pereira *et al.*, 1999; Delmas *et al.*, 1995a] and the LBA (Large Scale Biosphere–Atmosphere Experiment) currently underway in Amazonia are, among others, exemplary in assessing pyrogenic emissions modeling using remote sensing from satellite or aircraft platforms. In Africa projects such as the 1992 and 2000 Southern Africa Fire-Atmosphere Research Initiative (SAFARI) [Swap *et al.*, 2001], the 8 year African burned biomass emissions program by Barbosa *et al.* [1999b], the Defense Meteorological Satellite Program (DMSP) to model emission factors over southern Africa [Elvidge *et al.*, 1992] and many other projects used satellite data paired with burnt area estimates to quantify region ecosystem emissions [Prasad *et al.*, 2002; DeFries *et al.*, 1999c; Zhan *et al.*, 2000d, Flasse & Verstrate, 1994]. Most studies mentioned here were reliant on 1-kilometer resolution NOAA AVHRR (National Oceanic and Atmosphere Administration Advanced Very High Resolution Radiometer) satellite data to estimate the area burnt or vegetation greenness to drive emission models. Recent studies increasingly use low spatial resolution ( $\leq 30$  meter resolution) satellite systems to validate or calibrate contemporary fire information from moderate to high resolution satellite systems or quantify fire activity at regional levels for emissions inputs [Michalek *et al.*, 2001; Eva & Lambin, 1998]. New fuel modeling methods to feed emission estimates use Net Primary Productivity (NPP) information based on Light Use Efficiency (LUE) approaches over a growing period to predict the live and dead tree and grass ratios that is aboveground biomass fuels available for burning over the whole southern African region [Hely *et al.*, 2002a]. The resolution of the NPP model is at one squared kilometer.

In this study local emission estimates are made for a 30-day window in September 2001 (from September 3 - October 4, 2001) for a study area in the southern and central Kruger National Park (KNP), South Africa. We use multi-sensor satellite fuel and fire information coupled with actual emission factors measured in KNP smoke plumes:

- i. To *derive* aboveground biomass fuel prediction regression equations we correlated the field measured biomass amounts, percent greenness of fuels and fractional land

observations of fuel components with concurrent pre fire Landsat ETM+ data captured over the same field sampling period during July and August 2000.

- ii. The amount of total fuel exposed to the fire (grass, wood and litter) actually consumed by the fire or combustion completeness (CC) was modeled using daily 250-meter MODIS data.
- iii. To *drive* the emissions estimates model the 2000 derived fuel biomass prediction equations were applied to a Landsat ETM+ image captured over the KNP on the 3<sup>rd</sup> of September 2001. Combustion completeness (CC) and burnt area information were calculated using differential mapping ratios for a 30-day period after the early September 2001 Landsat ETM+ image. The fire CC and area was mapped with daily cloud free and good quality MODIS (at 250 meter resolution) overpasses.
- iv. The per pixel fire and biomass information was multiplied by emission factors (EF, g/kg) of gaseous species that were measured aboard the University of Washington's Convair-580 instrumented aircraft during prescribed burning over the KNP-area in 2000 [Hobbs *et al.*, 2002A].
- v. Total emission estimates for all detected burned areas within the observation period were calculated per pixel and for some important species illustrated as spatial explicit maps.

By relating the field biotic factors distribution and field fire information to concurrent multi-sensor satellite data we intend to capture the actual land cover present, rather than modeling the potential natural vegetation. Emission results obtained by substituting Average airborne EF from savanna fires are tested against EF determined as a function of the combustion efficiencies of the fuel mixtures calculated. By using the explicit high-resolution Landsat ETM+ fuel models and the mixtures of fuels to estimate the EF (as a function of the estimated combustion efficiency of the fuel components) we aim to reduce the uncertainties for most particulates in pyrogenic emission estimates over the KNP region.

## 2.4.2 Methods

### 2.4.2.1 Study area

Pre fire grass biomass, woody biomass, percent greenness and fractional land cover components observations were measured along a 120-kilometre long sampling transect (within a study area of 8020km<sup>2</sup>) on 18 sites in the KNP covering several distinct savanna types according to Gertenbach [1983a]. Several prescribed burn sites within the Madikwe Game Reserve (MGR) on the western boundary of South Africa were supplementary sampled (Figure 26 and Table 6). The Madikwe site was included in the study to gain confidence in spatial modeling of fuels and methods to predict aboveground biomass fuel, thereby creating statistically and spatially coherent regression models. Biomass sampling was done in the peak dry or fire season in late July and early August when the vegetation is most senescent. Table 6 gives a complete overview of the sampling sites, their respective location, their savanna type, elevation, precipitation per annum, degree of slope and biomass fuel ranges [gDM/m<sup>2</sup>] [DM=dry matter]. The fuel load is the amount of aboveground biomass (in grams per unit surface area) available for burning, i.e. within the flaming zone. This includes grass mass, woody biomass up to a height of two meter and dry matter litter mass (twigs, wood debris, leaf and tree bark).

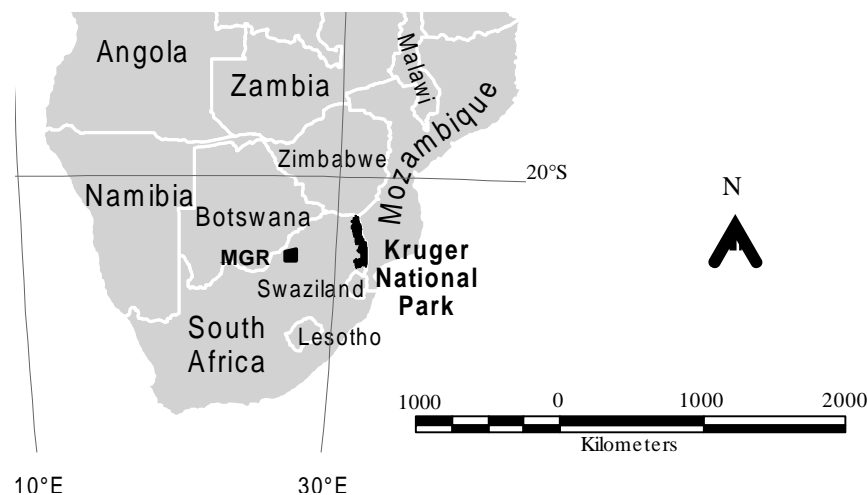


**Figure 26:** The map shows Southern African states and the location of the two biomass sampling sites. The Kruger National Park (KNP) is located near the border to Mozambique and Madikwe Game Reserve (MGR) is situated on the western border of South Africa, 900 kilometres west from the KNP.

Savanna type	Kruger National Park			Madikwe Reserve
	<i>Terminalia sericea/Dichrostachys cineria</i> open tree savanna	<i>Combretum spp./Terminalia sericea</i> woodland	<i>Sclerocarya birrea/Acacia</i> open tree savanna	<i>Acacia spp./Boscia</i> sp. open tree savanna
No. of prescribed burn sites*	6	6	6	7
Location (long. /lat.)	25°7'22.51"S, 31°14'12.29"E	25°6'37.47"S, 31°23'57.66"E	24°24'14.11"S, 31°46'13.68"E	24°40'53.68"S, 26°26'18.51"E
Annual Precipitation (mm)	750-1000	500-750	500-750	500-750
Elevation (m)	~600	~600	~500	~500
Average slope (degrees)	3 to 5	3 to 5	3 to 5	<4
Average tree cover density (percent)	26	20.6	1.3	9.2
Aboveground biomass ranges [gDM/m <sup>2</sup> ]**	700-1500	400-1300	350-550	300-1440

\* some sites were cloudy in either the pre or the post fire Landsat ETM+ data; these had to be excluded from the regression modeling

\*\*only standing grass and wood below <2m

**Table 6:** Field sampling and characterization sites descriptions

All sites are broadly defined as being semi-arid savanna [Cole, 1986] and are in protected unperturbed ecosystems ecosystems. In these savannas systems inherent soil properties, plant competition, and specific physiological attributes naturally regulate biomass production [Kauffman *et al.*, 1992], i.e. biomass fuel production available for burning. Typical semi-arid savanna grasses found in KNP and MGR are *Aristida spp.*, *Hyperthelia dissolute*, *Diheteropogon amplexans*, *Heteropogon contortus* and *Setaria flabellate* [Scholes, 1997a; Hao *et al.*, 1996b]. Typical faster growing and less palatable grasses species such *Elionurus muticus* and *Hyparrhenia hirta* are primarily found in the southern KNP region [Gertenbach, 1983b] These ‘Sourveld’ grasses produce high grass fuel loads and are associated with soils that are deeply leached and have high sand contents. Poorly drained clay soils are usually support more palatable, shorter grasses such as *Aristida spp.* and are primarily found in the ‘sweetveld’ areas of the KNP and Madikwe.

### 2.4.2.2 Fuel sampling

Site characterization and fuel sampling was made before (and after) the fires within a 120m x 120m sampling frame on prescribed burn plot (Figure 27). The 120m x 120m site dimension was an efficient size for field measurement averaging, a small enough size to manage and sufficiently large to minimize potential problems with Landsat ETM+ navigation. The KNP experimental burn plots, on which the 120-meter sampling area was placed, all have a size of seven hectare, whilst those in Madikwe were variable in size. The 120-meter sampling frame was judged from extensive pre-fire field inspection and examination of the Landsat ETM+ data to have homogenous vegetation and soils. This is important as some of the KNP experimental burn plots have a high soil variability, and are attenuated by so called ‘edge effects’ due to unnaturally fire induced heavy herbivore pressures and the small size of the plots [Trollope *et al.*, 1998; Van Wilgen *et al.*, 2000].

**Grass** is the most important savanna fuel [Trollope and Potgieter, 1986] and it was measured systematically within the 120 meter sampling frame with most precision. The disc pasture meter (DPM) developed by Bransby & Tainton [1977] was used to estimate compaction height [cm] of standing grass by recording the settling height every 6m and changing direction every 30m (Figure 27). The disc meter regression equation from Trollope & Potgieter [1983] was used to express grass load in gDM/m<sup>2</sup> as an average for the sampling area. However to improve the accuracy of the disc meter reading grass was also clipped in 50cm by 50cm quadrats every 30m along the same sampling transect. The grass clippings were made a year later in 2001: the grass was ambient dried, weighted and compared with corresponding DPM heights [cm] consecutively to improve the disc meter calibration equations. Grass and wood fuel moisture content level drop to near zero [%], after being ambient air dried for several days.

The **woody** fuel load was estimated using published allometry equations according to Netshiluvhi & Scholes [2001] applied to the individual measurements of tree and shrub height [m], number of stems, and basal diameter [cm] of dominant species in three 10meter x 10meter plots located randomly across the sampling frame (Figure 27). The grass and wood biomass sampling methods have are also extensively covered by Kraus and Samimi [2001a].

**Litter** material such dead grass, wood debris, twigs litter (=1.5 cm in diameter) and leaf litter was collected in the 50cm clipping quadrats, dried, weighed and expressed in gDM/m<sup>2</sup> as average for the whole sampling frame.

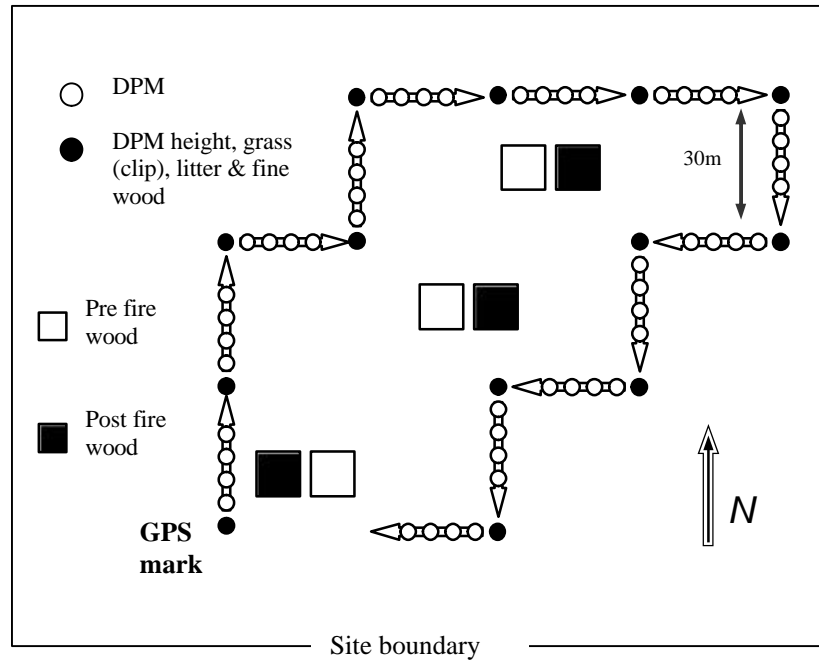


**Figure 27:** Sampling design (120 by 120 meter) implied on prescribed burn plots. The settling height of grass was recorded every 6 m with a disc pasture meter (DPM) and also clipped in 50 cm quadrats every 30 m. Dry matter leaf litter and twig fall (=1.5 cm in diameter) was also collected in the quadrats, dried and weighted. Wood mass was sampled before and after the fire in three randomly selected 10-meter plots in the centre of the sampling frame using non-destructive measurement methods.

Additionally to the biomass measurements fractional land cover component percentages of individual vegetation components (trees, shrubs, and grasses), their percent greenness, percent of area covered by bare surfaces and rocks were determined. This was done through visual inspection by three investigators using a consistent protocol for each sampling site. Other auxiliary information that was measured included the average [%] tree cover density, using a spherical densiometer at 16 points within the sampling frame [Lemon, 1957]. The average tree cover density for each sampling area is needed to calculate the leaf litter amounts and the fractional cover components are, in particular, needed to validate vegetation greenness from Landsat ETM+ vegetation index information.

We recognize the statistical (theoretical) inaccuracies by averaging in particular the wood mass of individual species and extrapolating these to the whole sampling frame. These inaccuracies are accounted in the regression equations with Landsat indices and discussed thoroughly in section 3.1.

### 2.4.2.3 Satellite data

Several Landsat ETM+ scenes were captured over the burning periods between June and September in 2000 and 2001. The ETM+ sensor has a pixel size of 30 meter in six reflective bands respectively imaging the same point on the Earth's surface every 16 days in the same orbit as MODIS [Goward *et al.*, 2001a]. The satellite cross-track covers 185 by 170 kilometers [Jensen, 1996]. This scale and the availability of the high resolution NIR and MIR wavelengths make it particularly suited to map vegetation status and fire occurrence covering the southern and central part of the KNP.

The Level-1G Landsat ETM+ data sets were geometrically corrected yet had to be co-registered to one another. Although the geo-location accuracy of the Landsat data was high, it was necessary to manually co-register the different dates to improve their co-registration to less than one 30m Landsat pixel. This was achieved by applying integer pixel translational offsets found using ground control points.

This and the radiometric calibration to surface reflectance are critical in multi-temporal data analyses [Elmore *et al.*, 2000a]. By performing spectral calibration to the same physical units, we assured that spectral differences among the images were due to fundamental change in surface characteristics and not due to changes in atmospheric contamination of imagery, solar elevation and azimuth, and possible sensor instrument noise. The atmospheric correction of satellite data allows for a better comparison to biotic field measurements.

The 6S radiative transfer code was used on the Level-1G Landsat ETM+ data to correct it to surface reflection [Vermotte *et al.*, 2002; Holben *et al.*, 1998]. The 6S code was run using Aerosol Robotic Network (AERONET) aerosol optical depth [nm], water volume [cm] and air mass (unitless) measurements. The Landsat ETM+ calibration and geo-location processes for the 2000 KNP and Madikwe ETM+ data sets are described in detail by Roy and Landmann [2002a, forthcoming]. Landsat ETM+ imagery is arranged in a unique path and row acquisition system (Goward *et al.*, 2001b): path 168, row 077 is the KNP detection path, and path 171, row 077 ascribes the Madikwe imagery. The surface reflection MODIS data tiles were geo-located and resampled to the Landsat ETM+ grid.

#### 2.4.2.4 Emissions modeling approach

##### *Fuel modeling*

Several Landsat ETM+ indices, spectral ratios, differential indices, such as the Normalized Differential Vegetation Index (NDVI), and single band spectra data averages were extracted for each sampling frame and correlated to average fuel mass and percent greenness of each corresponding field sampling frame. Of the tested indices the Landsat ETM+ Tasseled Cap brightness index [Huang *et al.*, 2001] and the NDVI were particularly useful to calculate fuel biomass parameters over KNP and Madikwe. The ETM+ Tasseled Cap brightness index uses all seven reflectance bands (from 468 nm-2230 nm) on at-sensor reflectance (?), and is sensitive to non-photosynthetic biomass while correcting for some soil background reflection/perturbations. The NDVI is sensitive to chlorophyll in photosynthetic active vegetation such as tree foliage and grass [Gitelson and Kaufman, 1998]. The NDVI was calculated using surface reflectance in the Landsat near-IR (NIR: 834 nm) and visible band (VIS: 661 nm). Fuel greenness largely determines the quality of combustion that is the level of oxidation in the combustion of fuels and enhances the emission values of smoldering gases such as CH<sub>4</sub> and CO [Delmas *et al.*, 1995b].

##### *Fire modeling*

The fire-affected area and the fraction of fuel that was consumed or combustion completeness (CC) was determined from daily 250-meter MODIS overpasses using the CC differential ratio (1). Recent work showed significant relationships between the Landsat ETM+ NIR band and the amount of biomass fuel consumed measured on prescribed burn plots in the KNP [Roy and Landmann, 2002b, forthcoming]. Therefore we attempted to test the CC relationship between Landsat ETM+ and contemporary MODIS data. CC can be defined as the amount of fuel exposed to the fire that is actually combusted by the fire [Shea *et al.*, 1996a], recognizing that features such as rocks or swampy areas as well as some tree foliage is not burnt on a site or remote sensing landscape scale. The combustion completeness is defined as the ratio between the post-fire satellite reflection and the pre-fire reflection

$$CC = (p_{t1} - p_{t2}) / p_{t1} \quad (1)$$

$$0 \leq CC \leq 1$$

where  $CC$  is the combustion completeness of the fire-affected area,  $p_{t1}$  and  $p_{t2}$  is the pre-fire and post-fire reflection respectively.

*Emission ratios and emission factors*

Emission factors (EF) and emission ratios (ER) were measured with the Airborne Fourier Transform Infrared Spectroscopy (AFTIR). The AFTIR system is designed to obtain FTIR spectra of air flowing through, or detained within, a multipass cell inside an aircraft [Yokelson *et al.*, 1999; Yokelson *et al.*, 2002a, this issue]. The AFTIR was mounted on a CV-8 Convair aircraft measuring ‘real-time’ concentrations of gases in smoke plumes over the KNP [Hobbs *et al.*, 2002, this issue B(a)]. Initially ER were derived from the concentrations of a gas  $X$  that was related to the simultaneous concentration of a reference gas usually CO or CO<sub>2</sub>. This is necessary since absolute concentrations in smoke plumes represent only the dilution of combustion gases or particulates in ambient air. The mixing ratios of gases may vary as a function of photochemical processes as the smoke ages [Hobbs *et al.*, 2002, this issue B (b)].

The EF fluxes are calculated and derived from the ER using the carbon mass balance equation, by reference to CO on the basis of an experimental ratio, being:  $ER = \Delta[X] / \Delta[CO]$  [Yokelson *et al.*, 2002b; Delmas *et al.*, 1995c]. As the carbon mass balance does not vary between biomass fuel types (biomass fuels usually contain up to 50% carbon) and type of combustion, we can use the experimental ratio above to derive the EF (described as  $X$ ).

The EF for the three sampled fires were related to the AFTIR measured modified combustion efficiency (MCE) of the fire as for some compounds the EF vary strongly depending on the MCE and hence also the type of combustion. The MCE is a measure of the oxidation of the fuel combusted and determined by the physical attributes of the fuel types and the type of combustion. MCE is defined as the fraction of carbon emitted as carbon dioxide relative to the total gaseous emissions of CO and CO<sub>2</sub> [Ward *et al.*, 1992a; Scholes *et al.*, 1996b].

$$MCE = CO_2 / [CO_2 + CO] \quad (2)$$

The sum  $[CO_2 + CO]$  represents generally more than 95% of the C released by the combustion. Table 7 shows the AFTIR results for emission ratios (ER) and emission factors (EF) for each gas measured in KNP smoke plumes. The combustion efficiency (MCE) is depicted for the three savanna fires investigated.

UW Flight Number	1815	1824	1834	
Date of fire (2000)	17-Aug	29-Aug	07-Sep	KNP-Area
Fire Name	<sup>1</sup> Skukuza (KNP)	KNP	Timbavati (KNP-Area)	Average
Fire Location(s)	-25.457, 31.582 -24.463, 31.836	-25.139, 31.401	-24.37, 31.25	by AFTIR
Modified				
Combustion				
Efficiency (MCE)	0.927	0.932	0.935	0.932
CO <sub>2</sub> EF	1678	1688	1696	1687
CO/CO <sub>2</sub> ER	0.0784	0.0726	0.0692	0.0734
CO EF	83.7	78.0	74.7	78.8
NO/CO <sub>2</sub> ER	0.0009	0.0011	0.0008	0.0009
NO <sub>2</sub> /CO <sub>2</sub> ER	0.0016	0.0019	0.0018	0.0018
NO <sub>x</sub> as NO EF	2.86	3.45	3.01	3.11
CH <sub>4</sub> /CO ER	0.0594	0.0704	0.0583	0.0627
CH <sub>4</sub> EF	2.84	3.14	2.49	2.82
C <sub>2</sub> H <sub>4</sub> /CO ER	0.0192	0.0156	0.0160	0.0169
C <sub>2</sub> H <sub>4</sub> EF	1.61	1.22	1.19	1.34
C <sub>2</sub> H <sub>2</sub> /CO ER	0.0033	0.0043	0.0034	0.0037
C <sub>2</sub> H <sub>2</sub> EF	0.26	0.31	0.24	0.27
HCHO/CO ER	0.0158	0.0104	0.0187	0.0150
HCHO EF	1.42	0.87	1.50	1.26
CH <sub>3</sub> OH/CO ER	0.0143	0.0202	0.0145	0.0163
CH <sub>3</sub> OH EF	1.37	1.80	1.24	1.47
CH <sub>3</sub> COOH/CO ER	0.0192	0.0169	0.0146	0.0169
CH <sub>3</sub> COOH EF	3.44	2.82	2.34	2.87
HCOOH/CO ER	0.0021	0.0054	0.0064	0.0046
HCOOH EF	0.29	0.69	0.79	0.59
NH <sub>3</sub> /CO ER	0.0076	0.0027	0.0016	0.0040
NH <sub>3</sub> EF	0.39	0.13	0.07	0.20
HCN/CO ER	0.0094	0.0059	0.0072	0.0075
HCN EF	0.76	0.44	0.52	0.57

<sup>1</sup>Two fires near Skukuza were averaged together as one fire when reducing AFTIR data.

**Table 7:** Initial emission ratios (ER) and emission factors (EF, g/kg) for fires investigated by the AFTIR on the University of Washington's (UW) Convair-580 aircraft covering a transect of ~100 km along which three fires were measured in the KNP-area during the SAFARI 2000 intensive research campaign.

*Emission calculation approach*

We used EF rather than autocorrelation with emission ratios (ER) based on the relative amount of CO and CO<sub>2</sub> emitted. A four way approach was adopted to optimize the emission factors (EF) and to test the sensitivity of the resulting emission estimates:

- (i) The AFTIR MCEs of fires measured in 2000 over the KNP were compared to the MCE of fuel mixtures that were modeled within the same location using Landsat ETM+ data sets from 2000. We shall call the method using the AFTIR MCE the *measurement* approach, and the Landsat derived MCE from the fuel mixture model the *model* approach. The modeled MCE for the study area were calculated from known MCE values measured for individual KNP fuel components during the SAFARI 1992 campaign [Shea *et al.*, 1996b; Ward *et al.*, 1996a]. The measured MCE were captured in three fires (Table 7) aligned along a 100-kilometer transect stretching from the open woody *Acacia spp.* savanna (in the middle of the park) to *Combretum spp.* dominated woody savanna in the south. The expected drop of measured MCE from open tree savanna to woody savanna fires was verified by the same corresponding drop in the modeled MCEs values determined for the three corresponding fire positions ( $R^2=0.97$ ,  $n=3$ ). The consistency between the two data sets implies that both approaches seem valid.
- (ii) EF for the gases in Table 7 were calculated using the 2001 Landsat ETM+ data. The MCE was modeled as a function of the ETM+ derived fuel mixtures (per pixel information) and as a function of the respective EF. To accurately define the linear relationship between the MCE and the EF we utilized the regression equations derived from all savanna fires that were AFTIR measured over Southern Africa during SAFARI 2000 [Hobbs *et al.*, 2002 (A)b]. The all-SAFARI regressions were statistically significant as opposed to the regression models available for only the KNP site. The all-SAFARI data was coherent with the KNP data points. The resulting EF (as a function of MCE) per pixel information gives some idea of the natural gradient in emission factors that results from savanna fires burning under a range of vegetative/environmental conditions and, therefore, with different mixtures of flaming and smoldering combustion factors for each smoldering compound (except CO<sub>2</sub> which is not a smoldering gas).
- (iii) The average AFTIR EF for measured gases from the KNP fires (Table 7) were applied in the emissions equation (3). This is the most efficient method since it omits the MCE modeling step and can be seen as accurate as it takes actual *in situ* data along the corresponding fuel sampling transect into account.

(iv) The average AFTIR KNP measured EF and the EF derived from the MCE models were substituted into the basic wildfire equation (3) [Braatz *et al.*, 1995c], resulting in two emission results for each gas respectively. The emission results using the two approaches were compared to one another. In this way the sensitivity of the two approaches can be defined which would substantiate the final result.

The emissions formulae can be applied to a region or for each burnt pixel:

$$\text{Emission (kg)} = \text{Area burnt (km}^2\text{)} * \text{fuel mass (gm}^{-2}\text{)} * \text{CC (g}^*\text{g}^{-1}\text{)} * \text{EF (gkg}^{-1}\text{)} \quad (3)$$

Where area burnt is the area size of the pixel (in km<sup>2</sup>), fuel mass is the total available above-ground fuel load per unit surface area [gDM/m<sup>2</sup>], CC is the combustion completeness [g\*g<sup>-1</sup>] and EF is the emission factor in grams per kg of dry fuel burnt [g/kg]. The retrieval of fire combustion completeness from MODIS multiplied by the high resolution ETM+ biomass information would provide a major advance over sometimes *anecdotal* estimates of combustion completeness that assume the entire satellite observation area as being burnt [*e.g.* Barbosa *et al.* 1999b].

## 2.4.3 Results and discussion

### 2.4.3.1 Predicting fuel mass and greenness

Due to the possible effect of misregistration and edge effects of the prescribed burn plot encapsulated in the Landsat ETM+ data we used several pixels well within the 120 meter sampling area that best matched the physical location.

As grass biomass is the most important savanna fuel [Stocks *et al.*, 1996] it should be sampled and determined with high accuracies. The best fit regression equation between grass mass for a total of 21 sites in KNP and Madikwe was achieved using the Landsat ETM+ Tasseled Cap brightness index ( $R^2=0.66$ , Figure 28). The data range and residual analyses showed that the data is normally distributed.

Above-ground wood (<2 meter), twig litter and woody debris litter smaller than 1,5 cm in diameter also correlated significantly to cloud free Landsat ETM+ index data for corresponding sampling areas ( $R^2=0.46$ ). The regression coefficient for wood was more depreciated than the grass model probably due to the fact that measuring vertical woody biomass in remote sensing is problematic [Franklin and Hiernaux, 1991]. In a recent study

*Kraus and Samimi* [2001b] found grass mass as compared to wood and foliage mass to also correlate (non-linearly) best with Landsat Thematic Mapper (TM) and Landsat ETM+ vegetation indices in Southern African savannas.

The grass and wood regression equation in Figure 28 show confidence (narrow interval) and prediction intervals (wide interval) at 95 percent, used to indicate mean variances of the data that is ascribed to the equation and prediction interval accuracies of the model respectively.

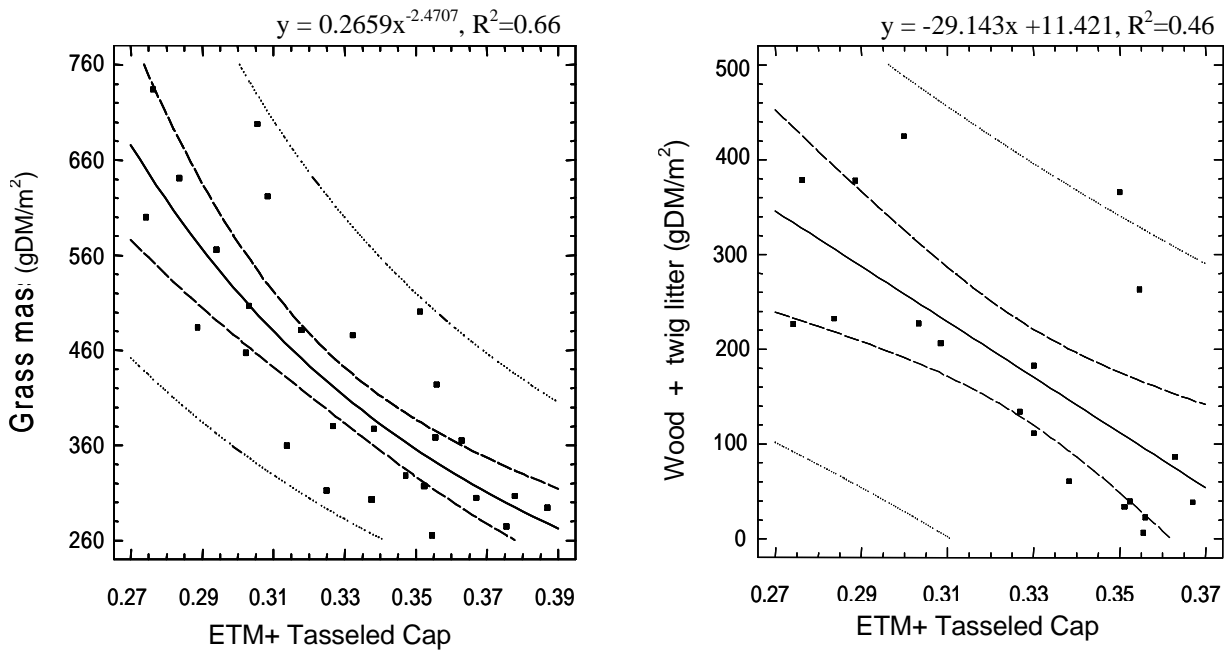


**Figure 28:** Aboveground grass and woody mass (=2 meter in height) including twig litter (gDM/m<sup>2</sup>) sampled on prescribed burn plots during 2000 and 2001 as a function of Landsat ETM+ Tasseled Cap (?) brightness. The regression was derived from field data sampled in several savanna types in the Kruger National Park and Madikwe Game Reserve. The regressions are shown with 95 % prediction intervals (widely defined as the bold, dashed line), the prediction intervals at 95% (narrow defined, dashed) for cloud-free 30m pixel averages pertaining to each 120m x 120m site (dots) and with non-linear and linear regression fits of these data (solid lines).

Average leaf litter [gDM/m<sup>2</sup>] averaged for each 120-meter sampling frame and collected in the 50 cm quadrats is best correlated to Landsat data using a two way approach (Figure 29). Firstly the tree cover density as [%] average per sampling frame was significantly linearly related to the Landsat ETM+ NDVI ( $R^2=0.62$ ). Secondly the sampled leaf litter mass was significantly non-linearly correlated to the measured tree cover density [%] for each sampling frame ( $R^2=0.75$ ) (Figure 29).

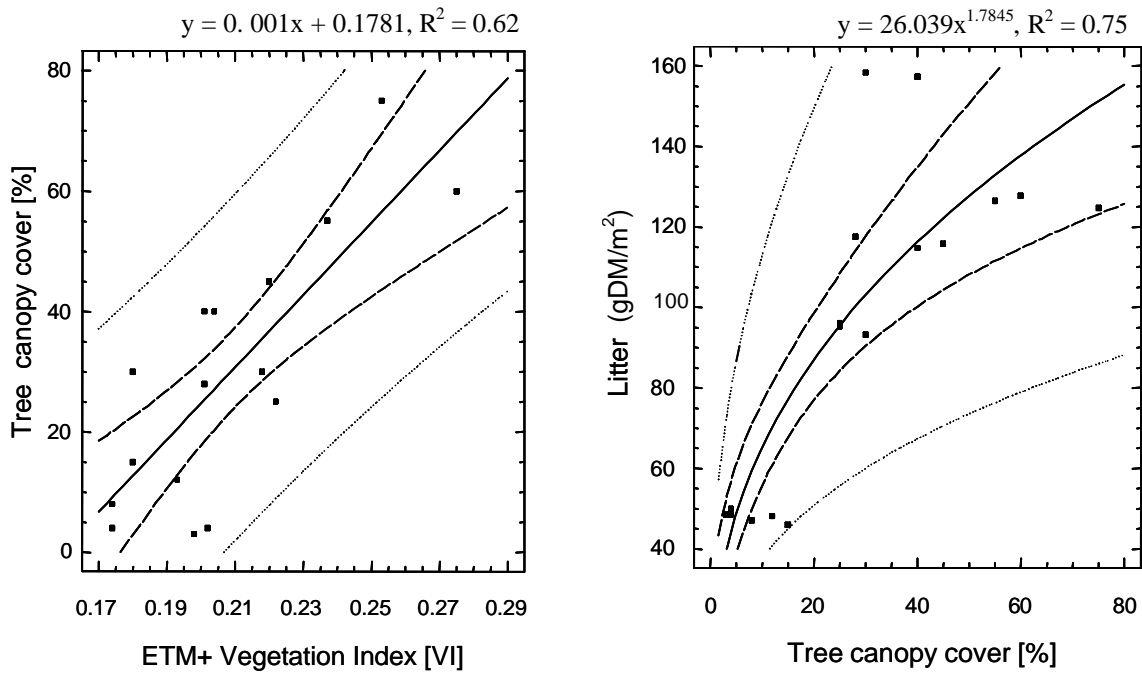


**Figure 29:** Recommended two-way approach that can be used to predict litter [gDM/m<sup>2</sup>] (grass and leaf litter). The site measured tree cover density [%] is significantly linearly related to Landsat ETM+; the tree cover density [%] can be used to predict the litter amount [gDM/m<sup>2</sup>] using the above non-linear regression. The regressions are shown with 95 % prediction intervals (widely, dashed line), the prediction intervals at 95% (narrow defined, dashed).

Percent pre burn fuel greenness from the fractional land cover estimates for trees, shrubs and grasses in several heights (as average per sampling site) was related to the Landsat ETM+ NDVI (Figure 30). As expected the result exhibited low greenness values for the Madikwe, similarly also in open woodland sites. Considerable higher greenness values were predicted for the *Combretum spp.* woodland sites in the southern KNP. Some broad leaved tree species may still have green foliage during the dry season depending on underlying soil physics, geology and if they are located in areas of enhanced moisture status [Scholes, 1997b]. Fuel greenness as a determinant of the combustion efficiency was also measured in KNP biomass fuels during the 1992 SAFARI campaign [Ward et al., 1996b].

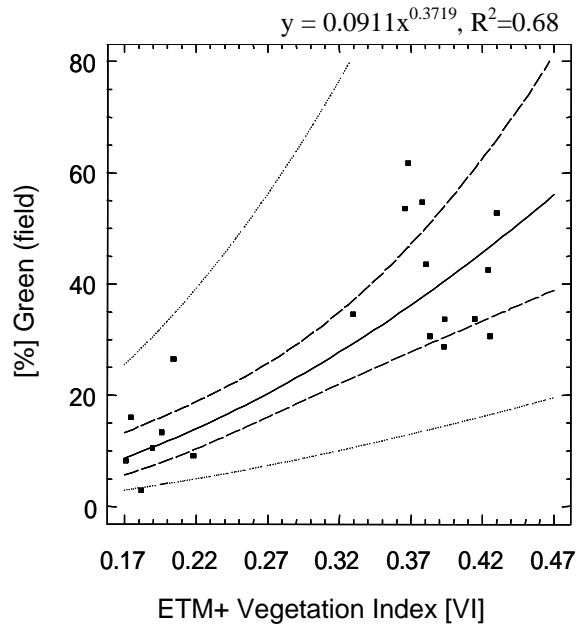


**Figure 30:** Percent [%] greenness from field observations on fractional land cover components and corresponding NDVI from Landsat ETM+. The regressions are shown with 95 % prediction intervals, the prediction intervals at 95% and with a non-linear regression fit of data points (solid lines).

We did not take into account a soil adjusted Vegetation Index (VI) [Huete *et al.*, 1985], as from our field observations the sampling areas only consisted of between 3 and 5% soil cover. All the regression equations used to predict grass, woody biomass, litter and greenness were significant ( $P=0.002$ ).

#### *Error and accuracy assessment*

Apart from the possible errors made during field sampling, field site misregistration, spectral calibration and mathematical errors in the regression equation models, there may be some error due to spectral satellite surface variability when merging field and remote sensed measurements [Elmore *et al.*, 2000b]. Moderate or coarse resolution satellites are mostly affected by changes in viewing, illumination geometries and instrument noise [Roy *et al.*, 2002c; Stroppiana *et al.*, 2000], yet they may still be prevalent in high resolution satellite data. These satellite and surface viewing effects may cause changes in surface properties that could possibly elevate or depreciate fuel mass in the regression equations. In especially multi-temporal image data sets differences that are due to fundamental changes are important to define [Roy and Landmann, 2002c, forthcoming]. To quantify the illuminous and viewing

effect, a range of surface cross track illumination corrections were implied on the surface reflection pre-burn data. The grass and tree mass was calculated and the result was compared with the original grass and tree mass modeled without illuminous corrections. The result showed that the error due to surface variation could result in the grass and shrub mass to vary between 0.5 and 3 percent for grass and wood mass respectively. This is assuming no other sensor noise.

Error sources in the fuel regression estimates may primarily be due to the extrapolation of individual dominant tree and shrub *species* mass to the whole sampling frame. The allometry reports used to estimate wood mass are only valid for the dominant species that were sampled in the randomly selected 10-meter plots (Figure 27). Due to these errors in the fuel variation and the above mentioned sensor variability the prediction and confidence limits in the fuel biomass regressions have to be carefully observed.

Vegetation with high tree cover and foliage densities that ‘hide’ underneath grass activities also had to masked out from the grass and wood fuel predictions [Thompson, 1993]. An empirical greenness threshold using the Landsat Vegetation Index (VI) was used for this. As a result a total of 6.5% of pixels in the September 2001 Landsat fuel image were masked out. These pixels were mostly outside the range of the prediction intervals (within a 95 percent confidence interval) or ascribed to areas of high percent greenness in river boundary vegetation and along seepage lines. A total quantifiable error range from the Landsat data was determined to be between 6.5 and 9.5 percent.

We recognize that other indices or ratios to estimate biomass parameters will exhibit similar or improved regression results within different savanna types at different scales and seasons. The high-resolution satellite models obtained can only be assumed to propagate accurate measurements along the 120 kilometer field sampling transect (and the 8020 km<sup>2</sup> sampling area in the KNP) within the boundary of the park.

The regression equations of the prediction models essentially measure the degree of accuracy using, for example, the goodness of fit squared multiple of the regression equations derived.

#### 2.4.3.2 Satellite fire information

The fire-affected area was extracted using daily 250-meter MODIS data tiles for the observation

period subsequently to the ETM+ 3<sup>rd</sup> September 2001 image. MODIS provides complete coverage of the study area. A linear regression between 30-meter Landsat mapped fire scar

sizes co-located to corresponding MODIS fire scars showed that only 7 % of the fire-affected area [km<sup>2</sup>] mapped was missed by 250-meter resolution MODIS. As 98 % of the missed fire scars were in the fragmented settlement areas next to the park, this uncertainty was seen to be negligible.

The CC information extracted from MODIS and Landsat ETM+ using the NIR channels respectively (841-876 nm) over a common acquisition period in August and September 2001 showed a highly significant agreement ( $R^2=0.87$ ) (Figure 31). Since we know that Landsat ETM+ is accurate in characterizing the fractional fuel consumption (CC) in the KNP [Roy and Landmann, 2002d, *forthcoming*] and the regression model in Figure 31 is significant we can make use of daily orbiting MODIS data to estimate CC of fuels in the KNP using the 250-meter NIR band (841-876 nm).

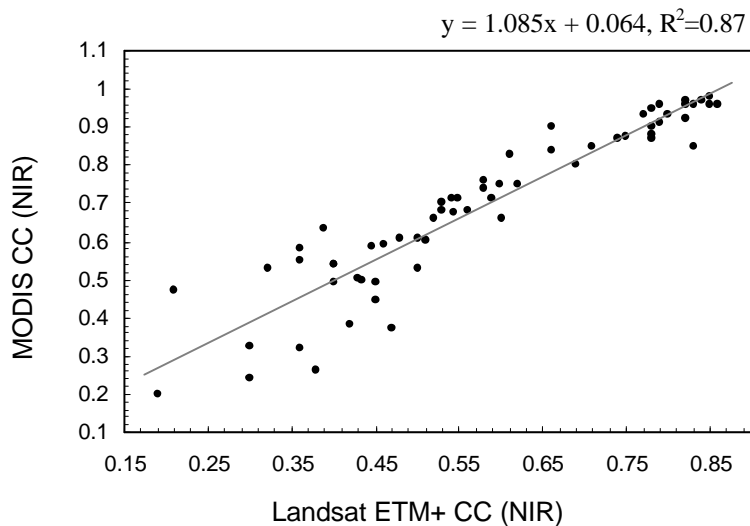


**Figure 31:** Regression equation showing 250-meter resolution MODIS CC using the NIR channel (841-876 nm) fire information as a function of the same information from co-located 30-meter resolution data from fires in the KNP. The regression shows that CC can be continuously and accurately ( $R^2=0.87$ ) estimated with daily MODIS fire information using the near-IR band.

The surface reflectance variation uncertainties imposed by residual aerosol loading in multi-temporal imagery, different sensor viewing, illumination geometries and surface property variations may affect the accuracy of MODIS derived CC information. This is explicitly visible in low combustion completeness fire pixels (CC values below  $\sim 0.5$ ; Figure 31). Some surface spectral reflectance changes on fire-affected areas may also be related to the fast regeneration of fire-affected areas in African savannas [Trigg and Flasse, 2000]. To exclude the temporal fire variations and other data ‘noise’ perturbations only cloud free good quality

MODIS observations with view zenith angles smaller than  $40^\circ$  and captured within two days after the fire occurrence were considered.

#### 2.4.3.3 Emissions estimates

The total aboveground fuel mass, the [%] greenness of fuels derived from the regression equations and the MODIS CC fire information were substituted into the basic wildfire emissions model in (3). Only the area within the park boundary in the southern and central part of the KNP was considered, the areas covering the corresponding field sampling transect ( $8020 \text{ km}^2$ ).

##### *Measured AFTIR EF versus fuel modeled EF*

We tested the emission results obtained by substituting the measured EF averages from the AFTIR against the emission results obtained from substituting the fuel modelled EF (as a function of the all-SAFARI 2000 measured CE). Both measurements are run for each respective gas over the September 2001 period and for the whole study area. Table 8 below shows minimum and maximum values for emissions (kg) calculated using the AFTIR measurement and the fuel modelling approach respectively. The [%] average difference in emission calculated for each gas using the two approaches respectively and the standard variation ( $1\sigma$ ) are also shown. The emission results from both approaches corroborate well on a one-to-one relationship. Evidently from Table 8 the results using the fuel modelling approach exhibited lower average emissions, the data points were also more variable and the minimum values were considerable lower than the results obtained by substituting the AFTIR measurements. The effect on  $\text{CH}_4$  (methane) was particularly pronounced as it exhibited an average difference of -11% between the two approaches. This may be due to  $\text{CH}_4$  being more sensitive to fuel mixtures and efficiencies of the burn than most of the other gases.

We can infer that the fuel model approach reduces the uncertainty for some gas estimates [Scholes *et al.*, 1996c; Ward and Radke, 1993a], in particular for some of the smoldering stage compounds such as  $\text{CH}_4$  and  $\text{NO}_x$ . The model approach seems more appropriate mainly due to the recognized complexity of savannas on a site and landscape scale and the higher sensitivity/variability in the results when using the fuel biomass composition and fuel consumption modelling method.

Gas	Approach	Min.	Max.	$1\sigma$	%
		emission [kg]	emission [kg]		difference (ave)
CO <sub>2</sub>	AFTIR	30168.9	79675.8	10399.2	0.4
	Fuel model	31099.7	79436.1	10182.9	
CO	AFTIR	1409.2	3721.7	485.7	-4.0
	Fuel model	917.2	3915.8	624.4	
NO <sub>x</sub> as NO	AFTIR	55.6	146.9	19.2	1.4
	Fuel model	59.0	165.9	22.4	
CH <sub>4</sub>	AFTIR	50.4	133.2	17.4	-11.8
	Fuel model	25.6	130.7	22.0	
C <sub>2</sub> H <sub>4</sub>	AFTIR	24.0	63.3	8.3	6.9
	Fuel model	16.2	63.5	9.9	
C <sub>2</sub> H <sub>2</sub>	AFTIR	4.1	12.8	1.5	0.0
	Fuel model	3.8	13.4	1.8	
HCHO	AFTIR	22.5	59.5	7.8	6.4
	Fuel model	15.1	58.1	8.9	
CH <sub>3</sub> OH	AFTIR	26.3	69.4	9.1	8.4
	Fuel model	15.0	67.3	10.9	
CH <sub>3</sub> COOH	AFTIR	51.3	135.5	17.7	-6.8
	Fuel model	30.6	139.9	22.8	
HCOOH	AFTIR	10.4	27.4	3.6	7.5
	Fuel model	10.7	37.9	5.7	
NH <sub>3</sub>	AFTIR	3.6	9.4	1.2	6.5
	Fuel model	3.5	14.2	2.2	
HCN	AFTIR	10.2	26.9	3.5	3.1
	Fuel model	8.7	26.9	3.8	

**Table 8:** Range (minimum and maximum), variations ( $1\sigma$ ) and percent differences of emission estimates derived by using the AFTIR measurements and Landsat ETM+ fuel modeled estimates.

#### *Total emission estimates and study context*

Table 9 shows resulting total cumulative pyrogenic emissions for the 8020 km<sup>2</sup> study area, emissions per unit area [g/m<sup>2</sup>] for the 30-day 2001 observation period and estimated KNP emissions for the 2001 burning season from June to October 2001 (for the equivalent study area). The emissions estimates for all fires occurring from June to late August 2001 were calculated from burned area estimates mapped using Landsat ETM+ imagery acquired on the 18<sup>th</sup> of August 2001. The total fuel mass and CC had to be assumed to be the averages

calculated for the ETM+ September observation period. As combustion efficiencies, EF, fuel composition and amounts vary between sites and seasons [Delmas *et al.*, 1995d] assumptions of accuracies are made using the comparison. Yet, it seems imperative to place our results into a spatio-temporal context.

Table 9 shows that between 24 and 29% of the dry season emissions of respective gases from June to early October 2001 occurred during our observation period. This once-off observation does not validate the hypothesis that burning and emissions south of the equator in Africa peak in September [Lacaux *et al.*, 1993c]. We note that cumulative CO<sub>2</sub> emissions measured for the observation period and area make up around 29 % of the total cumulative dry season emissions from June to September October 2001. CO emissions make up 26% of the dry season emissions; most other ‘smoldering’ gases also have a considerably lower percentage contribution than CO<sub>2</sub>. The reason for the elevated percentage CO<sub>2</sub> contributed may be related to the time of burning, as peak dry season fires are usually associated with more flaming combustion [Hely *et al.*, 2002b]. Peak dry season fires usually exhibit higher levels of oxidisations as biomass fuel moisture contents during that period are comparatively lower. September is the peak dry season in the KNP region.

Table 8 shows that CO<sub>2</sub>, CO, NO<sub>x</sub>, and CH<sub>4</sub> emissions are significant higher than most other compounds. Emissions of oxygenated volatile organic compounds (OVOC: alcohols, acids, aldehydes) were found to be considerable. This is an important finding, since OVOC were known to comprise about one-half of the organic emissions from temporal and boreal ecosystems [Yokelson *et al.*, 2002c] and were never before determined/considered in South African emissions inventories. OVOC are significant since they strongly influence smoke chemistry (to form OH and HO<sub>2</sub>) through photochemical processes [Mason *et al.*, 2001]. CO<sub>2</sub>, CO, NO<sub>x</sub>, and CH<sub>4</sub> are also important because reactions between them regionally probably contribute to the annual tropospheric ozone anomaly in Southern Africa [Scholes *et al.*, 1996d]. NO<sub>x</sub> explicitly causes ozone destruction in the stratosphere while it forms ozone in the troposphere [Graedel and Crutzen, 1997] and may thus contribute to regional climate changes.

Compound gas	Total September Emissions (tones) <sup>a</sup>	Emissions per unit area burnt (g/m <sup>2</sup> )	Total estimated emissions for study area (tons) from June-August 2001 <sup>b</sup>
Carbon dioxide (CO <sub>2</sub> )	187806 <sup>c</sup>	616.52	664650
Carbon monoxide (CO)	8367	27.47	31046
Nitrogen oxide (NO <sub>x</sub> ) <sup>d</sup>	383	1.26	1225
Methylcarbon (CH <sub>4</sub> )	272	0.89	1111
Ethene (C <sub>2</sub> H <sub>4</sub> )	137	0.45	528
Acetylene (C <sub>2</sub> H <sub>2</sub> )	29.8	0.10	106
Formaldehyde (HCHO)	126	0.41	496
Methanol (CH <sub>3</sub> OH)	142	0.47	575
Acetic acid (CH <sub>3</sub> COOH)	295	0.97	1131
Formic acid (HCOOH)	83.6	0.27	232
Ammonia (NH <sub>3</sub> )	30.6	0.10	78.8
Hydrogen cyanide (HCN)	60.9	0.20	225

<sup>a</sup> Based on the study area of 8020km<sup>2</sup>

<sup>b</sup> Estimated from burned areas extracted from high-resolution Landsat imagery captured over the same study area prior to September 2001, assuming invariable fuel/fire conditions at the time of burn.

<sup>c</sup> Assuming a C net content of 50 %

<sup>d</sup> NO and NO<sub>2</sub>, usually referred to as NO<sub>x</sub> [Lobert and Warnatz, 1993]

**Table 9:** Total emission estimates [t] and emissions per unit surface area [g/m<sup>2</sup>] for September 2001 over the Kruger National Park (KNP), covering an area of 8020km<sup>2</sup>. As a comparison cumulative emissions [t] are shown for all fires proceeding the observation period from June to August 2001.

#### *Spatial evaluation of important compounds*

Figures 32 to 35 show the spatial distribution of important reactive carbons (CO and CH<sub>4</sub>), NO<sub>x</sub> and CH<sub>3</sub>COOH as exhibiting the highest emissions from the OVOC gases. The

cumulative fire emissions [kg] released within the 30-day observation period are superimposed on the MODIS burned area data (Figures 32-35). The border between the KNP and other adjoining private reserves is shown as a continuous black line. To the left of the border the landscape is considerably fragmented by the high population density resulting in smaller fires (*Frost, 1999*). Due to overgrazing and wood fuel removal through harvesting in these highly utilized and populated areas emissions per unit surface area would be considerably less than in the pristine savanna areas (e.g. KNP).

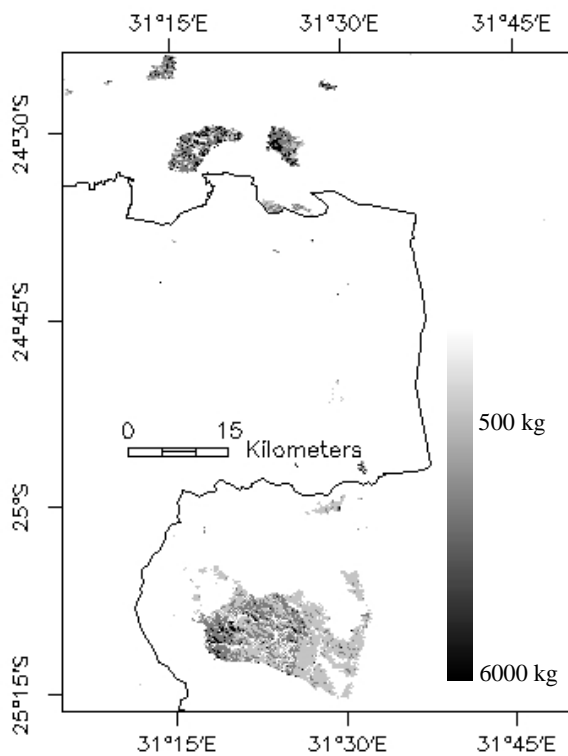


**Figure 32:** Cumulative CO emissions (kg) for the 30-day satellite observation period in September 2001

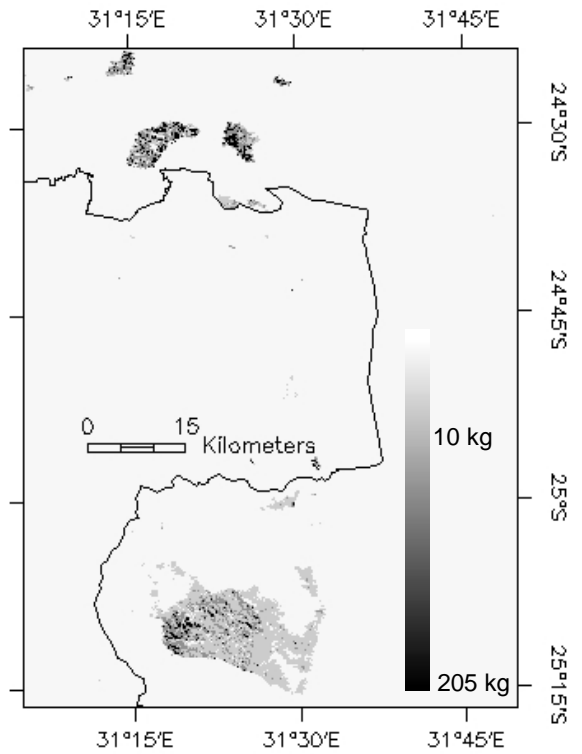


**Figure 33:** Cumulative NO<sub>x</sub> emissions (kg) for the 30-day satellite observation period in September 2001

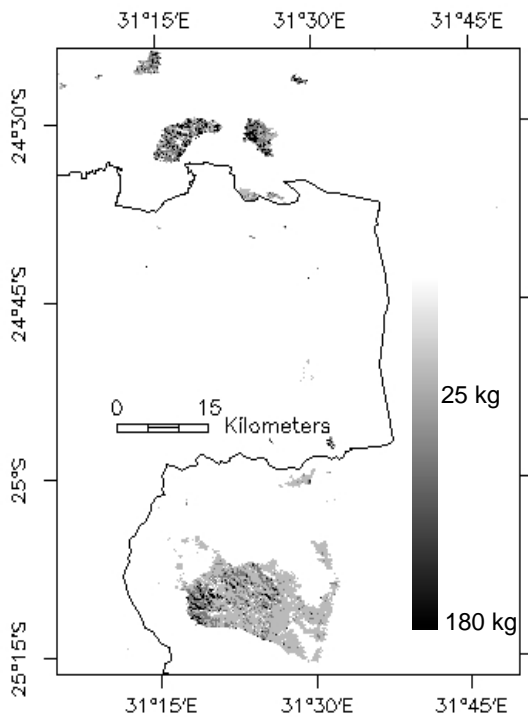


**Figure 34:** Cumulative  $\text{CH}_3\text{COOH}$  emissions (kg) for the 30-day satellite observation period in September 2001

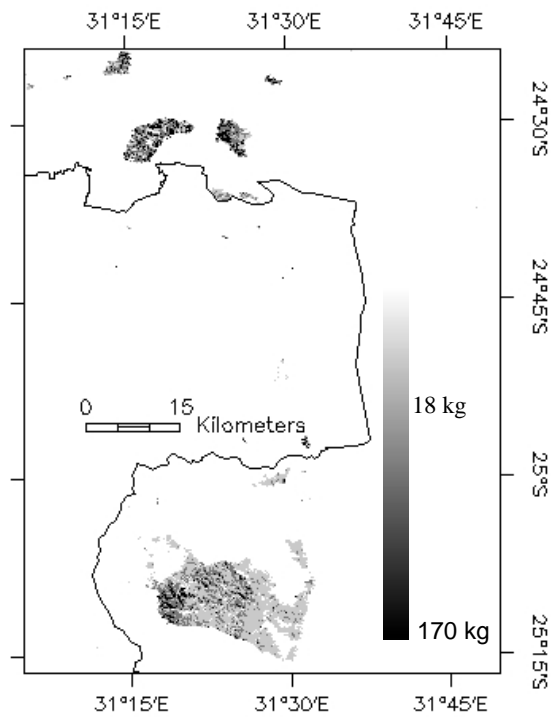


**Figure 35:** Cumulative  $\text{CH}_4$  emissions (kg) for the 30-day satellite observation period in September 2001

A significant finding in the spatial data is that emissions for all gases (especially  $\text{CO}_2$ ) were elevated in the central KNP regions (near the  $-24^\circ 30'$  latitude) as opposed to emissions over the southern KNP fires (lighter shades of grey). The central KNP fire sites were in the open woodland *Acacia spp.* savannas. In these sites the CC was on average 13% higher than in the *Combretum spp.* dominated (southern) broadleaved savanna sites. This implies that CC is an important and highly variable parameter affecting wildfire emissions. Broadleaved savannas usually produce larger diameter fuel wood [Scholes *et al.*, 1995] and to a lesser degree fine and dry fuels that usually burn more readily in flaming combustion [Luke and McArthur, 1977].

#### 2.4.4 Conclusion

The extensive biomass and site characterization sampling allowed us to determine the fuel mixture available for burning more accurately, instead of making (linear and theoretical) modeling assumptions about the fuel composition in savannas. The fuel mixture modeling approach, using the MCE versus the emission factor data, inherently also accounts for the

type of fire (smoldering or flaming combustion), which is largely determined by the fuel type and mixture [Delmas *et al.*, 1995d]. This knowledge and the airborne emission data recording which is weighted according to the combustion ratios at the time of sampling [Ward and Radke, 1993b] may consider the flaming to smoldering ratio in savannas more accurately and effectively (than for instance laboratory or field measurements). Corroborating the *in situ* emission factor data with inherent knowledge on the biomass ecosystem using spatially explicit and validated high-resolution vegetation regression models, and synoptic satellite fire observations provided useful information. The CC models provide a major advance over assumptions that the entire satellite observation area burned especially when coarse resolution satellite data is used as burned area input estimate. We also found CC to be a prime parameter in emissions estimates that is also highly variable over the study area.

All the above may considerably increase the accuracies in local emission estimates. However, to apply these methods operationally over a phenological diverse ecosystem is problematic due to the cloud problem in optical satellite data, the surface and remote sensing instrument variabilities mentioned and the typical low temporal resolutions of high-resolution satellites such as Landsat ETM+.

The AFTIR allowed us the capability to spatially measure the most 10 abundant gases in South African savanna fires. The emissions of OVOC gases from biomass burning were never before determined in South African savannas. The area unit emission mass data for the most abundant fire compounds (from Table 8) can provide data comparability with other explicit and spatially distinct fuel biomass consumption and emission models, pending their availability in the near future.

Finally we note that there is clearly a future need for more synthesis studies that couple *in situ* ecosystems data sets on fire behaviour, fuel data with known chemical elementary composition knowledge and high-resolution remote sensing as a function of time, location and fire regime. Stimulation of interactions between combustion scientists and atmospheric chemists proved useful in this study and should be further encouraged.

## 2.4.5 Summary

Before implementing emission factors into spatial flux calculations, site-specific coherent accurate and spatial explicit data on aboveground fuel available for burning, fuel consumption rates and burned area extend data is imperative. A 30-meter Landsat ETM+ spatially explicit model on fuel mass and type derived and augmented with synoptic daily observations of

burned area and combustion completeness (CC) from moderate resolution MODIS satellite is derived. The study area encompasses 8020 km<sup>2</sup> in the Kruger National Park (KNP), South Africa. The satellite fuel and fire data is corroborated with *in situ* smoke plume measurements of emission ratios (ER) and emission factors (EF) from Airborne Fourier Transform Infrared Spectroscopy (AFTIR) over prescribed fires in the KNP. The EF were determined for the twelve most abundant and important particulates found in smoke plumes of fires worldwide; most of these gases such as oxygenated organic molecules were never before estimated for fires over South Africa. The EF were related to the combustion efficiency (CE) of the fuel mixtures derived from the Landsat fuel models. Some smoldering fire phase compounds such as CH<sub>4</sub> were found to be highly sensitive to the variation in CE as a function of the EF. The main outcomes are spatial explicit cumulative emission maps for each gas [kg] for a 30-day observation period (3 September 2001- 4 October 2001). The results for oxygenated organic molecules (methanol, formaldehyde and acetic acid) in relation to the emissions of other compounds were found to be considerable. This is a significant finding since oxygenated organic molecules have a highly reactive photochemical potential. By combining real time satellite observations of burned area, CC, the spatial explicit fuel model data with EF measures as a function of the fuel mixtures we show that it is possible to improve existing fuel and fire inputs into emissions models.



## **2.5 The relevance of remote sensing burned area information for future fire management policies in the Kruger National Park (KNP)**

T. LANDMANN and N. GOVENDER

(submitted to *Koedoe*)

T. Landmann, Council for Scientific and Industrial Research (CSIR), Environmental Technology (Environmentek), P.O. Box 395, Pretoria 0001, South Africa (tlandmann@csir.co.za); N. Govender, Scientific Services, South African National Parks, Private Bag X 402, Skukuza, South Africa.

### **2.5.1 Introduction**

Fire is a key management issue in the Kruger National Park (KNP) and is an important agent capable of affecting structural change in KNP plant ecosystems and associated faunal diversities (Biggs & Potgieter 1999). KNP fire management policy is evolving with changing integrated attitude towards ecosystem management. In April 2002 the Kruger National Park (KNP) implemented a new Integrated Fire Management System that stipulates setting prescribed fires based on vegetation biomass and species composition, cumulative monthly burn area targets, and fire suppression efforts if a security threat or a burnt area target is reached (Biggs 2002a).

Both fire suppression activities and management objectives to monitor and modify fire management programs require accurate and timely information on the location, spatial distribution and timing of fire. Spatial information on fire severity would help to classify fire regimes and fuel types, fuel amounts combusted and help to compare burns regionally or seasonally (Chaffey & Grant 2000). Knowledge related to fire such as fire behaviour and fuel status provides a sound bases to fire management activities (Fernandes 2001).

Satellite imagery has the potential to provide fire information rigorously and spatially explicit typically over large or remote areas where direct characterization of fires cannot be feasibly measured or observed by park managers. Remote sensing methods use portions of the electromagnetic (EM) spectrum which is not visible to the eye to extract a wide range of fire

related information such as *before the fire* biomass fuel information, such as vegetation status, *during the fire* observations on the intensity of the active fire flame and *after the fire* assessments that describe the burnt area (Flasse *et al.* 2002a). Fire managers can utilize fire remote sensing information from each of the fire stages. However, studying active fires is problematic in remote sensing because burning may not occur at the time of the satellite overpass (Roy *et al.* 1999). Mapping fire scar characteristics using remote sensing data, such as fire severity or combustion completeness mapping, is increasingly being accomplished in fire remote sensing (Patterson & Yool 1998a; Michalek *et al.* 2001a; Miller & Yool 2002a; Roy & Landmann, 2002, forthcoming).

Satellite data sets on fire scar information can further corroborate field fire reports made by the park rangers and significantly improve the accuracy of the data used in future park management decisions. Depending on the turnaround of securing the satellite data, newly lit prescribed burns may be assessed in order to help plan further ignitions (Brockett *et al.* 2002a). Explicitly, remote sensing can assess and assist fire management policies by:

- improving knowledge of the current fire situation
- assisting strategic fire management decision making
- eventually assessing the effectiveness of fire management objectives.

Many studies have shown the potential usefulness of remote sensing to effectively map fire related information for resource managers (e.g. Pereira *et al.* 2000; Thompson & Vink 1997; Hetherington 1997). In South Africa several image based fire mapping techniques such as single or multi-temporal imagery, derived indices, simple level slicing, isodata clustering models, principal component analysis and spectral vegetation indices (VI's) have been investigated for extracting fire scar mapping in national parks (Flasse *et al.* 2002b). Most commonly indices or band ratios are used to extract fire information from satellite data. Spectral indices consist of individual bands that use defined wavelength, combinations in the form of ratios, ratios of differences divided by the sums (normalized differences) or linear band combinations. Thompson (1993) investigated the use of single-date Landsat-5 Thematic Mapper (TM) Normalized Differential VI (NDVI) in as a once-off study in a South African park to map fires in the Hluhluwe-Umfolozi Game Reserve in eastern South Africa. Hudak *et al.* (1998) used multi-spectral principle component classification (PCA) methods to map fire severity between two Landsat acquisition phases in Madikwe Game Reserve in northwestern South Africa. Roy *et al.* (2002b) is currently developing time-series burn scar information for

the Southern Africa using well calibrated, atmospherically and bi-directional corrected daily orbiting Earth Observing System (EOS) MODIS data sets. However there is clearly a need for accurate automated methods to satellite map and characterize burnt areas with high accuracies over larger phonological diverse regions (Rogan & Franklin 2001). Satellite burn scar mapping methods are less automated than active fire mapping and are often applicable only on a local scale using empirical thresholds on spectral satellite data to extract the area burnt. In this study we attempt to show simple fire extraction methods using Landsat ETM+ data to delineate/map the area burnt. The spatial accuracy of 500-meter resolution MODIS data to map fires as time-series and continuously over the whole KNP area is investigated. We will only investigate the reflective bands in MODIS and Landsat ETM+. Lastly suggestions are made of how these and other recent findings pertaining to the satellite characterization of burnt areas and the burned area time-series MODIS fire product information can effectively be used to complement future fire policies in the KNP.

## 2.5.2 Background

### 2.5.2.1 Imaging characteristics and data description

Objects and landscapes reflect and emit different amounts of radiation at different wavelengths. In the visible (VIS) to middle infrared (mid-IR), this response is measured using reflectance (Flasse *et al.* 2002c). Different sections of electromagnetic radiation responses are defined in spectral bands (usually measured in micrometers -  $\mu\text{m}$ ), and each spectral band is differently sensitive to e.g. ashes and charcoal. The narrowness and amount of bands are defined as the satellite sensor's spectral resolution. The temporal and spatial resolution is largely determined by the orbit characteristics of the satellite and the area on the ground covered by the satellite, *i.e.* detection footprint. High-resolution satellites have smaller detection footprints and longer revisit cycles, because of the inherently larger data volumes they transmit and store (Arvidson *et al.* 2001). High-resolution satellites are less likely to be attenuated by so called illuminous and satellite viewing effects on the surface of the earth than moderate or low resolution satellites (Stroppiana *et al.* 2001a). These effects cause reflectance variabilities in each satellite pixel that may not be coherent with the changes in land cover. Pixels or image elements make up the lines and samples of a satellite image within a certain defined grid.

The MODIS satellite onboard NASA's<sup>1</sup> Terra satellite platform senses the earth's surface in 36 spectral bands spanning the visible (0.415 $\mu\text{m}$ ) to thermal infrared (14.235 $\mu\text{m}$ ) spectrum at nadir spatial resolutions of 1 km, 500m and 250m (Barnes *et al.* 1998). MODIS provides daily coverage for all areas globally above approximately latitudes of 30°. The detection footprint of MODIS is 2330 km. The first seven MODIS reflective bands at 500-meter resolution are primarily used for fire monitoring and land cover observations (Table 10).

In this study we used high-resolution Landsat Enhance Thematic Mapper (ETM+) reflective data that was acquired in the context of the extensive Southern African MODIS fire validation campaign in 2000 and 2001 (Roy *et al.* 2002c; Justice *et al.* 2000). Landsat ETM+ is collected on the Landsat-7 platform in a near-polar, near-circular, sun-synchronous orbit, imaging the same point on the Earth's surface every 16 days. Landsat-7 ETM+ data have a spatial resolution of 15m and 30m in the reflective bands and senses the earth in seven spectral reflective bands from the visible (0.479 $\mu\text{m}$ ) to the middle infrared (mid-IR) (2.209 $\mu\text{m}$ ). In this paper the two corresponding MODIS and Landsat ETM+ mid-IR bands are called the short mid-IR (SMIR) and the long mid-IR (LMIR) bands respectively. This spectral region is otherwise called the shortwave thermal infrared (SWIR in Table 10). Landsat scans an area corresponding to 175 km by 180 km on the ground. We used three Landsat ETM+ images captured consecutively over the Skukuza area in the southern KNP during 2000 to imply simply mapping method in multi-temporal data sets. Two ETM+ scenes were also acquired in 2001 to verify the spatial accuracy of MODIS. The 2001 burn season was selected for the ETM+ to MODIS spatial analyses because good quality and cloud free MODIS tiles were available in this period.

Table 10 shows the spectral, spatial and temporal characteristics of both Landsat ETM+ and MODIS reflective bands, as well as data sources and data costs. The ETM+ data and quick-looks are available by searching the EOSDIS Data Gateway website listed in Table 10. The Landsat ETM+ satellite series has is an operational satellite programme that guarantees the routine availability of remotely sensed data over longer time periods. MODIS on the contrary is a lesser operational satellite, since there will be no predecessor after the five year life span of MODIS. Yet research results from MODIS may input and complement improvements and developments in future satellite missions.

---

<sup>1</sup> National Aeronautics and Space Administration

Spectral characteristics	Landsat ETM+		MODIS (500m bands)	
	Channel	Central wavelength	Channel	Central wavelength
Visible Blue	1	0.48	3	0.47
Visible Green	2	0.56	4	0.56
Visible Red	3	0.66	1	0.65
Near Infrared (NIR)	4	0.83	2	0.86
Short wave infrared (SWIR)	-	-	5	1.24
Short middle infrared (SMIR)	5	1.65	6	1.64
Long middle infrared (LMIR)	7	2.21	7	2.13
Visible near-IR (VNIR) <sup>a</sup>	8	0.71	-	-
<b>Spatial characteristics and practical issues</b>				
Spatial coverage	175 by 180 km		2330 cross track	
Temporal resolution	16-day cycle		4 times daily <sup>b</sup>	
Pixel size	15-30 m		250-500m <sup>c</sup>	
Data costs	~450 USD		no costs	
Data source	<a href="http://edcimswww.cr.usgs.gov/pub/imswelcome/">http://edcimswww.cr.usgs.gov/pub/imswelcome/</a>		<a href="http://redhook.gsfc.nasa.gov/~imswww/pub/imswelcome/plain.html">http://redhook.gsfc.nasa.gov/~imswww/pub/imswelcome/plain.html</a> (or left)	

<sup>a</sup> Pancromatic 15-meter spatial resolution VNIR band (0.52 $\mu$ m- 0.9 $\mu$ m).

<sup>b</sup> MODIS is on two satellite platforms: one morning and night pass (on EOS-AM-1) and one afternoon and early morning pass (on EOS-AQUA) respectively.

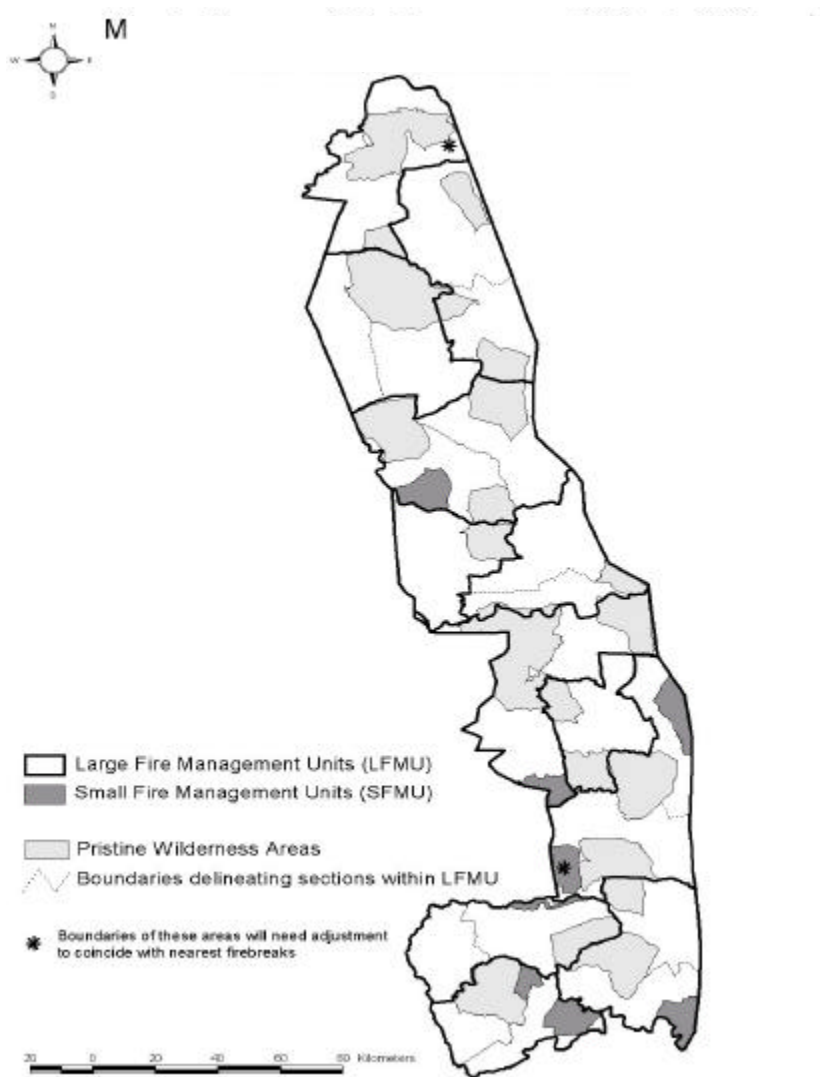
<sup>c</sup> The Red Visible (0.65 $\mu$ m) and the near-IR (0.86 $\mu$ m) bands have a spatial resolution of 250 meter; the other reflective bands have a spatial resolution of 500m respectively.

**Table 10:** Spectral, spatial and temporal characteristics as well as practical considerations compared for Landsat ETM+ and MODIS satellite data. The Visible bands are assigned to the visible color sequence (Red, Green and Blue).

### 2.5.2.2 Description of the KNP Integrated Fire Policy

The integrated KNP fire policy is flexible and dynamic to allow arson fires (illegal trans-migrant), lightning fires (natural) and prescribed point ignited fires (management) to contribute to a monthly burn area target stipulated for a certain fire management area. Point ignitions are lit within the designated area to create so called fire patch mosaics (Brockett *et al.* 2002b). The KNP is divided into two types of Fire Management Units (FMU). Map I illustrates the different FMU proposed:

- In the Large Fire Management Units (LFMU) fuel biomass and species composition as well as the percent of the area that is targeted to be burnt will determine burn procedures. In Pristine Wilderness Areas (PWA's) within the LFMU no species composition assessments are done prior to burning. Ignition points will be located as randomly as possible. Together with management and illegal immigrant fires, the LFMU is burnt towards the monthly target until the end of September. Lightning fires are allowed to contribute to the monthly target and will only be suppressed when over 50% of the FMU burn target is achieved. All management fires are stopped at the end of September and lightning fires are given a chance to burn.
- In the Small Fire Management Units (SFMU) biomass and species composition also determines randomly set point ignited burns until the monthly targets, which contribute towards a year end target. Lightning fires are aggressively combated within SFMU with only management fires as an ignition source.



**Map 4:** Proposed Fire Management Units in the KNP and Pristine Wilderness Areas

It is an existing objective in KNP fire management policies to monitor long term changes in the ecosystem with respect to fires (distribution, intensity, frequency, size and cause). These ecosystem descriptors are measured by so called “thresholds of potential concern” (TPCs) (van Wilgen *et al.* 2002). The TPC’S are upper or lower levels along a continuum of change of a selected environmental indicator which, when reached, prompts an assessment of the causes that will lead to management action to be taken to re-calibrate or moderate these causes (Anon 1997).

There is evidently a need for spatial information that can effectively differentiate burned, unburned, date of burn as well characterize burned areas to monitor long term changes in the TPCs.

## 2.5.3 Technical Approach

### 2.5.3.1 Spectral analyses of burnt areas

Two approaches were considered to simply separate fire reflectance spectra from other landscape features in the KNP and map the fire-affected area. We firstly investigated field and laboratory reflectance from the Analytical Spectral Devices (ASD) radiometer instrument to emulate the satellite reflection of ashes, burnt areas and savanna vegetation. This would allow us to investigate spatial mapping issues. Secondly we investigated the temporal evolution of fire affected areas on experimental burn blocks using multi-date (i.e. multi-temporal) Landsat ETM+ imagery captured in 2000 (15 August 2000, 31 August 2000 and 18 October 2000). The average spectral reflectance for a selected 3 by 3 pixel Landsat ETM+ window was investigated. The window average is less affected by possible misregistration between scenes and 'noise' perturbations in the data sets.

The ASD field radiometer was used to capture the spectral signature in the EM range between 0.43  $\mu\text{m}$  to 2.21  $\mu\text{m}$  (at a measuring interval of 0.01  $\mu\text{m}$ ) on fire-affected areas near Skukuza and Pretoriuskop in the KNP. The ASD was hand held over the fire-affected area, taking reflective measurements every 10 seconds through walking motion. To capture the temporal fire scar evolution, fire scars of different ages were measured (2 hour, 1 day and 7 days old fire scars). Ash, charcoal and samples of unburnt non-photosynthetic vegetation such as leaves, grass, twigs and bark found on newly burnt scars were also collected and subsequently analysed in the laboratory using the same ASD instrument and wavelength resolution. The field data and laboratory spectral ash signatures were averaged/resampled to the corresponding Landsat ETM+ wavelengths.

The ETM+ imagery was captured over experimental burned areas in the southern and central KNP during 2000. The KNP experimental burn plots (EBP) that were sampled were homogeneously burnt under similar micro-meteorological conditions. All EBP investigated exhibited soil fractional cover between 3 and 5 % of the total land cover and the tree cover density ranged from 20 to 26%. This is known from extensive field work performed on the EBP during the SAFARI campaign in 2000 and reported by Kraus and Samimi (2001). As it is critical in multi channel or multi-temporal satellite data to render spectral comparability between data from different acquisition dates, and between satellite data and laboratory or field radiometer reflectance, the ETM+ sets were calibrated (normalized) to the same physical units, surface reflection (?). An atmospheric transfer model (6S) (Vermote *et al.* 1997) was used to calculate surface reflection (?) from the digital numbers (DN) data sets (Level-1G).

There are also other numerous strategies available to calibrate at-sensor digital numbers to surface reflectance. The two most common techniques are Temporally Invariant Surface Features (TISFs) (Hall *et al.* 1991) and Empirical Line Calibration that uses field or radiometer reference spectra from landscape features and linearly correlates or matches these to the same features identified on an image (Kruse *et al.* 1990).

The Landsat ETM+ surface reflection (?) spectral information using the same wavelengths of fire-affected area showed a good point to point and line fit corroboration with the ASD measured fire spectra. This comparison shows that the calibration was accurate.

### 2.5.3.2 Spatial corrections

The Landsat ETM+ imagery of 2000 was co-located to one another to account for a slight shift in-between the ETM+ images. The co-registering result showed that registration was well within one pixel throughout the image. Further, the Landsat corrected imagery of 2001 was co-located to 500-meter MODIS imagery using an automated resampling process in the remote sensing software.

## 2.5.4 Mapping the fire-affected area

### 2.5.4.1 Spectral considerations in Landsat

Figure 36 below illustrates the resultant spectra simulated from laboratory ASD measured black ash, ASD field reflectance captured over a one week old fire-affected areas, laboratory ASD measured reflectance of KNP non-photosynthetic typical vegetation and the spectral signature for photosynthetic live vegetation (green grass). The green grass reflectance spectrum was provided by the United States Geological Survey (USGS) Digital Spectral Library (Clark *et al.* 1993) and included to represent the ideal 'green' reflectance as comparison. A soil reflectance spectrum is not included, since it exhibits a non-photosynthetic vegetation similar reflectance.

The narrow resolution spectral measurements are resampled to the reflective Landsat ETM+ bands (from 0.47  $\mu\text{m}$  to 2.2  $\mu\text{m}$ ), thereby simulating ETM+ reflectance spectra as the satellite would see them under near optimal atmospheric, illuminous and nadir viewing conditions. The position of the visible (VIS), red wavelength region, the near-IR (NIR) and the two mid-IR (MIR) wavelength regions (SMIR=short mid-IR; LMIR=long mid-IR) are shown. The shown ETM+ wavelength band centre regions also cover the reflective spectrum of MODIS wavebands (Table 10), and correspond to MODIS central wavebands.

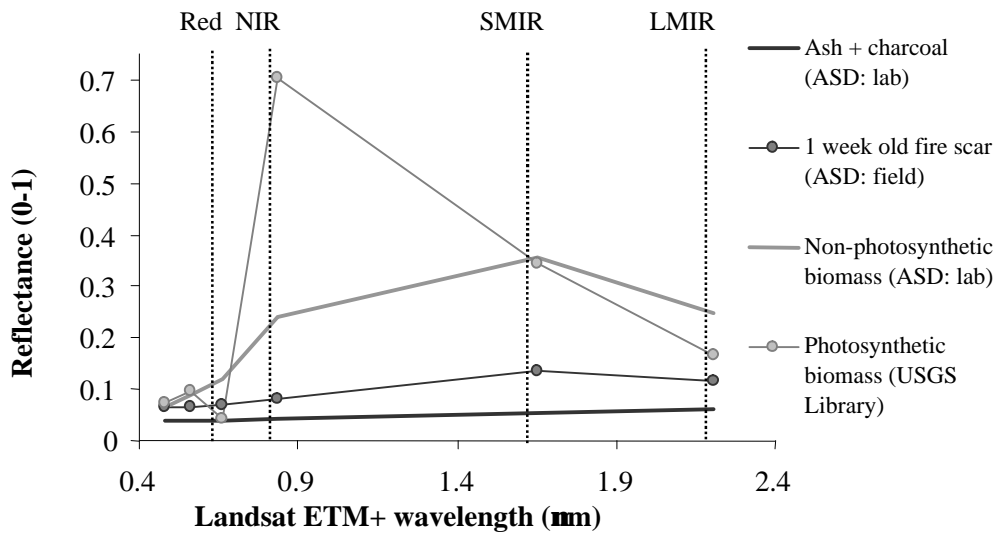


**Figure 36:** Simulated reflectance spectra of ASD derived ash reflectance, fire scar spectra and biomass reflectance spectra (solid lines). The non-photosynthetic biomass and ash spectra were derived from laboratory measurements using an ASD radiometer (grey and black line). The one week old fire scar reflectance spectra was derived using hand held field ASD radiometer measurement (averages) on one week old burn scars in the KNP (dark grey solid line with points). The photosynthetic biomass reflectance spectra was derived from the USGS spectral library (grey line with points). The simulated reflectance (y-axis) is shown as a function of the resampled Landsat ETM+ wavebands from 0.47  $\mu\text{m}$  to 2.2  $\mu\text{m}$ . The fire scar sensitive central wavebands are marked with vertical dotted lines.

As apparent from Figure 36, the SMIR region is better suited to discriminate the fire-affected area from the two biomass curves since both ash spectra are largely separate from the biomass curves. The NIR and the LMIR are second most discriminative. The difference between the SMIR and the LMIR for the ash spectra are negative to near slight positive. The same relationships for the two vegetation curves are pronounced positive. The SMIR is sensitive (high reflection) to non-photosynthetic fuel biomass, yet with increasing wavelengths in the MIR the signal is more insensitive for plant moisture content (Trigg & Flasse 2000a; Stroppiana *et al.* 2002b) and hence the reflectance decreases in the LMIR. This spectral response is typical in non-photosynthetic fuel biomass in savannas. The fuel biomass in the KNP during the burning season is characteristic non-photosynthetic.

Therefore, the differing nature of the two MIR channels used a differential index or Burn Index (*BI*) is a good tool for delineating and discriminating fire-affected areas from prevalent savanna vegetation

$$BI = \frac{\rho_{SMIR} - \rho_{LMIR}}{\rho_{SMIR} + \rho_{LMIR}}$$

where  $BI$  is the Burn Index,  $\rho_{SMIR}$  is the short wave middle infrared reflectance ( $\rho$ ) and  $\rho_{LMIR}$  is the long wave reflectance middle infrared reflectance ( $\rho$ ) respectively. The BI can be calculated with daily MODIS 500-meter overpasses using the two mid-IR channels 6 (1,628-1.652 $\mu$ m) and 7 (2.105-2.155 $\mu$ m) (Table 10).

To extract fire scars more accurately on a larger scale a second ratio (variable) to discriminate water bodies from burns must be applied. A differential ratio between the LMIR and the NIR region (BI2) can be used:  $BI2 = (\rho_{LMIR} - \rho_{NIR}) / (\rho_{LMIR} + \rho_{NIR})$ . Water bodies, swamp areas and moist surfaces with enhanced moisture status also have low mid-IR reflectance, especially in the SMIR, and hence spectral confusion in the SMIR spectral region would occur. In the LMIR spectral region, however, fire scars are “warmer” than moist areas, as fire-affected areas have a higher surface heat flux in the LMIR (Eva & Lambin 1998a). The depreciated NIR channel reflectance of fire scars (Figure 36) due to the decrease in chlorophyll and vegetation moisture on fire scars (Patterson & Yool, 1998b) makes this spectral region also suitable for fire scar discrimination. The NIR is sensitive to vegetation chlorophyll found in photosynthetic vegetation such as leaves and live grass (Gitelson & Kaufman 1998). The BI2 is commonly and effectively used to discriminate fire scars in temperate forest areas (Koutsias & Karteris 2000).

The mentioned differential ratios can be used to simply visualize the burnt area. Thresholds implied are only applicable on a local scale and can hence only be derived empirically. We do not attempt to show the accuracies or measure the discriminate properties of the differential ratios mentioned, although some topographic and illuminous effect normalizations when using reflectance spectral ratios have been observed in other studies (Kitchin & Reid 1999; Salvador *et al.* 2000; Stroppiana *et al.* 2002c). The magnitude of the index does not quantitatively measure fire severity or combustion completeness, especially as comparative between sites that may exhibit different tree cover densities or soil conditions. For example a fire-affected area in woody savannas could be mapped as less severe than a fire in a grassland site with the same intensity simple because unburnt woody cover would obstruct the reflection of ash underneath the tree canopy.

#### 2.5.4.2 Temporal considerations

Figure 37 below shows the mean temporal reflective fire scar evolution of all experimental burn blocks. We used three cloud free consecutive Landsat ETM+ data sets during the 2000 burn season and extracted the average reflective values for each prescribed burn block. Only the fire bands sensitive to changes associated with fire are used (ETM+ bands 3 to 7). The Normalized Difference Vegetation Index (NDVI), which is a ratio between so called RED visible region of the EM spectrum (0.63-0.69 $\mu\text{m}$ ) and the NIR (0.78-0.9 $\mu\text{m}$ ), shows less sensitivity to the burn scar evolution over time. The NDVI is known to be less capable in discriminating ash from vegetation in African savannas (Eva & Lambin 1998b). During the burning season in South African savannas the vegetation moisture contents and chlorophyll contents are low, which may

limit the use of the NDVI index to discriminate fire-affected areas from KNP savanna vegetation.

However, the difference between the two MIR bands in Figure 37 exhibits a pronounced sensitivity to fire temporal evolution, especially during the first seven days of re-generation after the fire event.

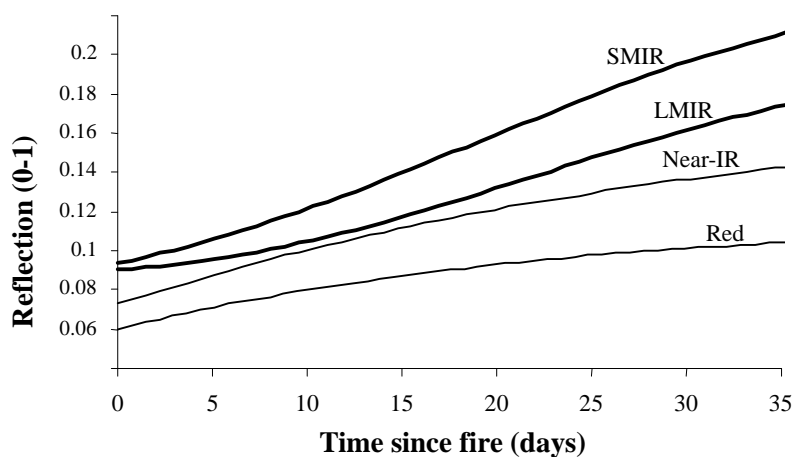


**Figure 37:** Temporal compositing of fire affected pixels using Landsat ETM+ bands 3 (0.66 $\mu\text{m}$ ) to 7 (2.2 $\mu\text{m}$ ). The exact burn day was gathered from field fire protocols made during the SAFARI 2000 intensive field campaign. The Landsat acquisition dates were: 15 August 2000, 31 August 2000 and the 18 October 2000.

The SMIR spectral region also is most sensitive to spectral change over time since the SMIR curve exhibits a steeper gradient (Figure 37). Therefore when using the MIR channels in fire mapping, only very recent burnt pixels can be mapped effectively. Observations from field

work in Namibian savannas verify that regeneration of fire-affected areas is fast as charcoal and ashes are rapidly removed by the elements (Trigg & Flasse 2000b; Langaas 1995).

#### 2.5.4.3 Validating MODIS fire information

Ultimately using regular time-series burn scar information from high temporal satellite sensors such as MODIS would be more effective and feasible. A three year MODIS burned area validation project was set up in 2000 to investigate the accuracy of time-series (automated) MODIS burnt areas information over Southern Africa (Roy 2000). Validation is performed with independent data from high spatial resolution (ETM+) satellite data sets that were acquired over representative sites within Southern Africa. The ETM+ imagery was mapped between two acquisition scenes, so identifying all fire activity within 16 days. Areas that could not unambiguously be identified as burnt were visited in the field and errors of omission and commission in the ETM+ mapping were noted (Roy *et al.* 2002c).

The Southern and central KNP (Landsat ETM+ scene path 168, row 077) is a MODIS fire validation site. ETM+ fire mapping and field validation was performed in the 2001 and 2002 dry seasons. The KNP images also cover the communal areas outside the park boundary. Validation field investigations showed that most mapping errors were caused by spectral confusion with freshly ploughed fields, low intense fires under tree canopy covers, fires that are patchy burned, mostly on swampy or seeped areas, and areas where re-generation of vegetation (green-up) was fast. Ambiguous fire areas were mostly found in the highly fragmented communal areas next to the KNP. At the time of writing research activities are still ongoing to fine tune, develop and improve the final MODIS burned area product with the supporting validation information from the different sites.

To test the spatial accuracy of 500-meter MODIS fire data in general for the KNP, we compared Landsat ETM+ fire scar areas with those mapped on MODIS. Fire scars were extracted from both satellites using the same Burn Index (BI) (manually), and using corresponding acquisition dates in 2001. We selected good quality cloud free MODIS imagery for a corresponding ETM+ detection area of approximately 100km by 100km. We used a simple linear regression to correlate fire-affected areas extracted from MODIS to collocated fire-affected areas on 30-meter Landsat ETM+ (Figure 38). The mapped Landsat pixels are considered as the true fire scar size and used to 'predict' corresponding 500m MODIS fire sizes. The significant agreement ( $R^2=0.98$ ) and low errors of omissions between Landsat and MODIS fires shows a good operational result. Only 7 percent of the area that was classified in Landsat as being burnt was undetected by MODIS, and 93% of this area was

outside of the park boundary. The minimum fire scar detection threshold in MODIS was below two square kilometres and is dependant of the “shape” of the fire affected area. The smaller fires outside the park may be due to the fragmentation of the land cover by settlements and roads (Frost 1999).

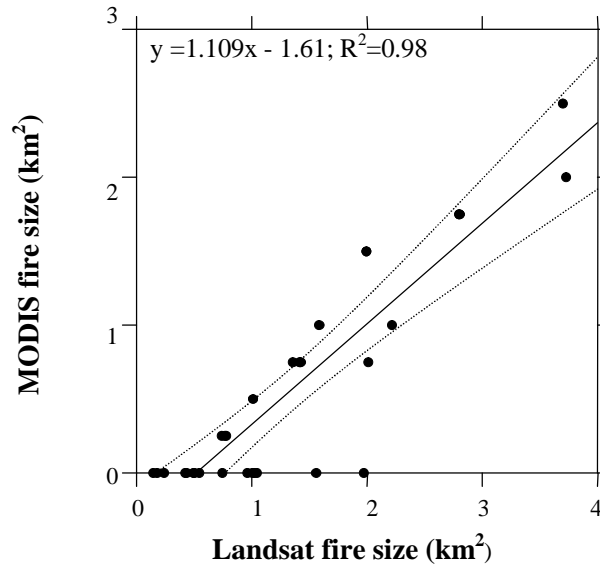


**Figure 38:** Regression equation between MODIS fire scar size (km<sup>2</sup>) and collocated Landsat ETM+ fire size for an observation period in September 2001. Only fires smaller than < 4 km<sup>2</sup> are shown with confidence limits at 95% depicted as dotted lines. The regression is shown as a solid line ( $R^2=0.98$ ;  $P<0.001$ ) and shows that fires  $\leq 2$  km<sup>2</sup> are hardly detected with 500m MODIS data. These areas are shown as data points on the x-axis, at  $y=0$ .

## 2.5.5 Relevance of results for fire KNP fire management

### 2.5.5.1 Fire mapping

Since we showed that the BI is sensitive to the spatial and temporal distribution of ash in the KNP biome, it provides a valuable tool to rapidly visualize fire-affected areas. The BI as well as the BI2 require low central processing unit (CPU) data overheads and can be easily applied whilst taking full advantage of the ‘fire sensitive’ reflective spectral range of Landsat ETM+ and MODIS data. Specifically the MODIS 2330 km detection footprint, no-cost data acquisition, daily overpasses, improved spectral characteristics (Table 10) and high fire mapping accuracies (from Figure 38) make it suitable to effectively extract fire scars over the

whole park region. The KNP covers an area of 330 km from north to south and an average of 55 kilometres wide. The imagery we acquired fitted well into the specific MODIS data tiles ordered for the location of Skukuza (24° 59' and 31° 34'), the administrative camp in the KNP.

Daily MODIS fire scar information could input the monthly KNP cumulative burning area target as set by the Integrated Fire Policy (Biggs, 2002b). This could give the fire manager information on whether to 'slack off' or carry on with prescribed fires to reach a specific monthly burn area target. Because MODIS tiles can be secured with a rapid turnaround time of around ~12 days, burned area information can be incorporated into current prescribed KNP ignition plans. For instance, the effectiveness of pre-empting unnatural fires up until end September (end of the burning season) through prescribed fires started from early in the season can be assessed by mid October. Further, the objective to prevent 'massive' unnatural or arson fires in early spring, starting from October can be assessed in retrospective. Comprehensive integrated knowledge on the area coverage of fires caused by unnatural causes, lightning and prescribed burns are one crucial component of the integrated fire management system (Biggs 2002c).

When considering a near real-time MODIS monitoring system (or direct broadcast) for the KNP area (Lynnes *et al.* 2000) 500m reflective band burned area information from MODIS can serve as baseline data for MODIS active fire location maps. Up to date fire scar information and the location/direction of the smoke plume can help to determine the location and ignition path of an unwanted active fire that may not require immediate suppression if it is burning towards a large area already visible or mapped as recently burned. The integrated fire policy embeds issues of fire security to protect humans and infrastructure in the case of possible fire threats.

#### 2.5.5.2 Fire regime monitoring

Although we do not aim to consider the use of remote sensing for biodiversity monitoring, spatial and more precise 'site specific' information on the fire regime using remote sensing may provide evidence on biodiversity and savanna vegetation dynamics or patchiness (Anderson *et al.* 1998; Justice & Korontzi 2000). The investigation into different fire and biodiversity patterns as a result of the different fire uses in the Fire Management Units (FMU) are key questions for the next decades (Biggs 2002d). The fire regime is characterized by the distribution of fires, their frequency, type of fire and essentially the fire intensity or severity (Bond 1997). Extensively validated time-series MODIS burn scar maps or self extracted burned areas per fire season enable the KNP fire managers to produce fire frequency and fire

seasonal maps, by simply comparing fire occurrence within or between one year/season to the next. Due to high temporal frequency of most coarse resolution satellites (such as MODIS) they are better suited to fire frequency and fire seasonality information, since this information depends on the time between dates of the fire occurrence.

Fire severity information, however, can only be accurately monitored with high-resolution data sets such as Landsat ETM+, and mostly coupled with field knowledge on fuel biomass consumption rates and fire intensity (Miller & Yool 2002b; Michalek *et al.* 2001b). In a recent study 30-meter Landsat ETM+ data was used to characterize the spatial distribution of ashes that are related to different fire severity levels. Whiter ash surfaces were found to be related to more pre burn biomass and increased burning efficiencies. Different fire severity levels could be derived for experimental burn blocks in the southern KNP (Landmann 2002, forthcoming).

Explicit fire severity, fire frequency and fire distribution information from hybrid integrated data sources (such as Landsat ETM+ and MODIS) can assist managers to monitor the long-term effects of the KNP Integrated Fire Management Policy by:

- Identifying current patterns in the fire regime and cross-referencing this information with ecological information on the desired fire regime, thereby highlighting areas where existing regimes are acceptable, or rather deviating, from the intention,
- Comparing fire regime patterns in areas where a range quality filter (before prescribed burning) has been applied to areas with random burning policies (such as in the Pristine Wilderness areas),
- Monitoring and comparing burn patterns and resulting biodiversity in areas determined by peak dry season prescribed patch fires, areas burnt by lightning or trans migrant fires at the end of the dry season (September to November) to areas burnt in the wet or pre dry season. Fires set at peak dry season are usually more severe and may be required to achieve certain management objectives (such as for example to suppress the woody savanna component in favour of the grass component) (van Wilgen *et al.* 1990).

Due to the low revisiting cycles of most high-resolution satellites (*e.g.* Landsat ETM+), cloud contamination in the data and constraint area coverage (Table 10), it may not be feasible to map fire severity over the whole KNP. Single fire events in different FMU could be selected and locally compared. A possible solution to low-temporal orbiting satellite data is using 15-30 meter high-resolution Advanced Spaceborne Thermal Emission and Reflection Radiometer

(ASTER) data onboard the daily orbiting Terra satellite platform. Aster is a pointer instrument and has Landsat ETM+ corresponding reflective wavelengths (from 0.55 $\mu\text{m}$  to 2.5  $\mu\text{m}$ ), covering a detection footprint of 60 km by 60 km on the ground (Maguchi *et al.* 1993). A request for Aster data can be submitted by investigators to capture a specific area of interest in consecutive orbits (<http://asterweb.jpl.nasa.gov>).

## 2.5.6 Conclusions and Recommendations

We found the MIR wavelength region, in particular the SMIR, to exhibit a large magnitude of reflective change when savanna vegetation is converted to charcoal and ash. Consequently straight differential band ratios using the MIR bands can be used effectively and are simple to extract fire scars using Landsat ETM+ and/or MODIS. The validated MODIS burned area information, that will be available in the near term, or the simple spectral fire extraction ratios shown here can effectively be used to feed the cumulative KNP burn area targets. To evaluate and monitor the effect of the KNP fire policy on fire and biodiversity patterns and possible habitat or fire regime shift through different Fire Management Units (FMU) high-resolution satellite data is better suited.

Figure 39 sums up the levels of remote sensing fire analyses investigated in this study to reach fire management objectives. With increasing data resolution, data costs and fire information detail the temporal resolution of the satellite systems usually decreases (e.g. Landsat ETM+ data). Aster is enclosed in a dashed line, because it does not really cover large areas of the KNP and its use must be requested. The theoretical system in Figure 39 is driven by the assessment needs to assimilate the (hierarchical) information levels.

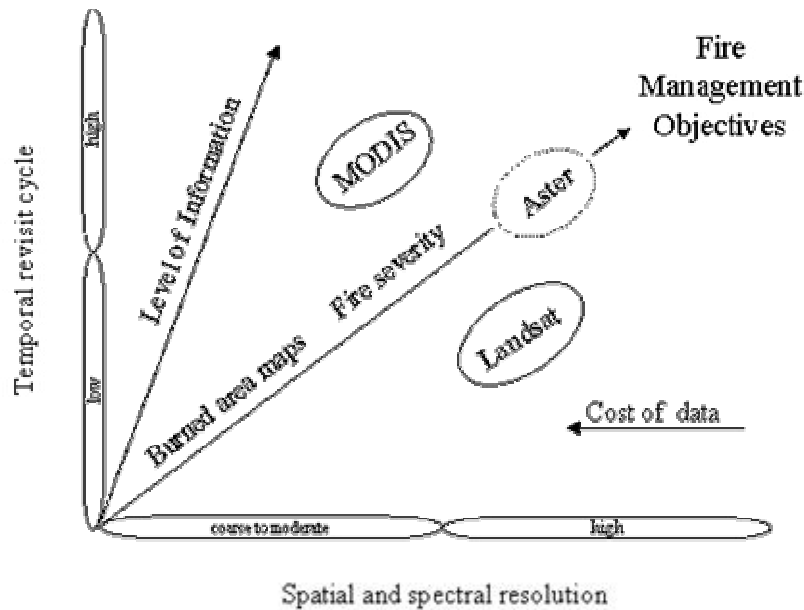


**Figure 39:** Fire remote sensing and its means to achieve fire management objectives. The positions of Landsat ETM+, MODIS and ASTER are shown (as ellipse circles) with regard to their spatial, spectral and temporal revisit cycles. The level and value of fire information increases considerable more with the temporal revisit cycle of a satellite. The cost arrow implies the lower costs of Landsat ETM+ or ASTER satellite data as compared with hyperspectral (very narrow bandwidth) airborne remote sensing data.

From Figure 39 it becomes apparent that there is a future need for high temporal (daily to twice weekly) and high spatially resolution satellite fire data encompassing large areas such as the KNP. The need for high temporal coverage is not only due to the fast temporal spectral fire changes we observed (Figure 37) but also due to the region exhibiting high cloud cover densities during the burning season. Low acquisition costs and enhanced capabilities in the MIR and NIR waveband regions would be an advantage. Ideally such a remote sensing satellite would be positioned near the top right in Figure 39. Future studies on the use of remote sensing for fire management objectives should also investigate the interdependences among the different information levels and other data inputs to the theoretical model in Figure 39. These inputs could be land cover, climate layers, topography information, biomass data as well as research and development inputs from experimental satellite or airborne remote sensing studies.

Essentially the assessment needs, and spectral and spatial resolutions of the satellites used will determine the method and abilities needed to corroborate future KNP fire management policies.

## 2.5.7 Summary

Concurrent to the introduction of the new Kruger National Park decision support fire policy is the final validation and refinement phase for time-series burn scar information from the MODerate Resolution Imaging Spectroradiometer (MODIS) satellite (Roy *et al.* 2002a). Within the recently completed Southern Africa Fire-Atmosphere Research Initiative (SAFARI) (Swap *et al.* 2001), fire and biomass fuel data as well as high-resolution satellite data such as Landsat ETM+ was collected and analysed to feed the refinement of MODIS burned area information. The primary aim of this paper is to comprehensively investigate the use of (= 30 meter resolution) Landsat ETM+ satellite data sets as well as burned area information from MODIS to corroborate KNP fire management policies. A simple burn scar index (BI) using 30-meter Landsat ETM+ data is derived using site specific spectral characteristics of fire-affected areas. The wavelengths used in the BI are found in most satellite sensors. Validation issues to verify the fire mapped area in MODIS using Landsat ETM+ are discussed: fire scars mapped with 500-meter resolution MODIS data sets were found to give a good agreements with corresponding fire scars mapped using 30-meter Landsat ETM+ satellite data ( $R^2=0.98$ ). The results show that daily 500m MODIS observations can be most effectively used to map burned areas to support fire management policies in large protected areas such as the KNP. More mapping detail can be achieved by using higher resolution satellite data, such as Landsat, but at higher data costs and lower temporal observation cycles.

**Key words:** Fire spectral characteristics, Landsat, MODIS validation, fire management.



## **Section 3: Overall Discussion and Conclusion**

### 3.1 Characterizing the fire-affected area

Temporally and spatially explicitly data on the distribution of aboveground fuel biomass available for burning is an important prerequisite for characterising the fire-affected, calculations on fuel consumption rates (ROY AND LANDMANN, forthcoming), fire severity models (MICHALEK *et al.*, 2000) and hence pyrogenic emission estimates. The fuel sampling protocol propagated in this study is efficiently designed to be applicable across large areas of diverse plant physiological and structural features. One drawback of the randomly designed fuel sampling technique is that large diameter downed logs that are sometimes sparsely distributed in woody savanna sites were often not accounted for. Ground-based fuel measurements for prescribed burns in Zambia suggest that up to 10% of fuels consumed was due to logs that continued smoldering for days (YOKELSON *et al.*, 2002). This remains to be corrected in future work.

From the sampled fuel data regression equations to predict fuel mass, percent greenness and vegetation structure (such as the tree wood to grass ratio) can be derived using Landsat ETM+ or 250-meter MODIS data. The Landsat ETM+ regression fuel estimates capture the actual (dynamic) state or cyclicity of the vegetation instead of modeling it. It should be noted, however, that this is not a physically based approach. Thus it requires enough sampling sites to develop the statistical relationships that can provide (say) grass mass ( $\text{g}/\text{m}^2$ ) predictions for a given satellite reflective index value.

In the near future (continuous) net primary production (NPP) models reliant on Rainfall Use Efficiencies (RUE), herbivory pressures and less empirical relationships between the tree and grass savanna components require more attention. Ideally they would be well validated and parameterized for several vegetation types. Previous released NPP fuel models are based on Light Use Efficiency (LUE) calculations for a single fuel biomass entity value, and thereby assuming a linear empirical relationship between savanna components (SCHOLES AND LANDMANN, forthcoming; HELY *et al.*, 2002).

The fire severity (FS) and combustion completeness (CC) models were investigated as hypothetical and/or illustrated with field and Landsat ETM+ data on fire experimental burn sites. The results demonstrate that:

- spectral variability/changes in multi-temporal fire mapping methods should be clearly defined by the sub-pixel information on fraction area burnt, CC and fire behavior factors such as the fire intensity and/or as a function of fire regime.
  - Characterizing the fire scars over large scale diverse fire regimes and physiological differing regions is problematic.
- complex algorithms must be applied with extensive atmospheric data corrections, and good pixel-to-pixel geo-location corrections
- sub-pixel information on the area fraction burnt and CC may be more accurate than ‘sometimes’ anecdotal burn scar aerial extend estimates that assume the whole pixel fraction burnt.
  - capturing CC and FS in ‘real-time’ with continuous satellite data observations may significantly improve future regional emission models.

Future work should focus on the interdependencies between spectral fire variations such as from the satellite viewing geometry versus the effect variability caused by solar and topographic shading effects (ROY *et al.*, 2002). These effects are pronounced in moderate to coarse resolution composite satellite data sets that have the potential to effectively cover larger areas (such as the whole KNP) with higher temporal frequencies. One way to determine only the viewing geometry effect would be to measure the constant fire energy from a fixed fire source (such as gas flares) in different MODIS view zenith angles and compare the energy emissions or brightness temperature releases to the changes in temperature or energy as a function of the view zenith angle.

### 3.2 Validation implication

The comparison between 250-500 meter resolution MODIS, Landsat ETM+ and field working results in this study can help to define validation protocols. The validation results show and imply that:

- errors of commission (such as ploughed fields) and omissions (such as sub-canopy low severity fires) occur at the KNP site and should be incorporated into automatic MODIS fire scar detection algorithms.
- defining combustion completeness and area fractions burnt information is possible with 250-meter MODIS data. There is an indication that the detection limit is around

0.5 CC or fraction burnt in MODIS because of the observed increase in data variability (and noise contribution) below that level.

- the MODIS 500-meter spatial resolution in seven reflective bands and 2330 km swath are suited to operational and effective fire mapping in the KNP, provided the mapped information is well validated.
- MODIS fire mapping and characterization mapping methods should consider the rapid burn scar re-generation potential verified by Landsat ETM+ multi-temporal mapped burn scars and field radiometer data in the KNP.

Future validation work should aim to investigate the implications of the temporal fire spectral signature evolution in MODIS fire mapping algorithms. The indications are that burned areas resemble a characteristic polynomial function over a 30-day period when observed in multi-temporal high-resolution imagery (using the fire sensitive wavebands: the near infrared and the middle infrared band). The spectral changes over time were found to be most pronounced in the first seven days after the fire event. The fire spectral signature resembles increasingly a soil reflective kind of spectral signature. This needs further investigation.

### 3.3 Local emission estimates

This section has illustrated the capabilities of new available EOS multi-sensor data to improve local emission estimates by capturing the ‘real-time’ fire activity and seasonal vegetation cyclicity (reliable and with known accuracies). The methods are less operational over larger regional areas (*i.e.* over Southern Africa). Yet, the derived Landsat ETM+ fuel biomass regression equations are applicable to subsequent studies over the KNP-area because they have been extensively validated with coherent data sets on biomass fuels over several savanna types. The emission results exemplify:

- The need for a high-resolution and spatially explicit fuel biomass map for emission studies.
- the fraction of oxygenated organic molecules to the total emissions (methanol, formaldehyde and acetic acid) was considerable. These compounds and their sources were never before determined or modelled in savanna fires over the KNP-area, yet they react photochemically to form HO<sub>x</sub>.
- characterizing combustion completeness and the fuel mixtures (*i.e.* the modified

combustion efficiency) spatially and explicitly can reduce some uncertainties in emission estimates as many so called smoldering gas compounds (such as CH<sub>4</sub>) are highly dependable on these parameters.

Future emission studies should increasingly exploit the relationship between the fire regime that largely determines the fuel mixtures, fire seasonality and hence the spatio-temporal distributions of gas emissions. The link between *in situ* emission factors determined through the airborne FTIR and (contextual) high-spatial resolution site-level fuel data may certainly reduce some of the uncertainties in emission models mentioned in the literature (*e.g.* JUSTICE AND KORONTZI, 2000; BARBOSA *et al.*, 1999; SCHOLLES AND LANDMANN, forthcoming). More synthesis studies of this sort are desirable.

Over and above this manuscript chapter shows how EOS hybrid data sets can potentially be used to derive explicit land-cover information, and how these information sources can be applied in emissions inventory reporting and with known accuracies. There is a programmatic need by the National Aeronautics and Space Administration (NASA) to use EOS data in the applications domain and for regional land managers to utilize satellite data and derived geophysical products.

### 3.4 The utility of results for fire management in the KNP

This manuscript chapter shows that new EOS data is operationally suited to effectively map fire scars in the KNP. Future operational fire monitoring systems that drive fire management strategies should be dynamic enough to include information from current research results (such as these) thereby subsequently utilizing new findings and data in their decision-making processes for fire management and reporting. Most importantly this chapter shows that:

- fire managers can acquire satellite data products that are increasingly available for free (*e.g.* EOS-MODIS data), or at substantially lower cost (in the case of Landsat-7), and easier accessible than before.
- regular satellite information on fire severity that may be related to the different burn practices of fire policies and biodiversity fluxes is currently only reliable using high-resolution satellites.
- there is a need for high-resolution continuous satellite data with several narrow bands and in the middle infrared spectral regions, a 1-2 day revisit cycle and a detection

swath of at least 100 kilometres. This need is in spite of the current spectral, spatial sensor improvements in satellite data and increased availability of biophysical and higher order fire products.

It is also hoped that research results presented in this thesis will be relevant to the next operational satellite systems planned by supplying some quantitative information on the accuracies of satellite fire mapping and characterization. One such planned operational satellite system is the new US National Polar Orbiting Environmental satellite System (NPOESS) to be launched later this decade. NPOESS provides moderate resolution data from 0.3 $\mu$ m to 14 $\mu$ m in 21 bands (NELSON AND CUNNINGHAM, 2002). NPOESS will provide direct (<1 day) long-term measurements of fire intensity (energy emissions from active fires), fuel moisture contents and fuel biomass data derived from net primary production (NPP) models. The European Space Agency (ESA) ENVISAT (Environmental Satellite) system is becoming operational in early 2003 and can, as well, provide comprehensive fire related information with unique atmospheric correction capabilities. The ATSR-2 and AATSR on ENVISAT have green, red, and near infrared channels for vegetation monitoring, in addition to the two short infrared and two thermal infrared channels on ATSR-1, that can deliver both nadir and "along track" views of the same surface location. The latter view passes through a longer atmospheric path, thus enabling improved corrections for atmospheric effects.

The results of this thesis show the utility of MODIS and Landsat ETM+ to map fires accurately over the KNP-area, to characterise fire scars that contribute significantly to atmospheric fire effect processes and ultimately how these data sets can corroborate fire management policies.



## **4. References**

- ACKERMAN, S.A., K.I. STRABALA, W.P. MENZEL, R.A. FREY, C.C. MOELLER, L.E. GUMLEY (1998): Discriminating clear sky from clouds with MODIS. *J. Geo. Res.* 103, D24: 32-141.
- ALLEAUME, S., HÉLY, C., LE ROUX, J., KORONTZI, S., ROY, D. P., SWAP, R. J., SHUGART, H. H., JUSTICE, C. O. (2002): Using MODIS to evaluate heterogeneity of biomass burning in Southern African savannas: Etosha region case study. Submitted to the *International Journal of Remote Sensing*.
- ANDERSON, A.N., R.J. WILIAMS, M.M. DOUGLAS, A.M. GILL, S.A. SETTERFIELD, W.J. MULLER, R.W. BRAITHWAITE, G. D. COOK & L.K. CORBETT (1998): Fire research for conservation management in tropical savannas: Introducing the Kapalga fire experiment. *Australian Journal of Ecology* 23 (2): 95-103.
- ANDREAE, M.O.(1997): Emissions of trace gases and aerosols from southern African savanna fires, in *Fire in Southern African Savannas: Ecological and Atmospheric Perspectives*, edited by B.W. van WILGEN, M.O. ANDREAE, J.G. GOLDAMMER, J.A. LINDESAY, pp. 161-183, Witwatersrand University Press, Johannesburg, South Africa,
- ANONYMOUS (1997): Revised management plan for the Kruger National Park. National Parks Board, Skukuza.
- ARINO, O., ROSAZ, J. (1999): 1997 and 1998 world fire atlas using ERS-2 ATSR-2 data. *Proceedings of the Joint Fire Science Conference, Boise, 15-17 June 1999.*
- ARVIDSON, T., J. GASCH & S.N. GOWARD (2001): Landsat 7's Long Term Acquisition Plan- An innovative approach to building a global imagery archive. *Remote Sensing of the Environment*, in press.
- BAILEY, A.W., BROCKETT, B.H., MENTIS, M.T. (1993): Fire management in Pilanesberg National Park, Bophuthatswana, using expert systems as aids to decision making. *African Journal of Range and Forage Science* (10): pp. 25-30.
- BARBOSA, P. M., D. STROPPIANA, J-M. GRÉGOIRE, J.M.C. PEREIRA (1999): An assessment of vegetation fire in Africa (1981-1991): burned areas, burned biomass and atmospheric emissions. *Global Biogeochemical Cycles*.13: 933-950.

- BARNES, W.L., T.S. PAGANO, V.V. SALOMONSON (1998). "Prelaunch characteristics of the Moderate Resolution Imaging Spectroradiometer (MODIS) on EOS-AM1", IEEE Transactions on Geoscience and Remote Sensing 36: 1088-1100.
- BARTON, J.M., J.W. BISTOW, F.J. VENTER. (1986): A summary of the Precambrian Granitoid rocks of the Kruger National Park. *Koedoe* 29:56-68.
- BIGGS, H.C. & POTGIETER, A.L.F (1999): Overview of the fire management policy of the Kruger National Park. *Koedoe* 42 (1):101-110.
- BIGGS, H.C. (2002): Proposed policy for the ecosystem management of fire in the Kruger National Park (KNP). Report, Skukuza, South African National Parks, unpublished report.
- BOARDMAN J.W., KRUSE F.A. (1994): Automated spectral analysis: a geological example using AVIRIS data, North Grapevine Mountains, Nevada. In Proceedings, ERIM Tenth Thematic Conference on Geologic Remote Sensing, Environmental Research Institute of Michigan, An, Arbor, pp. 1407-1418.
- BOND W.J. (1997): Fire. In *Vegetation of Southern Africa*, ed. R.M. Cowling, D.M. Richardson and S.M. Pierce, pp. 421-446, Cambridge, Cambridge University Press, UK.
- BRAATZ, B.V., S. BROWN, A.O. ISICHEI, E.O. ODADA, R.J. SCHOLE, Y. SOKONA, P. DRICHI, G. GASTON, R. DELMAS, R. HOLMES, S. AMOUS, R.S. MUYUNGI, A. DEJODE, M. GIBBS. (1995): African greenhouse gas emission inventories and mitigation options: forestry, land-use change, and agriculture, In: *African greenhouse gas emission inventories and mitigation options: forestry, land-use change, and agriculture Environmental Monitoring and Assessment*, edited by BRAATZ, B.V., S. BROWN, A.O. ISICHEI, E.O. ODADA, R.J. SCHOLE, pp. 109-126, Vol. 38, Kluwer Academic Publishers, The Netherlands.
- BRANSBY, D.I., TAINTON, N.M. (1977): The disc pasture meter: possible applications in grazing management, *Proceedings of the grassland society of Southern Africa* (12), pp. 115-118.
- BROCKETT, B.H. (1992) Calibrating a disc pasture meter to estimate grass fuel loads on the Zululand Coastal Plain, *African Journal of Range and Forage Science* (2), pp. 34-38.
- BROCKETT, B.H., H.C. BIGGS & B.W. VAN WILGEN. (2002): A patch-mosaic burning system for conservation areas in southern African savanna. *International Journal of Wildland Fire*, in press.

- CAETANO M.S.R., MERTES L., CADETE L., PEREIRA J.M.C. (1995): Assessment of AVHRR data for characterizing burned areas and post-fire vegetation recovery. In: Proceedings of the EARSel Workshop on Remote Sensing and GIS Applications to Forest Fire Management, pp. 49-52. University of Alcalá de Henares, Spain.
- CAHOON, D.R., B.J. STOCKS, J.S. LEVINE, W.R.C. COFER, K.P.O'NEILL (1992): Seasonal distribution of African savanna fires. *Nature* 359: 812-815.
- CAHOON, D.R., STOCKS, B.J., LEVINE, J.S., COFER W.R., PIERSON, J.M., (1994): Satellite analysis of the severe 1987 forest-fires in northern China and southeastern Siberia, *Journal of Geophysical Research-Atmospheres*, 99, 18627-18638.
- CHAFFEY, C.J. & GRANT, C.D. (2000): Fire management implications of fuel loads and vegetation structure in rehabilitated sand mines near Newcastle, Australia. *Forest Ecology and Management* 129: 269-278.
- CHENEY, P., SULLIVAN, A. (1997) Grassfires fuel, weather and fire behavior. CSIRO Publishing, pp. 102 –110.
- CLARK, R.N., G.A. SWAYZE, A.J. GALLAGHER, T.V.V. KING & W.M. CALVIN (1993): The U. S. Geological Survey, Digital Spectral Library: Version 1: 0.2 to 3.0 microns, U.S. Geological Survey Open File Report 93-592, 1340 pages, <http://speclab.cr.usgs.gov>.
- COCHRANE M.A, SOUZA, C.M. (1998): Linear mixture model classification of burned forests in the eastern Amazon. *International Journal of Remote Sensing*, 19, 3433-3440.
- COLE, M.M. (1986): *The Savannas: Biogeography and Geobotany*, London: Academic Press.
- COOPER, M.A.R. (1987): *Control Surveys in Civil Engineering*, Collins Professional Books, London, pp. 125-126.
- CRUTZEN, P.J., M.O. A. (1990): Biomass burning in the tropics: Impacts on atmospheric chemistry and biogeochemical cycles. *Science* 250: 1669-1678.
- CRUTZEN, P.J., M.O. A. (1990): Biomass burning in the tropics: Impact on atmospheric chemistry and biogeochemical cycles, *Science*, 250, 1669-1678.
- DEFRIES, R., C. FIELD, I. FUNG, G. COLLATZ, L. BOUNOUA (1999): Combining satellite data and biogeochemical models to estimate global effects of human-induced land cover change on carbon emissions and primary productivity, *Global Biogeochemical Cycles*, 13(3): 803-815.

- DELMAS, R., LACAUX, J.P., BROCARD, D. (1995): Determination of biomass burning emission factors: Methods and results, in African greenhouse gas emission inventories and mitigation options: forestry, land-use change, and agriculture Environmental Monitoring and Assessment, edited by Braatz, B.V., S. Brown, A.O. Isichei, E.O. Odada, R.J. Scholes, pp. 75-98, Vol. 38, Kluwer Academic Publishers, The Netherlands.
- DYWER, E., S. PINNOCK, J.M.GREGOIRE, J.M.C. PERREIRA (2000): Global, spatial and temporal distribution of vegetation fire as determined from satellite observations. *International Journal of remote sensing* 21: 3473-3497.
- ELMORE A.J., MUSTARD J.F., MANNING, S.J., LOBELL D.B. (2000): Quantifying vegetation change in semiarid environments: Precision and accuracy of spectral mixture analysis and the Normalized Difference Vegetation Index. *Remote Sensing of the Environment*. 73, 87-102.
- ELVIDGE, C.D., H.W. KROEHL, E.A. KIHN, K.E. BAUGH, E.R. DAVIS, W.M. HAO (1996): Algorithm for retrieval of fire pixels from DMSP operational linescan system data, in Biomass Burning and Global Change. Remote Sensing, Modeling and Inventory Development, and Biomass Burning in Africa, edited by J. S. Levine, MIT Press, Cambridge, Mass, London, England, Vol. 1, pp 73-85.
- EVA, H., LAMBIN, E.F. (1998a): Remote sensing of biomass burning in tropical regions: Sampling issues and multisensor approach, *Remote Sensing of Environment*, 64, 292-315.
- EVA, H., LAMBIN, E.F. (1998b): Burnt area mapping in Central Africa using ATSR data, *International Journal of Remote Sensing*, 1998, 19, 3473-349.
- EVA, H. & E.F. LAMBIN. 1998. Burnt area mapping in Central Africa using ATSR data. *International Journal of Remote Sensing* 19: 3473-3497.
- FERNANDES, P.A.M. (2001): Fire spread prediction in shrub fuels in Portugal. *Forest Ecology and Management*, 144: 67-74.
- FLASSE, S., M.M. VERSTRAETE (1994): Monitoring the environment with vegetation indices: comparison of NDVI and GEMI using AVHRR data over Africa, in: *Vegetation, Modelling and Climatic Change Effects*, editors F. Veroustrate and R. Ceulemans, SPB Academic Publishing, The Hague, The Netherlands, pp.107-135

- FLASSE, S., TRIGG, S., CECCATO, P., PERRYMAN, A., HUDAK, A., THOMPSON, M., BROCKETT, B., DRAMÉ, M., NTABENI, T., FROST, P., LANDMANN, T., LE ROUX, J. (2003): Remote Sensing of Vegetation Fires and its Contribution to a Fire Management Information System (8). In: Fire Management Handbook, in press.
- FRANKLIN, J., P. HIERNAUX (1991): Estimating foliage and woody biomass in Sahelian and Sudanian woodlands using a remote sensing model, *International Journal of Remote Sensing*, 12(6), 1387-1404.
- FRASER, R.H., LI, Z., CIHLAR, J. (2000): Hotspot and NDVI differencing synergy (HANDS): A new technique for burned area mapping over boreal forest, *Remote Sensing of Environment*, 74, 362-376.
- FREDERICKSEN, P., S. LANGAAS, M. MBAYE (1990): NOAA-AVHRR and GIS based monitoring of fire activity in Senegal- a provisional methodology and potential applications In: J.G. GOLDAMMER (ed.). *Fire in Tropical Biota*. pp. 179-215. Springer-Verlag, Berlin.
- FROST, P. G. H., ROBERTSON, F. (1987): The ecological effects of fires in savannas, In: *Determinants of Tropical Savannas*, edited by B. H. Walker, pp. 93-104, IRI Press, Oxford, England.
- FROST, P.G.H. (1999): Fire in Southern African woodlands: origins, impacts, effects, and control. Proceedings of an FAO meeting on public policies affecting forest fires. FAO Forestry Paper, 138: 181-205.
- FULLER, D.O., PRINCE, S., ASTLE, W.L. (1997): The influence of canopy strata on remotely sensed observations of savanna-woodlands, *International Journal of Remote Sensing*, 18, 2985-3009.
- GERTENBACH W.P.D. (1983): Landscapes of the Kruger National Park. *Koedoe*. 26, 9-121.
- Gitelson, A.G. & Y.J. Kauffman (1998): MODIS NDVI optimization to fit the AVHRR data series-spectral considerations. *Remote Sensing of Environment* 66: 343-350.
- GOWARD, S.N., B. MARKHAM, D.G. DYE, W. DULANEY, J. YANG (1990): Normalized difference vegetation index measurements from the advanced very high resolution radiometer. *Remote Sensing Environment* 35:257-277.
- GOWARD, S.N., MASEK, J., WILLIAMS, D. L., IRONS, J. (2001): The Landsat-7 Mission: Terrestrial Research in the 21st Century. *Remote Sensing of Environment*, in press.

- GRAEDEL, T.E., P.J. CRUTZEN (1997): *Atmosphere, Climate, and Change*, Scientific American Library, New York, USA.
- GUPTA, P. K., V. K. PRASAD, C. SHARMA, A. K. SARKAR, Y. KANT, K. V. S. BADARINATH, A. P. MITRA (2001): CH<sub>4</sub> emissions from biomass burning of shifting cultivation areas of tropical deciduous forests – experimental results from ground-based measurements, *Chemosphere - Global Change Science*, 3 (2), 133-143.
- HALL, F. G., D.E. STREBEL, J.E. NICKESON & S.J. GOETZ (1991): Radiometric rectification-toward a common radiometric response among multirate, multisensor images. *Remote Sensing of the Environment* 35: 11-27.
- HAO, W.M., M.H. LIU, P.J. CRUTZEN (1990): Estimates of annual and regional releases of CO<sub>2</sub> and other trace gases to the atmosphere from fires in the tropics, based on FAO statistics for the period 1975-1980, pp. 440-462. Springer Verlag, New York.
- HAO, W.M., D.E. WARD, G. OLBUR, S.P. BAKER (1996): Emissions of CO<sub>2</sub>, CO, and hydrocarbons from fires in diverse African savannah ecosystems, *Journal of Geophysical Research*, 101, 23,577-23,584.
- HÉLY, C., DOWTY, P., ALLEAUME, S., CAYLOR, K.K., KORONTZI, S., SWAP, R.J., SHUGART, H.H. (2002): Regional fuel load for two climatically contrasting years in southern Africa. *Journal of Geophysical Research*, in press.
- HÉLY, C., DOWTY, P. R., CAYLOR, K., ALLEAUME, S., SWAP, R. J., SHUGART, H.H. (2001): A temporal and spatially explicit primary production model for savanna fuel load allocation over the southern African region. Submitted to the *Journal of Ecological Modelling*, in press.
- HETHERINGTON, D.S. (1997): *Geographic information and remote sensing tools to assist fire management protocols in the National Parks of South Africa*. MSc thesis, The University of Greenwich, United Kingdom.
- HIL, J. (1990): Neue Wege zur geowissenschaftlichen Interpretation multispektraler Fernerkundungsdaten. *Geogr. Rundschau*, 50, 113-119.
- HOBBS, P. V., An Overview of the University of Washington's Airborne Measurements in SAFARI-2000, *Journal of Geophysical Research*, in press (A)

- HOBBS, P.V., P. SINHA, B. JILEK, L. JAEGLE, R. J. YOKELSON, T. KIRCHSTETTER, D. R. BLAKE, Emissions from a Savanna Fire from Biomass Burning in Southern Africa, *Journal of Geophysical Research*, in press (B)
- HOLBEN B.N., ECK T.F., SLUTSKER I., TANRE D., BUIS J.P., SETZER A., VERMOTE E., REAGAN J.A., KAUFMAN Y., NAKAJIMA T., LAVENU F., JANKOWIAK I. AND SMIRNOV A. (1998): AERONET -A federated instrument network and data archive for aerosol characterization. *Remote Sensing of the Environment*, 66, 1-16.
- HOROWITZ, L.W., S. WALTERS, D.L. MAUZERALL, L.K. EMMONS, P.J. RASCH, C. GRANIER, X. TIE, J.-F. LAMARQUE, M.G. SCHULTZ, G.P. BRASSEUR. 2002. A global simulation of tropospheric ozone and related tracers: Description and evaluation of MOZART, version 2. *Journal of Geophysical Research*, in press.
- HUANG C., WYLIE B., HOMER C., YANG L., VOGELMAN J. (2001): A Tasselled Cap Transformation for Landsat 7 ETM+ At-Satellite reflectance. *International Journal of Remote Sensing*, in press.
- HUDAK, A.T., B.H. BROCKETT & C.A. WESSMAN. 1998. Fire scar mapping in a southern African savanna. In: *Proceedings of the International Geoscience and Remote Sensing Symposium*, Seattle, Washington, CD-ROM.
- HUETE, A.R, J.C.N. EPIPHANIO (1995): Dependence of NDVI and SAVI on Sun/Sensor Geometry and Its Effect on fAPAR Relationships in Alfalfa, *Remote Sensing of Environment*, 51 (3), 351-360.
- JENSEN, J. R. (1996): *Introductory to Digital Image Processing: A Remote Sensing Perspective*, Englewood Cliffs, N.J.: Prentice-Hall.
- JUSTICE C.O., P.R. DOWTY, R.J. SCHOLLES, J.D. KENDALL (1996): Satellite remote sensing of fires during the SAFARI campaign using NOAA Advanced Very High Resolution Radiometer data, *Journal of Geophysical Research*, 101, 23,851-23863.
- JUSTICE, C.O., F. AHERN, A. FREISE (1999): *Regional Networks for implementation of the Global Observation of Forest Cover (GOFC) Projects in the Tropics*, START Report #4, START Secretariat, Washington D.C.
- JUSTICE, C.O. & S. KORONTZI (2000): A Review of the Status of Satellite Fire Monitoring and the Requirements for the Global Environmental Change Research, In: Ahern, F., J-M. Grégoire & C. Justice (ed.). *Forest Fire Monitoring and Mapping: A Component of Global*

- Observation of Forest Cover, Report of a Workshop, November 3-5 1999. pp. 1-18. Joint Research Centre, Italy: European Commission.
- JUSTICE, C.O., J. TOWNSHEND, E. VERMOTE, R. SOHLBERG, J. DESCLOITRES, D.P. ROY, D. HALL, V. SALOMONSON, G. RIGGS, A. HUETE, K. DIDAN, T. MIURA, , Z. WAN, A. STRAHLER, C. SCHAAF, R. MYNENI, S. RUNNING, J. GLASSY, R. NEMANI, N. EL SALEOUS & R. WOLFE (2000): Preliminary land surface products from the NASA Moderate Resolution Imaging Spectroradiometer (MODIS), In: Proceedings of IEEE Geoscience and Remote Sensing Symposium 2000 (IGARSS), Honolulu, Hawaii, 24-28 July 2000.
- JUSTICE, C.O., L. GIGLIO, S. KORONTZI, J. OWENS, S. ALLEAUME, J. MORISETTE, D.P. ROY, F. PETITECOLIN, J. DESCLOITRES, Y. KAUFMAN (2002): Global fire products from MODIS. (Special Issue of) Remote Sens. of Environment, in press.
- KASISCHKE, E.S., N.H.F. FRENCH (1995): Locating and estimating the areal extent of wildfires in Alaska boreal forest using multi season AVHRR NDVI composite data. Remote Sens. Environment 51: 263-275.
- KAUFFMAN, J.B., K.M. TILL, R.W. SHEA (1992): Biogeochemistry of deforestation and biomass burning, in The Science of Global Change: The impacts of Human activities on the Environment, ACS Symp. Ser., vol. 483, edited by D.A Dunnette, and R.J. O' Brien, pp. 426-456, Am. Chem. Soc. Washington, D.C.
- KAUFMAN, Y.J., C.O. JUSTICE, L.P. FLYNN, J.D. KENDALL, E.M. PRINS, L. GIGLIO, D.E. WARD, W.P. MENZEL, A.W. SETZER (1998): Potential global fire monitoring from EOS-MODIS. Journal of Geophysical Research, D103: 32215-32238.
- KAUFMAN, Y., JUSTICE, C.O. (1998): MODIS Fire Product (Version 2.2 Nov. 10 1998), Algorithm Technical Background Document (ATBD). NASA/GSFC, Greenbelt, MD.
- KITCHIN, M. & N. REID. (1999): Fire history-what can you do without it? Deriving the context for a fire ecology study by integrating satellite imagery and local information. In: Proceedings of the Australian Bushfire Conference, Albury, July 1999, Australia.
- KITUYI, E., L. MARUFU, S. O. WANDIGA, I. O. JUMBA, M. O. ANDREAE, G. HELAS (2001): Carbon monoxide and nitric oxide from biofuel fires in Kenya, Energy Conversion and Management, 42 (13), 1517-1542.
- KNAPP, A.K., SEASTEDT, T.R. (1986): Detritus accumulation limits productivity of tallgrass prairie, BioScience, 36, 662-668.

- KOUTSIAS, N. & M. KARTERIS (2000): Burned area mapping using logistic regression modeling of a single post-fire Landsat-5 Thematic Mapper image. *International Journal of Remote Sensing* 21 (4): 673-687.
- KRAUS, T. & C. SAMIMI (2002): Biomass estimation for land use management and fire management using Landsat-TM and -ETM+, *Erdkunde* 56 (2): 130-144.
- KRUGER, A.C., L.B. MAKAMO, S. SHONGWE (2002): An analysis of Skukuza climate data. *Koedoe* 45/1: 1-7.
- KRUSE, F.A., K.S. KIEREIN-YOUNG & J.W. BOARDMAN (1990): Mineral mapping at Cuprite, Nevada with a 63-channel imaging spectrometer. *Photogrammetric Engineering and remote sensing* 56: 83-92.
- LACAUX, J.-P., H. CACHIER, R. DELMAS (1993): Biomass burning in Africa: an overview of its impact on atmospheric chemistry, in *Fire in the environment: The Ecological, Atmospheric, and Climatic Importance of Vegetation Fires*, edited by P.J. Crutzen and J.G. Goldammer, pp. 151-191, *Environ. Sci. Rep.* 13, John Wiley and Sons Ltd, New York.
- LANDMANN, T. (1999): A methodology to monitor fires in South African grasslands using Landsat Thematic Mapper satellite data, M.Sc thesis, Department of Landscape Ecology, University of Goettingen, Germany.
- LANDMANN, T. (2002): Mapping fire severity in multitemporal reflective wavebands in burn plots in the Kruger National Park. *South African Journal of Sciences*, In press.
- LANGAAS, S. (1995): Night-time observations of West-African bushfires from space: Studies on methods and applications of thermal NOAA/AVHRR satellite data from Senegal and the Gambia, Ph.D. thesis, Department of Geography, University of Oslo, Norway.
- LEMMON, P. E. (1957): A new instrument for measuring forest overstory density. *Journal of Forestry*: 666-669.
- LEVINE, J.S., Ed. (1996): *Biomass Burning and Global Change*, MIT Press, Cambridge, MA.
- LEVINE, J.S. (1996): Introduction: Global biomass burning: Atmospheric, climatic, and biospheric implications, In: *Global Biomass Burning: Atmospheric, Climatic, and Biospheric Implications*, edited by J. S. Levine, MIT Press, Cambridge, Mass, pp. 278-295.

- LEVINE, J.S., D.A.B. PARSONS, R.G. ZEPP, R.A. BURKE, D.R. CAHOON, W.R. COFER III, W.L. MILLER, M.C. SCHOLLES, R.J. SCHOLLES, D.I. SEBACHER, S. SEBACHER, E.L. WINSTEAD (1997): Southern African savannas as a source of atmospheric gases, in *Fire in Southern African Savannas: Ecological and atmospheric perspectives*, edited by B.W. van Wilgen, M.O. Andreae, J.G. Goldammer, J.A. Lindesay, Witwatersrand University Press, Johannesburg, pp. 135-160.
- LOBERT, J.M., J. WARNATZ (1993): Emissions from combustion processes in vegetation, in *Fire in the environment: The Ecological, Atmospheric, and Climatic Importance of Vegetation Fires*, edited by P.J. Crutzen and J.G. Goldammer, pp. 151-191, Environ. Sci. Rep. 13, John Wiley and Sons Ltd, New York.
- LOBERT, J.M., W.C. KEENE, J.A. LOGAN, R. YEVICH (1999): Global chlorine emissions from biomass burning: Reactive Chlorine Emissions Inventory. *Journal of Geophysical Research* 104: 8373-8390.
- LOPEZ GARCIA, M.J., CASELLES, V. (1991): Mapping burns and natural reforestation using Thematic Mapper data, *Geocarto International*, 1, 31-37.
- LUKE, R.H. & MCARTHUR, A.G. (1978): *Bush fires in Australia*, Australian Government Publishing Service, Canberra.
- LYNNES, C., P. SMITH, L. SHOTLAND, T. EL-GHAZAWI, M. ZHUN (2000): Level 1 Processing of direct broadcast MODIS data. In: *Proceedings of the 4<sup>th</sup> international meeting on direct broadcast of Earth Observation Data in Dundee, Scotland*.
- MAGUCHI, H., H. TSU & H. FUJISADA (1993): Scientific bases of ASTER instrument design. In: *Proc. SPIE*, vol 1939, P.p. 150-160.
- MASON, S.A., R.J. FIELD, R.J. YOKELSON, M.A. KOCHIVAR, M.R. TINSLEY, D.E. WARD, W.M. HAO (2001): Complex effects arising in smoke plume simulations due to inclusion of direct emissions of oxygenated organic species from biomass combustion. *J Geophys. Res.* 106. 12527-12539.
- MATSON, M., J. DOZIER (1981): Identification of subpixel high temperature sources using a thermal IR sensor. *Photo. Enfr. And Rem. Sens.* 47: 1311-1318.
- MCDONALD, A.J., GEMMELL, F.M., LEWIS, P.E. (1998): Investigation of the utility of spectral vegetation indices for determining information on coniferous forests, *Remote Sensing of Environment*, 66, 250-272.

- MICHALEK, J.L., J.E. COLWELL, N.H.F. FRENCH, E.S. KASISCHKE, R.D. JOHNSON (2000): Using Landsat TM data to estimate carbon release from burned biomass in an Alaskan spruce forest complex. *International Journal of Remote Sensing* 21: 329-343.
- MILLER, J.D. & S.R. YOOL (2002): Mapping post-fire canopy consumption in several overstory types using multi-temporal Landsat TM and ETM data. *Remote Sensing of the Environment* 82: 481-496.
- MILNE, G. (1936): Some suggested units of classification and mapping, particularly for East African soils. *Soils research* 4: 183-98.
- MUIRHEAD, K., CRACKNELL, A. P. (1984): Identification of gas flares in the North Sea using satellite data. *International Journal of Remote Sensing* 5: 199-212.
- MUNSELL COLOR CO. (1971): Munsell soil color charts. 13 tables, 8 pp. Baltimore, MD, USA.
- Nelson, S.C., J.D. Cunningham (2002): The National Polar-Orbiting Operational Environmental Satellite System future U.S. Environmental Observing system. NPOESS Integrated Program Office. Silver Spring, Maryland.
- NETSHILUVHI, T.R., SCHOLES, R.J., 2001, Allometry of South African woodland trees, CSIR Environmentek, Pretoria, ENV-P-I 2001-007, South Africa.
- PATTERSON, M.W. & S.R. YOOL (1998): Mapping fire-induced vegetation mortality using Landsat Thematic Mapper Data: A comparison of linear transformation techniques. *Remote Sensing of the Environment* 65: 132-142.
- PEREIRA J.M.C, CHUVIECO E., BEAUDOIN A., DESBOIS N. (1997): Remote sensing of burned areas. In *A review of remote sensing methods for the study of large wildland fires*, ed E. Chuvieco, pp. 127-183. University of Alcala, Spain.
- PEREIRA, J.M.C. (1999): A Comparative Evaluation of NOAA/AVHRR Vegetation Indices for Burned Surface Detection and Mapping, *IEEE Transaction on Geoscience and Remote Sensing*, 37, 217-226.
- PEREIRA, J.M.C., A.C.L. SÀ, A.M.O. SOUSA, J.M.N. SILVA, T.N. SANTOS, J.M.B. CARRIERAS (1999): Spectral characterisation and discrimination of burnt areas, in *Remote Sensing of Large Wildland Fires*, editor E. Chuvieco, Berlin Heidelberg: Springer-Verlag, pp. 123-138.

- PEREIRA, J.M.C., S. FLASSE, A. HOFFMAN, J.A.R. PEREIRA, F. GONZÁLEZ-ALONSO & S. TRIGG (2000): Operational use of remote sensing for fire monitoring and management: regional case studies. Pp. 98-110. In: Ahern, F., J-M. Grégoire & C. Justice (ed.). *Forest Fire Monitoring and Mapping: A Component of Global Observation of Forest Cover*, Report of a Workshop, November 3-5 1999. Joint Research Centre, Italy: European Commission - Joint Research Centre, EUR 19588 EN.
- POTTER, C. S., V. BROOKS-GENOVESE, S. A. KLOOSTER, M. BOBO, A. TORREGROSA (2001): Biomass burning losses of carbon estimated from ecosystem modeling and satellite data analysis for the Brazilian Amazon region, *Atmospheric Environment*, 35(10): 1773-1781.
- PRASAD, V.K., Y. KANT, K.V.S. BADARINATH (2002): Estimation of potential GHG emissions from net primary productivity of forests- a satellite based approach. *Adv. Space Res.* 29, No. 11: 1793-1798.
- REICHENBACH, S.E., KOEHLER, D.E., STRELOW, D.W. (1995): Restoration and reconstruction of AVHRR images, *IEEE Transactions on Geoscience and Remote Sensing*, 33, 997-1007.
- Roberts D.A., Green R.O., Adams J.B. (1993): Discriminating green vegetation, non-photosynthetic vegetation and soils in AVIRIS data. *Remote Sensing of the Environment*. 44, 255-270.
- ROGAN, J. & J. FRANKLIN (2001): Mapping burn severity in southern California using spectral unmixing analysis. In: *Proceedings of the International Geoscience and Remote Sensing Symposium (IGARRS '01)*. Sydney, Australia.
- ROGAN, J. & S.R. YOOL. 2001. Mapping fire-induced vegetation depletion in the Peloncillo Mountains, Arizona and New Mexico. *International Journal of Remote Sensing* 22: 3101-3121.
- ROY, D.P., L. GIGLIO, J.D. KENDALL, C.O. JUSTICE (1999): Multi-temporal active-fire based scar detection algorithm. *International Journal of Remote Sensing* 20: 1031-1038.
- ROY, D.P. AND THE MIOMBO NETWORK FIRE WORKING GROUP (2000): MODIS Southern Africa Fire Products Validation Protocol, developed by consensus from a travelling meeting held 11-19<sup>th</sup> July 2000 in Zimbabwe and Zambia, October 26<sup>th</sup> 2000, NASA GSFC.

- ROY, D.P., P.E LEWIS, C.O. JUSTICE (2002): Burned area mapping using multi-temporal moderate spatial resolution data - a bi-directional reflectance model-based expectation approach. MODIS Land special issue of Remote Sensing of Environment, in press.
- ROY, D.P, LANDMANN, T. (2003): Estimating combustion completeness of fires from space in South African savanna ecosystems. In Proceedings, Third meeting of the GOFC/GOLD Southern Africa Fire Network (SAFNet), University of Botswana, Gaborone, ed P. Dube. University of Botswana, Botswana.
- ROY, D.P. & T. LANDMANN (2002): Characterizing the surface heterogeneity of fire effects using multi-temporal reflective wavelength data. International Journal of Remote Sensing, in press.
- ROY, D.P., P.E LEWIS, C.O. JUSTICE (2002): Burned area mapping using multi-temporal moderate spatial resolution data - a bi-directional reflectance model-based expectation approach. MODIS Land special issue of Remote Sensing of Environment, in press.
- ROY, D.P., C.O. JUSTICE, P. FROST, T. LANDMANN, J. LE ROUX, S. MAKUNGA, K. GUMBO, F. MKOSANA, K. DUNHAM, R. DU TOIT, K. MHWANDAGARA, A. ZACARIAS, B. TACHEBA, P. DUBE, J.M.C. PEREIRA, J. MORISETTE, P. MUSHOVE, D. DAVIES (2003): The Southern Africa Fire Network (SAFNet) regional burned area product validation protocol. International Journal of Remote Sensing, in press.
- RUTHERFORD, M. C. (1978): Primary production in South Africa, in Biogeography and Ecology of Southern Africa, pp. 621-659, Junk, The Hague.
- SALVADOR R., VALERIANO, J., PONS, X., DIAZ-DELGADO R. (2000): A semi-automatic methodology to detect fire scars in shrubs and evergreen forest with Landsat MSS time series. International Journal of Remote Sensing 21, 655-671.
- SCHOLES, M.C., M.O. ANDREA (2000): Biogenic and pyrogenic emissions from Africa and their impacts on the global atmosphere. *Ambio* 29: 23-29.
- SCHOLES, R.J. (1995): Greenhouse gas emissions from vegetation fires in Southern Africa, in African greenhouse gas emission inventories and mitigation options: forestry, land-use change, and agriculture Environmental Monitoring and Assessment, edited by Braatz, B.V., S. Brown, A.O. Isichei, E.O. Odada, R.J. Scholes, pp. 63-73, Vol. 38, Kluwer Academic Publishers, The Netherlands.

- SCHOLES R. J., KENDALL J., JUSTICE C.O. (1996): The quantity of biomass burned in southern Africa, *Journal of Geophysical Research*, 101, 236676-23676.
- SCHOLES, R.J. (1997): Savanna. In: *Vegetation of Southern Africa*, edited by R.M. Cowling, D.M. Richardson, and S.M. Pierce, pp. 258-277, Cambridge: Cambridge University Press.
- SCHOLES, R.J., T. LANDMANN (2002): A simple savanna biomass fuel model for the Kruger National Park (KNP). *J. Geophys. Res.*, to be submitted.
- SCHULZE, R.E. (1997): Climate. In *Vegetation of Southern Africa*. Ed. R.M. Cowling, D.M. Richardson and S.M. Pierce, pp. 2-42, Cambridge: Cambridge University Press.
- SETTLE J., CAMPBELL N. (1998): On the errors of two estimators of sub-pixel fractional cover when mixing is linear, *IEEE Transaction on Geoscience and Remote Sensing*, 36, 163-170.
- SHEA, R. W. (1996): Fuel biomass and combustion factors associated with fires in savanna ecosystems of South Africa and Zambia. *Journal of Geophysical Research*, Vol. 101, No.D19, pp. 23551-23568.
- SOKAL, R. R., ROHLF, F.J. (2000): *Biometry – The principle and practice of statistics in biological research*. Third Edition. WH Freeman and Company (Publ.), New York: 850p.
- STOCKS, B.J, VAN WILGEN, B.W., TROLLOPE, W.S.W., MCRAE, D.J., MASON, J.A., WEIRICH, F., POTGIETER, A.L.F. (1996): Fuels and fire behavior dynamics on large-scale savanna fires in Kruger National Park, South Africa, *Journal of Geophysical Research*, Vol 101, No.D19, pp 23541-23550.
- STRONACH, N.R.H, MCNAUGHTON, S.J. (1989): Grassland fire dynamics in the Serengeti Ecosystem, and a potential method of retrospective estimating fire energy, *Journal of Applied Ecology*, 26, 1025-1033.
- STROPPIANA, D., S. PINNOCK, J.-M. GREGOIRE (2000): The global fire product: daily occurrence from April 1992 to December 1993 derived from NOAA AVHRR data, *International Journal of Remote Sensing* 21, 1279–1288.
- SWAP, R.J., ANNEGARN, H.J., SUTTLES, J.T., HAYWOOD, J., HELMLINGER, M.C., HELY, C., HOBBS, P.V., HOLBEN, B. N., JI, J., KING, M., LANDMANN, T., MAENHAUT, W., OTTER, L., PAK, B., PIKETH, S.J., PLATNICK, S., PRIVETTE, J., ROY, D.P., THOMPSON, A.M., WARD, D., YOKELSON, R. (2002): The Southern African Regional Science Initiative (SAFARI 2000): overview of the dry-season field campaign, *South African Journal of Science*, 98, 125-130

- THOMPSON, M. W. (1993): Quantitative biomass monitoring and fire severity mapping techniques in savanna environments using Landsat Thematic Mapper imagery, External Contract Report FOR-DEA 587, Division of Water, Environment and Forest Technology, CSIR, Pretoria, South Africa.
- THOMPSON, M.W. & E. R. VINK (1997): Fire Scar Mapping in Pilanesberg National Park. CSIR internal Report FOR. 16, Environmentek, CSIR.
- TRIGG S. AND FLASSE S. (2000): Characterizing the spectral-temporal response of burned savanna using in situ spectroradiometry and infrared thermometry, *International Journal of Remote Sensing*, 21, 3161-3168.
- TROLLOPE, W. S. W. (1983): Control of bush encroachment with fire in the arid savannas of southeastern Africa, PhD thesis, University of Natal, Pietermaritzburg.
- TROLLOPE, W. S. W., Potgieter ALF (1985): Fire behavior in the Kruger National Park. *Journal of the Grassland Society of South Africa*, 2, (2): pp.17-22.
- TROLLOPE, W. S. W., POTGIETER, A. L. F. (1986): Estimating grass fuel loads with a disc pasture meter in the Kruger National Park. *Journal Grassland Society Southern Africa* 3: pp. 148-152.
- TROLLOPE, W. S. W., TANTON, N. M. (1986): Effect of fire intensity on the grass and bush component of the Eastern Cape Thornveld, *Journal of the Grassland Society of Southern Africa* 2(2): pp. 27-42.
- TROLLOPE W. S. W. (1992): Fire behavior and its significance in burning as a veld management practice. In *Proceedings, Prestige Farmers Day Proceedings 1991 – 1992*, C. R. HURTAND P. J. K. ZACHARIAS (eds).
- TROLLOPE, W.S.W., A.L.F. POTGIETER, H.C. BIGGS, L.A. TROLLOPE (1998): Report on the Experimental Burning Plots (EBP) trial in the major vegetation types of the Kruger National Park, Unpublished report no. 9/98, Skukuza, South African National Parks.
- VAN DE VIJVER C. (1999): Fire and Life in the Tarangire: Effects of burning and herbivory on an East African Savanna System. pp. 149-159. Doctoral Thesis, University of Wageningen, Wageningen, The Netherlands.
- VAN WAGNER, C. E. (1968): The line intersect method in forest fuel sampling. *Forest Science* 14: pp. 20-26.

- VAN WILGEN, B.W., C.S. EVERSON & W.S.W. TROLLOPE (1990): Fire management in Southern Africa: Some examples of current objectives, practices and problems. Pp. 179-215. In: J.G. Goldammer (ed.). *Fire in Tropical Biota*. Springer-Verlag, Berlin.
- VAN WILGEN, B.W., H. C. BIGGS, S.P. O'REGAN & N. MARÉ (2002): Fire Regimes in savanna ecosystems in the Kruger National Park, South Africa between 1941 and 1996. *International Journal of Wildland Fire*. in press.
- VERMOTE E.F., TANRE D., DEUZE J.L., HERMAN M., MORCRETTE J. (1997): Second Simulation of the Satellite Signal in the Solar Spectrum, 6S: An overview, *IEEE Transaction on Geoscience and Remote Sensing*, 35, 675-686.
- VERMOTE, E.F., AND A. VERMEULEN (1998): Atmospheric correction algorithm: spectral reflectances (MOD09), ATBD version 4.0, NASA/GSFC, Greenbelt, MD.
- VERMOTE, E. F., EL SALEOUS N.Z., JUSTICE C.O. (2002): Atmospheric correction of the MODIS data in the visible to middle infrared: first results. *MODIS Land special issue of Remote Sensing of Environment*, in press.
- VERSTRAETE, M.M. AND PINTY, B. (1996): Designing optimal spectral indexes for remote sensing applications, *IEEE Transactions on Geoscience and Remote Sensing*, 34, 1254-1265.
- WARD, D.E., R.A. SUSOTT, J.B. KAUFFMAN, R.E. BABBITT, D.L. CUMMINGS, B. DIAS, B.N. HOLBE, Y.J. KAUFFMAN, R.A. RASMUSSEN, A.W. SETZER (1992): Smoke and fire characteristics for cerrado and deforestation burns in Brazil: BASE-B Experiment, *Journal of Geophysical Research*, 97 (D13), 14601—14619.
- WARD, D.E., L.F. RADKE (1993): Emission measurements from vegetation fires: A comparative evaluation of methods and results, in *Fire in the environment: The Ecological, Atmospheric, and Climatic Importance of Vegetation Fires*, edited by P.J. Crutzen and J.G. Goldammer, pp. 53-76, *Environ. Sci. Rep. 13*, John Wiley and Sons Ltd, New York,
- WARD D.E., HAO W.M, SUSOTT R.A., BABBITT R.E., SHEA R.W., KAUFFMAN J.B., JUSTICE C.O. (1996): Effect of fuel composition on combustion efficiency and emission factors for African savanna ecosystems. *Journal of Geophysical Research* 101, 23569-23576.
- YOKELSON, R. J., J. G. GOODE, I. BERTSCHI, R. A. SUSOTT, R. E. BABBITT, D. E. WARD, W. M. HAO, D. D. WADE, D. W. T. GRIFFITH (1999): Emissions of formaldehyde, acetic acid, methanol, and other trace gases from biomass fires in North Carolina measured by

airborne Fourier transform infrared spectroscopy (AFTIR), *J. Geophys. Res.*, 104, 30, 109-30, 125.

YOKELSON, R.J., R.A. SUSOTT, R.E. BABBITT, D.E. WARD, W. M. HAO (1999): Trace gas emissions from specific biomass fire-types. In: *START Synthesis Workshop on Greenhouse Gas Emission, Aerosols and Land Use and Cover Change in Southeast Asia*, ed. by T. Moya, SARCS, IGAC, LUCC, IGBP, pp. 329-343, China-Tapei, Taipei.

YOKELSON, R.J., T. ISAAC, T. BERTSCHI, J. CHRISTIAN, P. V. HOBBS, D. E. WARD, W-M. HAO. (2002): Trace gas measurements in southern Africa, biomass-burning, smoke and haze by airborne FTIR. *Journal of Geophysical Research*, in press.

ZHAN, X., R.S. DEFRIES, S.O. LOSAND, Z.L. YANG (2000): Application of Vegetation Continuous Fields Data in Atmosphere-Biosphere Interaction Models, *Proceedings of IEEE 2000 International Geoscience and Remote Sensing Symposium*, 1948-1951, IGARSS, Honolulu, Hawaii.





**Table 12:** Examples of field parameters measured on prescribed burn sites in the KNP and Madikwe during the SAFARI-2000 campaign (R= biomass according to RUTHERFORD; S= biomass according to NETSHILUVHI & SCHOLES; CC\_S= combustion completeness using wood mass according to NETSHILUVHI & SCHOLES (2001).

Name of sampling site	R_wood (t/ha)	S_wood (t/ha)	Tree cover [%]	Grass (t/ha)	S_leaf (t/ha)	Munsell soil color (pre-burn)	Date of fire	Munsell soil color (after-burn)	CC_S
Madikwe 1	1.52	1.62	5	3.59	0.14	4/4, dark yellowish brown (10YR)	2000-08-18	4/4, dark yellowish brown (10YR)	79
Madikwe 2	26.83	64.28	5	3.12	0.14	4/6, yellowish red (5YR)	2000-08-18	4/6, yellowish red (5YR)	65
Madikwe 3	7.01	10.07	15	4.57	0.33	4/4 (dark) brown (5.7YR)	2000-08-19	5/6 strong brown (7.5 YR)	73
Madikwe 4	0.00	0.00	0	4.81	0.08	4/8 red (2.5YR)	2000-08-17	4/6 red (2.5YR)	60
Madikwe 5	0.09	0.03	0	2.75	0.05	4/6 strong brown (7.5YR)	2000-08-17	4/6 strong brown (7.5YR)	35
Madikwe 6	3.60	5.23	3	6.98	0.17	4/4 reddish brown (2.5YR)	2000-08-18	4/4 reddish brown (2.5YR)	80
Madikwe 7	8.99	19.70	15	5.65	0.34	4/6, yellowish red (5YR)	2000-08-18	4/6, yellowish red (5YR)	45
Skukuza 6	10.98	27.51	25	4.87	0.50	6/2 light brownish grey (10YR)	2000-08-10	5/2 grayish brown (10YR)	X
Skukuza 12	5.54	12.35	20	4.13	0.40	5/3 brown (7.5 YR)	2000-08-10	5/3 brown (7.5 YR)	X
Skukuza 4	30.27	72.58	15	5.28	0.34	5/3 brown (10 YR)	2000-08-10	5/2 grayish brown (10YR)	X
Naphe 1	9.57	21.36	20	5.07	0.42	5/2 grayish brown (10YR)	2000-08-11	5/3 brown (10 YR)	X
Naphe 3	65.52	107.26	20	2.65	0.38	5/3 brown (10 YR)	2000-08-10	5/3 brown (10 YR)	48
Naphe 6	24.65	54.18	30	4.84	0.58	5/2 grayish brown (10YR)	2000-08-14	5/2 grayish brown (10YR)	X
Shabeni 10	20.28	43.66	15	6.22	0.35	4/3 (dark) brown (10YR)	2000-08-14	4/3 (dark) brown (10YR)	75
Shabeni 1	13.11	32.68	20	3.80	0.40	4/4 (dark) brown (7.5 YR)	2000-08-14	4/4 (dark) brown (7.5 YR)	70
Shabeni 3	42.18	104.66	15	4.02	0.32	4/3 (dark) brown (10YR)	2000-08-14	4/4 (dark) brown (7.5 YR)	70
Kambeni 7	16.42	37.71	55	3.69	0.98	5/2 grayish brown (10YR)	2000-08-15	5/2 grayish brown (10YR)	61.5
Kambeni 5	32.65	77.18	60	7.34	1.12	4/3 (dark) brown (10YR)	2000-08-15	4/3 (dark) brown (10YR)	68
Kambeni 11	17.33	35.63	45	6.41	0.86	5/2 grayish brown (10YR)	2000-08-14	4/3 (dark) brown (10YR)	67
Marheya, 1	4.03	9.80	1	3.05	0.07	3/4 dark brown (7.5.YR)	2000-08-22	3/4 dark brown (7.5.YR)	80
Marheya 3	3.35	7.32	3	3.17	0.10	3/4 dark brown (7.5.YR)	2000-08-22	3/3 dark brown (10YR)	70
Marheya 10	1.52	0.93	0	4.23	0.07	3/3 dark brown (10YR)	2000-08-22	3/4 dark brown (7.5.YR)	84
Satara 1	3.36	6.37	7	5.00	0.20	3/4 dark brown (7.5.YR)	2000-08-22	3/3 dark brown (10YR)	70
Satara 7	5.75	1.82	2	3.65	0.09	3/4 dark brown (7.5.YR)	2000-08-22	3/4 dark brown (7.5.YR)	73.5
Satara 9	0.38	0.33	7	3.69	0.18	3/4 dark brown (7.5.YR)	2000-08-23	3/4 dark brown (7.5.YR)	80

## **Acknowledgements**

I would like to express my sincere gratitude to a number of people. Firstly I thank David Roy for his generous assistance and support during the nearly four years of work. My sincere gratitude also goes to my supervisor Prof. G. Gerold for technical support and ideas. Special thanks goes to Bob Scholes for his extraordinary mentorship, guidance and inspirational input into this study. I would like to acknowledge many of the staff members of the Kruger National Park, Scientific Services, over and above Andre Potgieter, Harry Biggs, Navashni Govender, David Woods and all the field scouts. Many thanks also to the staff of the Madikwe Game Reserve and North West Parks, explicitly Bruce Brockett and Piet Nel; to Brian Harris from the Timbavati Nature Reserve and to Dave Balfour from Kwa-Zulu Natal Wildlife. Staff members (too many to mention) of CSIR Environmentek deserve a special thank you: Helen de Beer especially. I also acknowledge the financial and resources support given to me by the Post-Graduate Program of the University of Göttingen and the Daimler-Benz Bursary Foundation in Ladenburg, Germany. In the context of the SAFARI-2000 initiative I would like to express my sincere gratitude to Prof. Harold Annegarn of the University of the Witwatersrand for his logistical and prompt support in urgent matters, Bob Yokelson for his excellent comments on my work, Bob Swap, Christelle Hely and many others.

Finally I would like to thank my family; especially my Grandmother for her overwhelming moral support, this thesis is dedicated to her. My sincere gratitude goes to Nina Rohwer for her companionship and patience.

## Danksagung

Mein besonderer Dank gilt Herrn Prof. Dr. Gerold für die Betreuung meiner Doktorarbeit. Insbesondere bedanke ich mich für die Bereitstellung des Arbeitsplatzes innerhalb der Abteilung für Landschaftsökologie und den großen Freiraum bei der Bearbeitung des Themas. Mein aufrichtiger Dank auch an Dr. David Roy für seine wertvollen Anregungen und Unterstützung bei Projektanträgen zur Finanzierung einzelner Komponenten dieser Arbeit. Einen besonderen Dank an Dr. Bob Scholes vom CSIR in Pretoria für wertvolle Diskussionen und Inspirative Ideen zum Arbeitsablauf. Dank und Anerkennung auch an etliche Mitarbeiter im Krüger National Park, insbesondere Andre Potgieter, Harry Biggs, Navashni Govender, David Woods und alle Feldassistenten. Dank auch an die Mitarbeiter und an das Management Team im Madikwe Wildpark, besonders Bruce Brockett und Piet Nel; an das Team vom Hluhluwe-Umfolozi Wildreservat und Brian Harris vom Timbavati National Park. Danke auch an alle Kollegen und Mitarbeiter im Geographischen Institut in Göttingen, und Mitarbeiter im CSIR in Pretoria für die Unterstützung bei der Anfertigung dieser Arbeit. Ich bedanke mich für die finanzielle Unterstützung bei der Gottlieb Daimler und Karl-Benz-Stiftung, der Graduiertenförderung der Universität Göttingen und Prof. Dr. Harold Annegarn vom SAFARI 2000 Projekt.

Schließlich möchte ich mich noch bei meiner Familie, besonders bei meiner Großmutter, bedanken; diese Arbeit ist ihr gewidmet. Vielen Dank auch an Nina Rohwer, insbesondere für ihre Hilfe, Zuneigung und Geduld.

---

 Curriculum Vitae

<b>Name:</b>	Landmann, Tobias	
<b>Adresse:</b>	Obere Mühle 8, 37077 Göttingen	
<b>E-Mail:</b>	tlandmann@csir.co.za	
<b>Geburtsdatum:</b>	08.05.1971	
<b>Geburtsort:</b>	Elim/Südafrika	
<b>Nationalität:</b>	deutsch	
<b>Familienstand:</b>	ledig	
<b>Schulbildung:</b>	1989	Deutsche Schule Hermannsburg, südafrikanischer Schulabschluss
	1990	Deutsche Schule Kapstadt, Abitur
<b>Zivildienst:</b>	03/1991-10/1992	Arbeiter Samariter Bund, Hannover, Hannover
<b>Universitätsbildung:</b>	10/1992-11/1998	Universität Göttingen, Diplomprüfung Hauptfach: Geographie Nebenfächer: Pflanzenbau in den Tropen und Subtropen und Sozioökonomie der Ruralen Entwicklung
	10/1995	Vordiplom
	07/1996-08/1996	Praktikum: Harbor & Masson Regional Planners and
	Architects, Durban	
	07/1997-10/1997	Praktikum: Agricultural Research Council (ARC); Institute for Soil, Climate and Water (ISCW), Pretoria
	02/1998-04/1998	Praktikum: Agricultural Research Council (ARC); Institute for Soil, Climate and Water (ISCW), Pretoria
	11/1998	Diplomprüfung; Resultat: sehr gut. Titel der Diplomarbeit: ‘Towards the development of a technique to monitor fires in South Africa using NOAA/AVHRR and Landsat Thematic (TM) satellite data’
<b>Doktorarbeit:</b>	02/1999-01/2003	Titel der Doktorarbeit: ‘Ableitung biophysikalischer Feuereigenschaften für das Testgebiet Skukuza, Südafrika, mittels EOS-MODIS Satellitendaten’, Schlüsselbegriffe: Vegetationsaufnahme, Charakterisierung von Brandflächen, Feuerintensitätsmodelle, MODIS-Validierung, Pyrogene Emissionen, Landsat Enhanced Thematic Mapper (ETM+)